# Brownian Dynamics Simulation of Polymer Beheaviors in Microfluidic Systems

**By**

**Zhu Xueyu**

**Supervisor: Ole Hassager, Henrik Bruus**

A THESIS SUMITTED IN PARTIAL FULFILLMENT OF THE REQUIEMENTS FOR THE DEGREE OF

Master of Engineering

**at**

**Danish Polymer Center**

**Technical University of Denmark**

**1st July 2005**

*To my parents, for your continuous encouragement and love in my whole life.*

# Preface

After almost half a year, this master thesis is finished eventually. The two-year master study will also be finished soon. Two years' study in DTU makes me not only possess a solid background in my major, but also get touch with a totally different culture from China. I think I would be benefited from this experience in my whole life.

In those two years, many people helped me a lot. Thanks to my advisors, Ole Hassager and Henrik Bruss for your support, patience, and guidance.

Thanks to my friends in Polymer Center, Yanwei Wang, Xiaoxue Yuan, Juan Jiang, Josè Marin for your help and many discussions.

Thanks to Bernd Dammann at High Performance Computing Center at DTU for providing the computing resources and advice on parallel computing

Thanks to Novozymes for offering the financial support to this master project.

Thanks to all members of Apple Kernel, communicating with you gives me lots of fresh idea.

Finally, special thanks to Ole again. Thank you for giving me an opportunity to come to this beautiful country and continuous encouragement to challenge myself in academia. I would say that it is my honour and luck to be your student. I think if I can become a professor someday, I would be a professor like you.

*Life is a random process, you can't expect what happens tomorrow. Hope everyone can enjoy his life and achieve his dream.*

# CONTENTS

# Abstract

This master thesis is entitled '*Brownian Dynamics Simulation of Polymer Behaviours in Microfuidic Systems* '. In this project, Brownian dynamic simulation is used to capture the most important features of dynamics of dilute polymer solution in the confined geometry, especially for dilute DNA solution. Two kinds of flow pattern in confined geometry are mainly examined:

*Homogenous flow.* A Brownian model of dilute DNA solution based on simple shear flow is developed and gives qualitatively agreement with experimental data and simulation results available now in free solution and confined geometries.

*Inhomogeneous flow*. Brownian models of dilute DNA solution based on pressure-driven flow are developed. Three kinds of models with different levels to treat hydrodynamic interaction are examined and compared: Free-draining model, Bulk hydrodynamic interaction model and Full hydrodynamic interaction model. Only Full hydrodynamic interaction gives correct predictions on the migration effect: DNA chain will migrate toward the center of the microchannel under pressure-driven flow.

Theoretical analysis on migration behaviour is carried on by following Jendrejack *et al*'s idea (2004). In addition, simple mechanism (reflection mechanism) on the migration behaviour is proposed from a physical perspective.

# Chapter 1 Introduction

In the last two decades, people made lots of efforts on molecular level understanding of the rheological properties of dilute solutions of flexible polymers, especially isolated polymer deoxyribonucleic acid (DNA) molecules. In 1990s, Steven Chu and his co-workers imaged the conformations of DNA molecules in well-defined flows (Perkins *et al*,1995). Before the appearance of the accurate results, it is difficult to test the predictions rigorously, though much effort has been devoted to predicting the molecular dynamics of polymer in various flows. In recently years, with the increase of experimental data, computer speed and developments of methods, simulations of the conformations of real polymers by predicting ensembles of coarse-grained chains become promising.

Solutions of polymer at extremely low concentrations ($\approx 10^{-5} c^*$.where $c^*$ is the polymer overlap concentration) can be called dilute, in which interchain interactions or entanglements are absent (Schroeder *et al*, 2005) and polymer chains interact primarily with the slovent. From a theoretical point of view, the interest of dilute polymer solutions comes primarily from their importance of understanding the molecular response to the hydrodynamic forces free from introducing the complication by entanglement. Understanding those classical problems of polymer fluid dynamics has proven to be useful for substantial applications. In recent years, the emerging biotechnology and nanotechnology is opening up opportunities in the area of “DNA processing”, especially for microfludic devices or “lab-on-chip” technology, where DNA molecules experienced pressure-driven or electrokineic flow fields, leading to DNA transport and stretching. Besides various flow fields, the interaction of DNA molecules with different surface patterns in such microfluidic device is ubiquitous due to the large surface-to-volume ratios of such devices (Chopra *et al*, 2002).

In such devices, *molecular migration* in flowing dilute polymeric solutions is a well-known phenomenon (During flow, the chain will migrate away from the confined wall). In the typical MEMS device, the gap size is about 10 $\mu m$, for example, while λ-

phage DNA has a radius of gyration ($\boldsymbol{R_G}$) on the order of 1 $\mu m$ and contour length of 21 $\mu m$ .In such systems where the size of the chain is comparable to the channel size, the confined effect becomes more and more important; rheology and chain dynamics are greatly affected (Jendrejack *et al* 2004)**.**

Due to this effect, it has been shown that near the confined wall, there exists a region called *depletion layer,* where chain segments are depleted due to the presence of the wall Therefore, chain concentration will vary from zero at wall to its bulk value over the length scale of this depletion layer. This variation is coupled with variation in other quantities such as the diffusivity of the chain and velocity profile. Traditionally, the detector of microchips can only detect the concentration of the molecule within the depletion layer. It can't penetrate into the depletion layer to measure the value in the bulk flow. Through simulations of the variation of the depletion layer, we can understand the migration behaviour in confined geometries better.

The most powerful tool of dealing with this range of length and time scale in dilute solutions during the flow is Brownian dynamics (BD). Compared to other numerical schemes, BD methods have considerable advantages. By coarsing away the uninteresting fast process, such as movements of solvent molecules, the time step in the simulation can be taken the value comparable to that of fastest process of real interest, which is the time required for the significant movement of macromolecules. These methods are based on rescaling the bead drag coefficient and the spring elasticity constant by using the suitable methods, in order to keep dynamic properties of the coarse-grained chains constant when the bead number in the model is changed. Similarly, the time step size can be adjusted within a wide range to optimise speed and accuracy without changing the mechanism of the process (Larson *et al*, 2005). Those methods have good agreements with the experiment results and are very useful in elucidating the experimental findings, especially for single DNA molecule in well-defined flows. Exciting results would be expected when we expand their use into single molecule in confined geometries under equilibrium and flow conditions.

## *Reference*

T.T.Perkins, D.E.Smith, R.G.Larson, Steven Chu, *Stretching of a Single Tethered Polymer in a Uniform flow*, Science, 268,1995

C.M.Schroeder, E.S.G.Shaqfeh, S.Chu, *Effect of Hydrodynamic Interaction on DNA Dynamics in Extensional Flow:Simulation and Single Molecule Experiment*, Macromolecules,9242-9256,2004

M.Chopra, R.G.Larson, *Brownian dynamics simulations of isolated polymer molecules in shear flow near adsorbin and nonadsorbing surface*, J.Rheol.46,831- 862,2002

R.M.Jendrejack, D.C.Schwartz, J.J.de Pablo, M.D.Graham, *Shear-induced migration in flowing polymer solutions: simulation of long-chain DNA in microchannels*, J.Chem Phys,120,2513-2529,2004

R.G.Larson, *The rheology of dilute solutions of flexible polymers: Progress and problems*, J.Rheol.49 (1), 1-70 , 2005

# Chapter 2 Theory

*"An actual polymer molecule is an extremely complex mechanical systerm with an enormous number of degrees of freedom. To study the detailed motions of this complicated system and their relations to noneuquilibrium properties would be prohibitively difficult. As a result, it has been customary for polymer scientists to resort to mechanical beheavior of macromolecule." (Ottinger, 1995). Those sentences highlight polymer molecules are quite different and complicated compared to other simple molecules, such as water and achcol. Therefore, how to describe this micromechanical system and various interactions inside the system will be introduced in this chapter.*

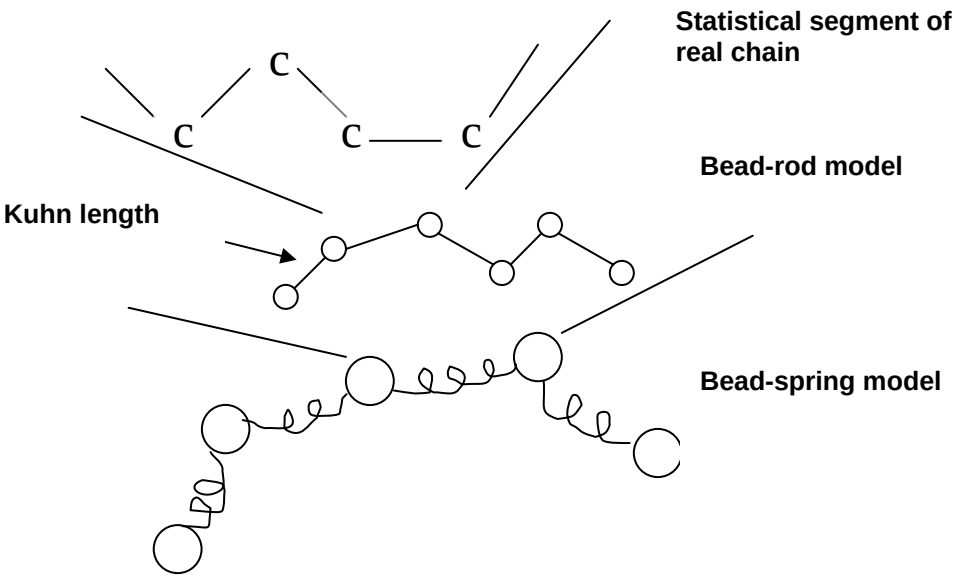


Fig.2.1 illustration of coarse-grain mapping of real polymer chain, with a carbon–carbon backbone containing fixed bond angles, onto a bead-rod chain whose configuration is that of a random walk, and further coarse-grain mapping of the bead-rod chain onto a bead-spring chain.

## *2.1 Bead-spring model and bead-rod model*

The choice of polymer model will depend on the real polymer one wants to model and the level of fine-scale molecular detail one needs to retain or can computationally afford to simulate (Doyle *et al*, 2004). To get the most accurate result, molecular simulation is the first choice. However, in the past days, the results by the atomic-level simulations of long chain polymer are frustrated, even using the most advanced

computer. Hence, it is needed to take a coarse-graining approximation in which we only track the slow variables capturing the coarse-grain features and assume that in the small scale, fast process remain at local equilibrium. Therefore, it is very important to choose a proper level of coarse-graining in a given flow. The most common coarse-grained models are the free jointed bead-rod and bead-spring models shown in Figure 2.1

### 2.1.1. Bead-rod model

In Kramer's bead-rod model, a polymer chain is constructed by $N_k$ beads connected by $N_k - 1$ rigid rods, which keep a constant length between each rod, corresponding to Kuhn length $b_k$ (equal to the mean square end-to-end length of the bonds in a statistical segment) shown in Figure 2.1.The beads serve to experience the drag force given by the solvent molecules. As defined in this way, it can be seen that bead-rod model is a discretized flexible chain with inextensible springs, whose flexibility can be adjusted by changing the number of beads on a constant chain length. In other words, the number of beads can be a parameter to control the internal freedom as well as the discretization of the hydrodynamic drag force. But the chains do not experience the excluded volume interaction between different chain segments (Hur *et al*, 2000). Although it can give us an accurate description on polymers, the problem is that this model is very computationally expensive due to the large number of dynamic variables (bead positions) and rapid motion of the individual rods, which requires smaller time steps. Therefore, we will use a model less demanding in computing resources– Bead-spring model to capture the feature of the real polymer chains in our project.

### 2.1.2. Bead-spring model

A bead-spring chain is represented by $N$ beads connected by $N_s=N-1$ entropic springs shown in Figure 2.1. Each spring represents a large number of Kuhn steps $N_{k,s}$ and spring constant is dependent on the number of Kuhn length. If the molecular weight increases, one can simply increase the number of Kuhn steps without wasting the computing time on the increase of the number of the springs. From a physical aspect, the springs do not represent the molecular interaction but entropic effects due to the loss of more local degrees of freedom. The equilibrium length is zero between the

successive beads. In addition, the model assumes that there is no excluded volume interaction and hydrodynamic interaction between beads.

## 2.2 Physical phenomena in the model

In these ranges of length scales (*nm* to *μm*) and time scales (*μs* to *s*), the following effects are of primary importance for rheological properties (Larson, 2005):

(1) Viscous drag

(2) Entropic elasticity

(3) Brownian forces

(4) Hydrodynamics interaction

(5) Exclued-Volume (EV) interaction

(6) Entanglement

Those effects have been ordered based on their importance. Viscous drag is a kind of frictional force exerted by surrounding solvent molecules, which is always important, even under the weak flow strength. Entropic elasticity will become important when the flow is strong enough to deform the configuration of polymer chains away from their equilibrium states. Moreover, the Brownian motion, due to the collisions between the polymer molecules and solvent molecules, will also influence the distribution of the conformations. In addition to HI, it means that the subchain will produce the disturbance to the flow field to influence the motion of other segments of the chain. This effect will play an important role for polymers with longer chain. EV interaction is the repulsive force which prevents two monomers to overlap, and will make the chains tend to expand beyond the ideal random-walk conformations in equilibrium. Fortunately, this interaction can be screened out in the good solvents at their theta temperature. However, it could become important when the length scale goes to the scale comparable to the radius of gyration of the chain. In addition to the entanglement, since our target system is dilute solution of polymers, so the interchain interaction can be neglected, which means we are focusing on the single molecule dynamics.

## 2.3 Equations for bead-spring model

Since the inertial force in the range of length scale of microdevices always can be negligible, the force balance on each bead including drag force, spring force, Brownian force leads to:

$$\mathbf{F}_i^{drag} + \mathbf{F}_i^s + \mathbf{F}_i^B = 0 \tag{2.1}$$

### 2.3.1. Drag force

Hydrodynamic drag force is the Stokes drag acting on the beads. If we neglect the hydrodynamic interaction and fluid inertia, it can be simplified as follows:

$$\mathbf{F}_i^{drag} = \zeta(\dot{\mathbf{r}}_i - v(\mathbf{r}_i)) \tag{2.2}$$

Where $\boldsymbol{\xi}$ is the drag coefficient, $\mathbf{r}_i$ is the velocity of the ***i***th bead and $\mathbf{v}(\mathbf{r_i})$ is the undisturbed velocity field (namely the solvent velocity) at the position of bead ***i***. For simple shear flow, if the velocity at origin is zero, $\mathrm{v}(\mathbf{r_i})=\boldsymbol{\kappa}\cdot\mathbf{r_i}$ ,where $\boldsymbol{\kappa}$ is the transpose of the velocity gradient tensor, $\boldsymbol{\kappa}=(\nabla\mathbf{v})^{\mathbf{T}}$**.** Substituting the Equation (2.2) into Equation (2.1) yields:

$$\frac{d\mathbf{r}_i}{dt} = \kappa\cdot\mathbf{r}_i + \frac{1}{\zeta}\left(\mathbf{F}_i^s + \mathbf{F}_i^B\right) \tag{2.3}$$

This *stochastic differential equation* is the famous *Langevin equation.* The analytical approach to this equation is beyond the scope of this project, a short introduction is given in *Öttinger's* book (1995).

### 2.3.2. Spring force

The effective spring force acting in the *i*th bead is given as

$$\mathbf{F}_i^s = \begin{cases} \mathbf{F}_1^{sb}, & i=1 \\ \mathbf{F}_i^{sb} - \mathbf{F}_{i-1}^{sb}, & 1<i<N \\ -\mathbf{F}_{N-1}^{sb}, & i=N \end{cases} \tag{2.4}$$

Where $\mathbf{F}_i^{sb}$ is the force that spring *i* acts on bead *i*.The spring force $\mathbf{F}_i^{sb}$ is a function of the extension $\mathbf{Q}_i$ of spring *i*, where $\mathbf{Q}_i=\mathbf{r}_{i+1}-\mathbf{r}_i$. Several force laws to describe the

effective spring are commonly used .The simplest form is the linear force law-Hookean law as follows:

$$\mathbf{F}_i^{sb} = H\mathbf{Q}_i \tag{2.5}$$

where H is the spring constant, which can be given as follows (Larson,2005):

$$H = 2k_B T \beta_s^2, \beta_s{}^2 = \frac{3}{2N_{k,s} b_k^2} \tag{2.6}$$

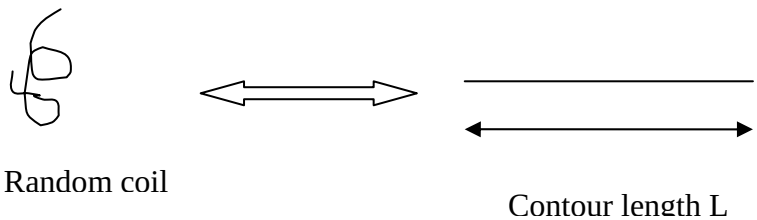


Figure 2.2 illustration of random coil stretched to its full length-contour length

However, a Hookean spring can be infinitely extended, which is unphysical. A more realistic model should give an upper limitation of the extension-$\boldsymbol{L_s = N_{k,s}\, b_k}$, which is the full extension of one segment of the chain represented by a single spring, ie. $\boldsymbol{L_s = L / N_s}$ where $\boldsymbol{L}$ is the contour length of the chain as shown in Figure 2.2. For a freely jointed chain, Kuhn and Grün showed the spring force law by statistical mechanical calculation as follows (Lasron, 2005):

$$\mathbf{F}_i = \frac{k_B T}{b_s} \mathbf{L}^{-1}\left(\frac{\mathbf{Q}_i}{L_S}\right) \tag{2.7}$$

which is called *inverse Langevin* force law and the **L** is the *Langevin* function given by

$$L = \coth\theta - 1/\theta \tag{2.8}$$

where $\coth\theta$ is the hyperbolic cotangent function . It can be seen that for the *inverse Langevin force law*, the force increases linearly with the extension in the small extension region; but grows rapidly for the large extension, especially the extension goes to the maximum length of the spring..

However, *Inverse Langevin force law* is not often used. Several their approximation forms are usually used in various analytical and numerical approaches. One of such approximation is *the Warner spring Law*:

$$F_i^{sb} = \frac{H\mathbf{Q}_i}{1 - \left(\frac{\mathrm{Q}_i}{L_S}\right)^2} \tag{2.9}$$

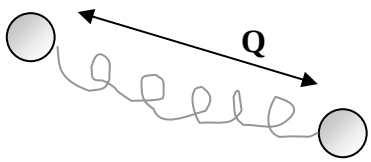


Figure 2.3 illustration of FENE dumbbell model

The simplest *Warner spring* model is FENE(Finitely extensible nonlinear elastisc) dumbbell, which incorporates non-linear effects into the *Hookean* dumbbell model where two beads are connected by a linear spring as shown in Figure 2.3. The maximum extension of the spring can be expressed as the dimensionless extensibility parameter **b** as follows:

$$b = HL / k_B T \tag{2.10}$$

Where $\boldsymbol{N_s}$**=1,** $L_S$=$L$. So $\boldsymbol{N_{k,s}}$ in the FENE dumbbell model will be equal to the total Kuhn steps $\boldsymbol{N_k}$ of the chain in bead-rod model. Combining Equation (2.6) and (2.10), it leads to:

$$b = (N_{k,s} - 1) b_k \tag{2.11}$$

A more accurate approximation, namely Cohen Padé approximation can be given as follows (Larson,2005) :

$$F_i^{sb} = \frac{H\mathbf{Q}_i}{3}\left[\frac{3-\left(Q_i / L_S\right)^2}{1-\left(Q_i / L_S\right)^2}\right] \tag{2.12}$$

which is much closer to the *Inverse Langevin force law.*

Since DNA and many other biopolymers have helical structures along the backbones, they are bendable but difficult to experience large torsional bond rotations. Yamakawa in 1979 established the wormlike chain model for this kind of polymer. By statistical mechanics calculations, this model leads to the approximate force law, namely *Marko-Siggia spring law* as follows (Larson, 2005):

$$F_i^{sb} = \frac{k_B T}{\lambda_p}\left[\frac{1}{4}\left(1-\frac{Q_i}{L_S}\right)^{-2} - \frac{1}{4} + \frac{Q_i}{L_S}\right] = \frac{2}{3} H L_S \left[\frac{1}{4}\left(1-\frac{Q_i}{L_S}\right)^{-2} - \frac{1}{4} + \frac{Q_i}{L_S}\right] \tag{2.13}$$

where $\lambda_P$ is the persistence length and Kuhn length $\boldsymbol{b_k}$ =2$\lambda_P$ .The spring constant is the same with the coefficient before. Since we have introduced those spring force law, the comparison of difference force law is presented in Figure 2.4.

It is important to note that various force laws in the bead spring model is derived by the equilibrium statistical properties, so it would raise a subtle problem when using the bead spring model in flow or nonequilibrium situation. Therefore, it is implicitly assumed that the springs are deformed slowly enough in such cases, so that its configuration space can be fully sampled. In a sense, we assume that a local equilibrium has been created in the phase space (Doyle *et al*, 2004).

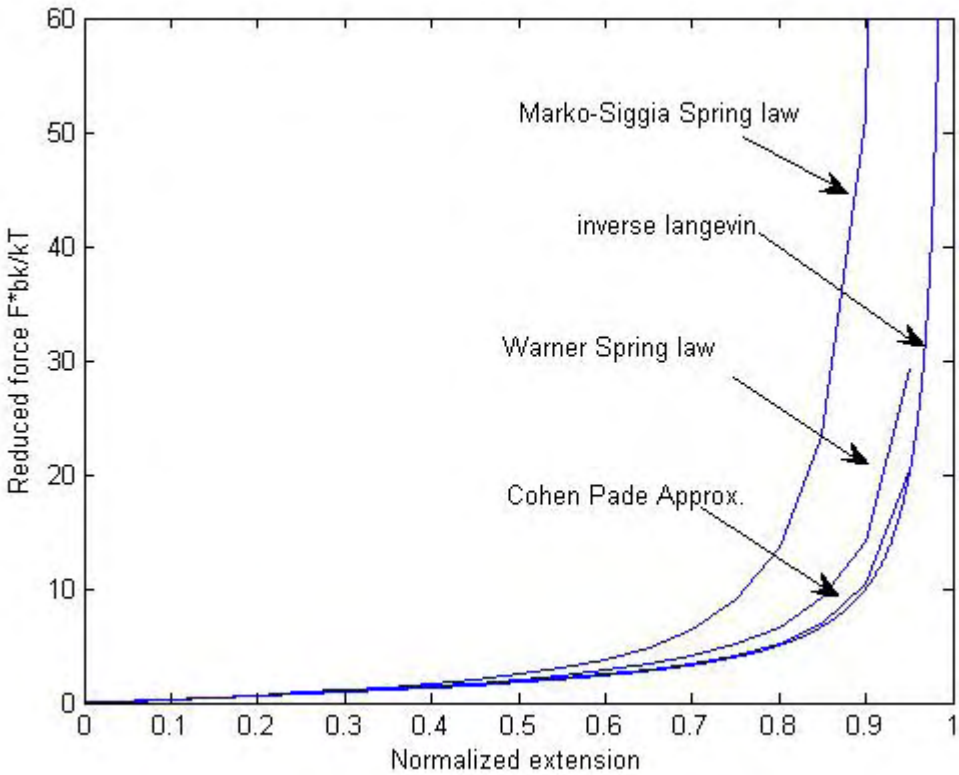


Figure 2.4 Comparison of different spring force law vs normalized molecule extension. The normalized extension is the distance between a bead and its successive bead divided by the maximum spring length.

### 2.3.3. Brownian force

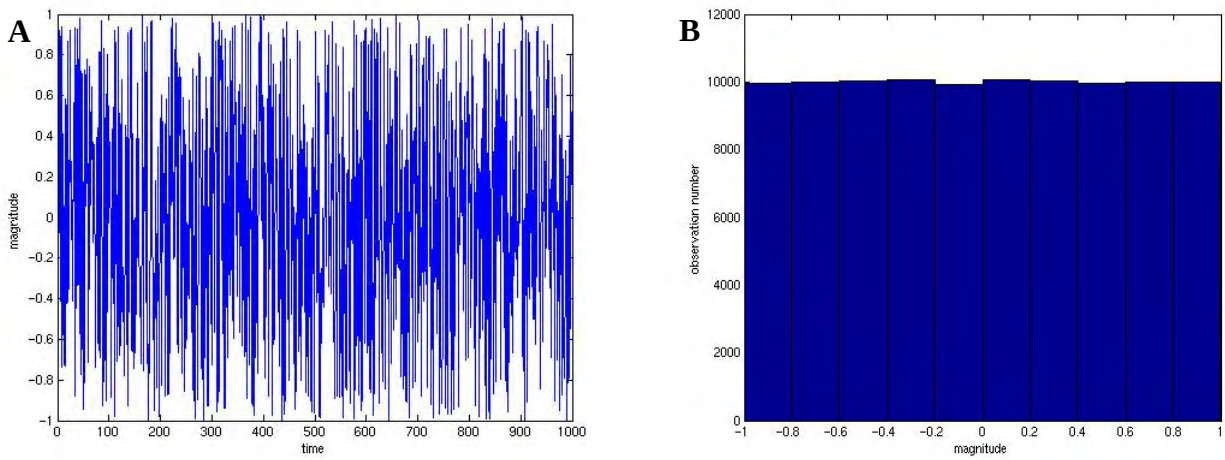


Figure 2.5 illustration of a set random number with zero mean value uniformly distributed in [-1,1] (A) and its histogram(B)

Although macromolecules have longer chain than small molecules, but they are small enough that Brownian kicks from the solvent molecules will change the positions and configurations rapidly. The characteristic time of this Brownian kicks is much smaller than the relaxation time of the polymer chain but this Brownian influence from the solvent is large enough to be treated as a kind of stochastic, random force (Schiek *et al* ,1997). Thus, the Brownian force over a time scale ***dt*** can be given by

$$\mathbf{F}^B(t) = \left( \frac{6k_B T \zeta}{dt} \right)^{1/2} \tag{2.14}$$

where **n** is a random three dimensional vector ,each component of which is random number uniformly distributed between [-1,1] as shown in Figure 2.5. The factors of $\boldsymbol{k_B T}$ and ζ come out due to the *fluctuation-dissipation theorem,* which bridges up Brownian force with drag force (Larson, 2005). A general form of the *fluctuation-dissipation theorem* in three dimensions is represented by

$$\begin{aligned} \left\langle \mathbf{F}^B(t) \right\rangle &= 0 \\ \left\langle \mathbf{F}^B(t)\mathbf{F}^B(t') \right\rangle &= A\delta\left(t - t'\right) \end{aligned} \tag{2.15}$$

Where δ ($t$-$t'$) is the delta function, when $t$ goes to $t'$ very close to 0, δ ($t$-$t'$).and **A** is a constant needed to be determined. Let's suppose a particle moves in a viscous solvent and only influenced by the random force from the solvent, the equation of motion can be expressed as following way:

$$\zeta \frac{d\mathbf{r}}{dt} = \mathbf{F}^B(t) \tag{2.16}$$

so the mean square displacement at given time t can be got from:

$$\left\langle \mathbf{r}(t)-\mathbf{r}(0)\right\rangle^2 = \frac{1}{\zeta^2}\left\langle \int_0^t F^B(t_1)dt_1 \cdot \int_0^t F^B(t_2)dt_2 \right\rangle \tag{2.17}$$

Which can be simplified to :

$$\left\langle \mathbf{r}(t)-\mathbf{r}(0)\right\rangle^2 = \frac{1}{\zeta^2}\int_0^t dt_1 \int_0^t dt_2 \left\langle F^B(t_1)\cdot F^B(t_2)\right\rangle \tag{2.18}$$

with Equation (2.15)

$$\left\langle \mathbf{r}(t)-\mathbf{r}(0)\right\rangle^2 = \frac{1}{\zeta^2}\int_0^t dt_1 \int_0^t A\delta(t_1-t_2)dt_2 = \frac{A}{\zeta^2}\int_0^t A dt_1 = \frac{A}{\zeta^2}t \tag{2.19}$$

In addition, the mean square displacement of particle is also satisfied with the Einstein equation:

$$\left\langle \mathbf{r}(t)-\mathbf{r}(0)\right\rangle^2 = 6Dt \tag{2.20}$$

Thus, it leads to the analytical form of **A:**

$$A = 6D\zeta^2 = \frac{6k_BT}{\zeta}\zeta^2 = 6k_BT\zeta \tag{2.21}$$

Therefore, the random force can be expressed as follows:

$$\begin{aligned} &\left\langle \mathbf{F}^B(t)\mathbf{F}^B(t')\right\rangle = 6k_BT\zeta\boldsymbol{\delta}(t-t') \\ &\mathbf{F}^B = \left[6k_BT\zeta\boldsymbol{\delta}(t-t')\right]^{1/2} = \left[6k_BT\zeta/dt\right]^{1/2} \end{aligned} \tag{2.22}$$

In the simulation, we will keep the time step constant and **n** is a random three dimensional vector ,each component of which is random number uniformly distributed between [-1,1]. In this way, we can not only mediate the magnitude of the random force, but also randomize the direction of the force. Therefore, the equation of motion only with Brownian force can be expressed as the following way based on Equation (2.16) and (2.22):

$$\frac{d\mathbf{r}_i}{dt} = \left(\frac{6k_BT}{\zeta dt}\right)^{1/2}\cdot\mathbf{n} = \left(\frac{6\mathbf{D}}{dt}\right)^{1/2}\cdot\mathbf{n} \tag{2.23}$$

where **D** is actually a 3x3 symmetric tensor, therefore, it should be at least a semi-definite tensor. We will discuss this issue in details in the next section.Substituting Equation (2.14) into Equation (2.1), it leads to the simplest form of *Langevin equation* for bead-spring model as follows:

$$\frac{d\mathbf{r}_i}{dt} = \kappa\cdot\mathbf{r}_i + \frac{1}{\zeta}\mathbf{F}_i^s + \left(\frac{6k_BT}{\zeta dt}\right)^{1/2}\mathbf{n}_i \tag{2.24}$$

or

$$\mathbf{r}_i(t+\Delta t) = \mathbf{r}_i(t) + \left(\kappa\cdot\mathbf{r}_i(t) + \frac{1}{\zeta}\mathbf{F}_i^s\right)dt + \left(\frac{6k_BTdt}{\zeta}\right)^{1/2}\mathbf{n}_i \tag{2.25}$$

This stochastic equation will govern the probability distribution of the configuration and position of the segments of the chain in the confined geometry. One needs to integrate this equation forward in time. The Brownian term will lead to many independent trajectories. By averaging them together, we can get the ensemble-averaged properties based on the time-evolution. Therefore, repetition of producing the independent trajectories is a time-consuming but necessary part of the simulation. After getting the time-averaged properties, it can be assumed as the steady state properties of molecules according to ergodic hypothesis (Doyle *et al*,2004).

### 2.3.4. Hydrodynamic interaction

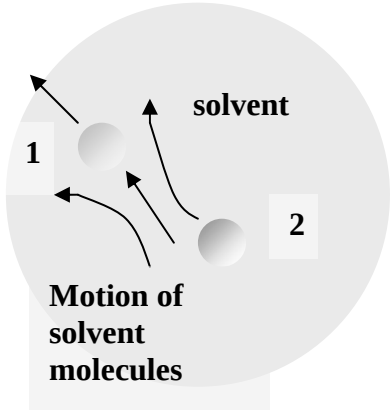


Figure 2.6 Movement of particle 1 generates the motion of solvent molecules, which eases the motion of particle 2 in the same direction.

Many practical applications in dilute polymer solutions are subject to hydrodynamic interaction (HI), such as gel permeation chromatography and the flow of biological fluids in the living systems. The important physical feature is that in a low Reynolds number flow, the hydrodynamic interaction due to a point force or boundary falls relatively slowly with the increasing distance. It becomes very important, especially if the length scale of the system is comparable to the characteristic length scale of polymers. In this section, three models with different levels to treat HI effects are introduced: ***Free-draining*** model (without HI effect), ***Bulk HI model*** (bead-bead interaction),***Full HI*** model (Bulk HI+ wall hydrodynamic effect)

**I. Hydrodynamic interaction in a free solution (Bulk HI model)**

The concept of hydrodynamic interaction is the motion of a segment will produce a disturbance to the velocity field in the flow due to the point force at this point, which will influence the motion of the entire chain accordingly shown in Figure 2.6. If the force is weak enough, the disturbance created by this force $\mathbf{F}_j^{drag}$ at $\mathbf{r}_j$ to the velocity

field at position $\mathbf{r}_i$ of bead $i$ can be approximated by a linear function of the hydrodynamic drag force $-\mathbf{F}_j^{drag}$ as follows:

$$\mathbf{v}_i' = -\mathbf{\Omega}_{ij} \cdot \mathbf{F}_j^{drag} = \mathbf{\Omega}_{ij} \cdot (\mathbf{F}_j^s + \mathbf{F}_j^B) \tag{2.26}$$

where $\mathbf{\Omega}_{ij}$ is the *hydrodynamic interaction tensor* or *mobility tensor*, which is the function of the displacement of $\mathbf{r}_i$-$\mathbf{r}_j$ between the bead $i$ and $j$. If we incorporate this effect into *Largevin equation*, the following stochastic equation can be get:

$$\frac{d\mathbf{r}_i}{dt} = \kappa \cdot \mathbf{r}_i + \sum_{j=1}^{N} \frac{\partial}{\partial \mathbf{r}_j} \cdot \mathbf{D}_{ij} + \sum_{j=1}^{N} \frac{\mathbf{D}_{ij}}{k_B T} \cdot \mathbf{F}_j^s + \left(\frac{6}{dt}\right)^{1/2} \sum_{j=1}^{N} \mathbf{B}_{ij} \cdot \mathbf{n}_j \tag{2.27}$$

where $\mathbf{D}_{ij}$ is *the diffusion tensor* and tensor $\mathbf{B}_{ij}$ can be represented as follows according to Eq (2.23):

$$\mathbf{D}_{ij} = \sum_{l=1}^{N} \mathbf{B}_{il} \cdot \mathbf{B}_{lj} \tag{2.28}$$

If Equation (2.28) is statisfied, a *Cholesky decompostion* can made between $\mathbf{D}_{ij}$ and $\mathbf{B}_{ij}$ as follows [1](Hsieh *et al*, 2005):

$$\begin{aligned} B_{\alpha\alpha} &= \left( D_{\alpha\alpha} - \sum_{\gamma=1}^{\alpha-1} B_{\alpha\gamma}^2 \right)^{1/2} \\ B_{\alpha\beta} &= \frac{\left( D_{\alpha\alpha} - \sum_{\gamma=1}^{\beta-1} B_{\alpha\gamma} B_{\beta\gamma} \right)^{1/2}}{B_{\beta\beta}}, \ \alpha > \beta \\ B_{\alpha\beta} &= 0, \ \alpha < \beta \end{aligned} \tag{2.29}$$

Here $\alpha, \beta, \gamma$ are the row and column positions of the elements in the tensor **D** and **B.** Here the diffusion tensors are supposed to be symmetric, positive-definite. However, this may be not the case during the simulation. This problem has its physical origin: on one hand, we assumed point particles or beads with zero radius during the derivation of *Oseen-Burgers* tensor; on the other hand, when calculating the frication coefficient for the given solvent, we implicitly assumed a bead radius $a$ given by Stokes law $\zeta = 6\pi\eta a$. Hence, *Oseen-Burgers* tensor only can lead to realistic results for the bead separation comparable to $2a$ (Ottinger *et al*, 1995)[2].Therefore, an alternative approach- *Chebyshev polynomial approximation* is introduced in the appendix A-2.

[1] Please refer Cholesky decomposition in appendix for details
[2] Please refer this part Appendix: A-3

For the diffusion tensor **D,** which is 3×3 block components of 3N×3N diffusion tensor, there are several forms in use. Mathematically, a Green function represents the influence of a bead being moved through the solution. The simplest one is the *Oseen-Burgers tensor* $\mathbf{\Omega}^{OB}$, which assumes that the beads can be regarded as point sources of drag in the solvent:

$$\mathbf{D}_{ij} = k_B T\left(\frac{1}{6\pi\eta_s a}\mathbf{I}\delta_{ij} + \mathbf{\Omega}_{ij}\right) \tag{2.30}$$

$$\mathbf{\Omega}_{ij} = (1-\delta_{ij})\mathbf{\Omega}_{ij}^{OB} \tag{2.31}$$

$$\mathbf{\Omega}_{ij}^{OB} = \frac{1}{8\pi\eta_S\left|\mathbf{r}_i - \mathbf{r}_j\right|}\left[\mathbf{I} + \frac{(\mathbf{r}_i - \mathbf{r}_j)(\mathbf{r}_i - \mathbf{r}_j)}{\left|\mathbf{r}_i - \mathbf{r}_j\right|^2}\right] \tag{2.32}$$

Where **I** is a unit tensor, $\delta_{ij}$ is the Kronecker delata and $\mathbf{r}_j - \mathbf{r}_i$ is the separation vector between the *i*th and *j*th beads. However, *Oseen-Burgers tensor* is not suitable for Brownian dynamics simulation, because it will become nonpositive when $\mathbf{r}_j - \mathbf{r}_i$ is comparable to or less than the bead radius as we mentioned before. Here $\mathbf{r}_i$ is the observation point to see the velocity perturbation due to the point force at $\mathbf{r}_j$ where $\mathbf{r}_j$ is the source point. Therefore, the perturbation to the flow field at any point is the sum of the perturbation from each bead around this point shown in Figure 2.7

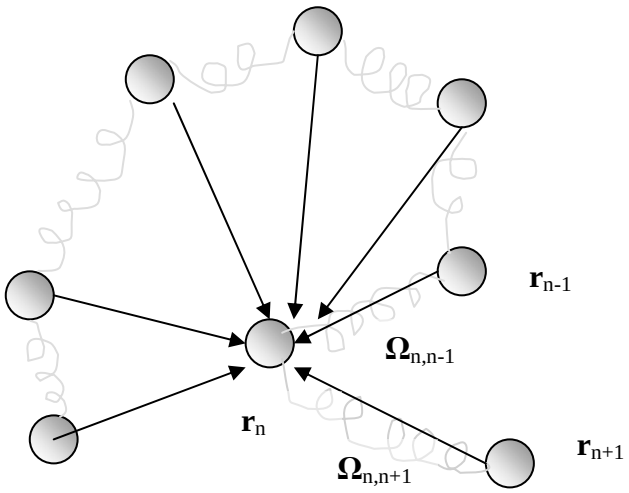


Figure 2.7 Motion of the *n*th bead is affected by the surrounding beads through hydrodynamic interaction

In Brownian dynamics simulation, the *Rotne-Prager-Yamakawa (RPY) Tensor* $\mathbf{\Omega}^{RPY}$ is always used to replace the *Oseen-Burgers tensor* (Larson, 2005):

$$\mathbf{\Omega}_{ij}^{RPY} = \frac{1}{8\pi\eta_S \left|\mathbf{r}_i - \mathbf{r}_j\right|}\left[C_1\mathbf{I} + C_2\frac{(\mathbf{r}_i - \mathbf{r}_j)(\mathbf{r}_i - \mathbf{r}_j)}{\left|\mathbf{r}_i - \mathbf{r}_j\right|^2}\right], \quad for \quad \left|\mathbf{r}_i - \mathbf{r}_j\right| \geq 2a \quad (2.33)$$

$$\mathbf{\Omega}_{ij}^{RPY} = \frac{1}{6\pi\eta_S a}\left[C_1'\mathbf{I} + C_2'\frac{(\mathbf{r}_i - \mathbf{r}_j)(\mathbf{r}_i - \mathbf{r}_j)}{\left|\mathbf{r}_i - \mathbf{r}_j\right|^2}\right], \quad for \quad \left|\mathbf{r}_i - \mathbf{r}_j\right| < 2a \quad (2.34)$$

$$C_1 = 1 + \frac{2a^2}{3\left|\mathbf{r} - \mathbf{r}_j\right|^2}$$
$$C_2 = 1 - \frac{2a^2}{\left|\mathbf{r} - \mathbf{r}_j\right|^2} \quad (2.35)$$

$$C_1' = 1 - \frac{9\left|\mathbf{r} - \mathbf{r}_j\right|}{32a}$$
$$C_2' = \frac{3\left|\mathbf{r} - \mathbf{r}_j\right|}{32a} \quad (2.36)$$

Here the first expression indicates the beads are well separated and the second means the beads have some overlaps with each other. However, it seems that the second case doesn't happen frequently in the simulation due to the *excluded volume effect*.

For *Oseen* tensor and *RPY* tensor, $\mathbf{\Omega}_{ij}$=0 for *i*=*j*, and $\partial/\partial\mathbf{r}_j \cdot \mathbf{\Omega}_{ij} = 0$ for all *i*, *j* in the free solution, things will be different in the confined geometry. Those modifications will be discussed in the next section.

The strength of HI effects between beads can be evaluated by the following parameters:

$$h^* = \frac{\zeta}{\eta_s}\left(\frac{H}{36\pi^3 k_B T}\right)^{1/2} = \frac{\zeta}{\left(12\pi^3\right)^{1/2} R_s\eta_s} = \sqrt{\frac{3}{\pi}}\frac{\zeta}{R_s} \quad (2.37)$$

where $H = 3k_B T / R_S^2$ is the elastic constant of the spring and $R_s = b_k\sqrt{N_{K,S}}$ is the root-mean-square end-to-end vector of a spring at equilibrium. Based on this definition, Equation (2.33)-(2.34) can be rewritten as follows:

$$\mathbf{D}_{ii} = \frac{k_B T}{6\pi\eta_S a}\mathbf{I} \quad (2.38)$$

$$\mathbf{D}_{ij}^{RPY} = \frac{k_B T}{8\pi\eta_S \left|\mathbf{r}_i - \mathbf{r}_j\right|} \frac{h^* \sqrt{\frac{\pi}{3}} R_s}{a} \left[ C_1 \mathbf{I} + C_2 \frac{(\mathbf{r}_i - \mathbf{r}_j)(\mathbf{r}_i - \mathbf{r}_j)}{\left|\mathbf{r}_i - \mathbf{r}_j\right|^2} \right], \quad for \quad \left|\mathbf{r}_i - \mathbf{r}_j\right| \geq 2a \quad (2.39)$$

$$\mathbf{D}_{ij}^{RPY} = \frac{k_B T}{6\pi\eta_S a} \frac{h^* \sqrt{\frac{\pi}{3}} R_s}{a} \left[ C_1' \mathbf{I} + C_2' \frac{(\mathbf{r}_i - \mathbf{r}_j)(\mathbf{r}_i - \mathbf{r}_j)}{\left|\mathbf{r}_i - \mathbf{r}_j\right|^2} \right], \quad for \quad \left|\mathbf{r}_i - \mathbf{r}_j\right| < 2a \quad (2.40)$$

It can be seen that the HI effect will be different due to the different choices of bead radius, which will make simulation result far from the experimental data. Therefore, when the simulation is carried out, the hydrodynamic interaction parameter could be another parameter to optimise.

**II. Hydrodynamic interaction in a confined geometry (Full HI model)**

Traditionally, people treat the HI effect to the level of bead-bead(which is named ***Bulk HI*** model in the above section), but the effect between the wall and bead comes into play in the confined geometry, especially when we have lowered down to a length scale comparable to the radius of gyration of the polymer. How to treat the hydrodynamic interaction and into which level? It is a critical point for us to explain dynamics of the biomolecules in the microchannel, because the Green function for hydrodynamic interaction is highly dependent on the geometry of the channel. In addition, the analytical solution only exists in few special cases, which are needed to be highly symmetric geometry. Here we introduced the method proposed by Jendrejack *et al* (2004) to evaluate the HI effect on a more accurate level, which is called ***Full HI*** model.

Usually, the Green function for the Stokes flow in a general geometry can be expressed as follows:

$$\mathbf{\Omega} = \mathbf{\Omega}^{OB} + \mathbf{\Omega}^{W} \quad (2.41)$$

Where $\mathbf{\Omega}^{OB}$ is the *Oseen* tensor or the Green function for the free solution. $\mathbf{\Omega}^{W}$ is the correction term which is responsible for the no-slip constraint at the wall. The velocity perturbation due to the point force $\mathbf{f}(\mathbf{x}_j)$ at source point $\mathbf{x_j}$ can be given as follows:

$$\begin{aligned} \mathbf{v}'(\mathbf{x}, \mathbf{x}_j) &= \mathbf{v}'_{OB}(\mathbf{x} - \mathbf{x}_j) + \mathbf{v}'_{W}(\mathbf{x} - \mathbf{x}_j) \\ &= \left[ \Omega^{OB}(\mathbf{x} - \mathbf{x}_j) + \Omega^{W}(\mathbf{x}, \mathbf{x}_j) \right] \cdot \mathbf{f}(\mathbf{x}_j) \end{aligned} \quad (2.42)$$

Since the Stokes equations are linear and homogeneous, the velocity produced by different forces and boundaries at the different points in the liquids are additive. Therefore, the velocity perturbation $\mathbf{v}'_w\left(\mathbf{x}_i,\mathbf{x}_j\right)$ can be get by the solving the classical incompressible Navier- Stokes flow problem:

$$-\nabla p+\eta_s\nabla^2\mathbf{v}'_W=0,\ \nabla\cdot\mathbf{v}'_W=0 \tag{2.43}$$

With the boundary condition:

$$\mathbf{v}'_{OB}+\mathbf{v}'_W=0 \quad \text{at the wall} \tag{2.44}$$

Thus, the boundary condition becomes $\mathbf{v}'_W=-\mathbf{v}'_{OB}$, which means $\mathbf{\Omega}^w(\mathbf{x}_i,\mathbf{x}_j)=-\mathbf{\Omega}^{OB}(\mathbf{x}_i-\mathbf{x}_j)$. Because we always use the *RPY tensor* instead of the *Oseen Tensor*, we should substitute Equation (2.33) into the boundary condition, then we would find the explicit velocity for the boundary.

Using this boundary condition and point force $f_1$ acting on the direction 1, this Stokes flow problem can be solved by finite element method (Jendrejack *et al*, 2004). Here we used the FEMLAB finite element software package(Comosol) to solve this classical fluid dynamic problem. After we get the velocity perturbation for the wall, the first column of the $\mathbf{\Omega}^w(\mathbf{x}_i,\mathbf{x}_j)$ could be given as the following way:

$$\begin{pmatrix}\Omega^W_{11}\\ \Omega^W_{21}\\ \Omega^W_{31}\end{pmatrix}=\frac{1}{f_1}\mathbf{v}'_W \tag{2.45}$$

Where *1,2,3* represents the three directions. The second and third column of the $\mathbf{\Omega}^w(\mathbf{x}_i,\mathbf{x}_j)$ can be got in the similar way by applying the point forces in the direction of *2* and *3*, respectively. Since we have the Green function $\mathbf{\Omega}^w(\mathbf{r}_i,\mathbf{r}_j)$ for wall, the total Green function can be expressed as following way:

$$\mathbf{\Omega}_{ij}=(1-\delta_{ij})\mathbf{\Omega}^{OB}(\mathbf{r}_i-\mathbf{r}_j)+\mathbf{\Omega}^W(\mathbf{r}_i,\mathbf{r}_j) \tag{2.46}$$

Compared to the flow of the free solution, $\mathbf{\Omega}_{ij}$ is nonzero and $\partial/\partial\mathbf{r}_j\cdot\mathbf{\Omega}_{ij}\neq 0$ for *i=j*, which will lead to a nonzero drift term in Equation (2.27).

The Green's function is evaluated on the grids before the Brownian simulation, which means we will make those grid data into a lookup table for a given geometry. During the simulation, Green's function and its divergence will be evaluated by the finite interpolation (please refer the detail in Appendix A-2).

From equation (2.32) and (2.33), it can be seen that the hydrodynamic interaction between beads decays relatively fast as $1/\boldsymbol{r}^2$ .For a particle close to the wall, it falls off with the distance to the point force as $1/\boldsymbol{r}$ (Jendrejack *et al*, 2004)**,** which means even the beads are far from the wall, the effect from the wall still exists beyond the range of excluded volume interaction from we will introduced in section 2.3.6. It indicates that hydrodynamic coupling to bounding surfaces could influence molecule's motions to a greater extent and over a longer range (Dufresne *et al*, 2000).

*Appendix:*

***Cholesky Decomposition***

Suppose we have a **symmetric** and **positive definite matrix**[3] **or semi-positive definite matirx**. It can be efficiently decomposed into lower and upper triangular matrix as follows:

$$\begin{pmatrix} a_{11} & \cdots & a_{1n} \\ \vdots & \ddots & \vdots \\ a_{m1} & \cdots & a_{mn} \end{pmatrix} = \begin{pmatrix} l_{11} & \cdots & 0 \\ \vdots & \ddots & \vdots \\ l_{n1} & \cdots & l_{nn} \end{pmatrix} \begin{pmatrix} l_{11} & \cdots & l_{n1} \\ \vdots & \ddots & \vdots \\ 0 & \cdots & l_{nn} \end{pmatrix}$$

the elements of the upper and lower triangular matrix can be get as follows:

$$\begin{aligned} a_{11} &= l_{11}^2 \rightarrow l_{11} = \sqrt{a_{11}} \\ a_{21} &= l_{21} l_{11} \rightarrow l_{21} = a_{21} / l_{11}, \cdots, l_{n1} = a_{n1} / l_{11} \\ a_{22} &= l_{21}^2 + l_{22}^2 \rightarrow l_{22} = \left( a_{22} - l_{21}^2 \right)^{1/2} \end{aligned}$$

we can also give a general form of the solution:

$$l_{ii} = \left( a_{ii} - \sum_{k=1}^{i-1} l_{ik}^2 \right)^{1/2} \tag{2.47}$$

$$l_{ij} = \left( a_{ij} - \sum_{k=1}^{j-1} l_{jk} l_{ik} \right) / l_{ii} \tag{2.48}$$

[3] A symmetric matrix is positive definite if all the eigenvalues are positive.

### 2.3.5. Excluded Volume Effect

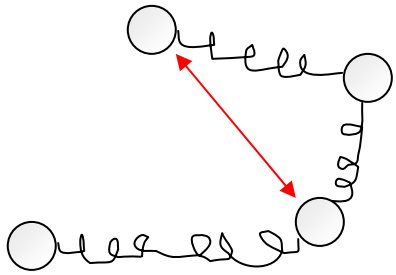

Figure 2.8 illustration of exclude volume interaction in a polymer chain

In order to include the solvent effects, the excluded volume effect should be considered in Equation (2.27). Different solvents will have different impacts on the properties of the dilute solutions of polymers. Those effects can be investigated qualitatively in the following way (Jendrejack *et al*, 2004).

In good solvents, the chain tends to swell since it prefers to be surrounded by the solvents. Consequently, solvent effects could be achieved by the repulsive bead-bead (two-sub molecules) potential. Each submolecule (segment) is considered to be deal with a Gaussian probability distribution. Considering the repulsive energy due to the overlap of two Gaussian coils (without deformation), the excluded volume potential can be expressed as follows (Larson, 2005, Jendrejack *et al*, 2004):

$$U_{ij}^{EV} = \frac{1}{2} v k_B T N_{K,s}^2 \left(\frac{9}{2\pi R_s^2}\right)^{\frac{3}{2}} \exp\left(-\frac{9\left|r_j - r_i\right|^2}{2R_s^2}\right) \tag{2.49}$$

where $R_s^2 = N_{k,s} b_k^2$ is the mean-square end-to-end distance of a spring with $N_{k,s}$ Kuhn segments and ν is the energy constant. Since we know the potential, the repulsive force on bead *i* from bead *j* can be written as the gradient of the potential:

$$\mathbf{F}_{ji} = -\nabla_{\mathbf{r}_i} U(r_i - r_j) = -\frac{\partial}{\partial x_i} U(\left|r_i - r_j\right|)\boldsymbol{\delta}_x - \frac{\partial}{\partial y_i} U(\left|r_i - r_j\right|)\boldsymbol{\delta}_y - \frac{\partial}{\partial z_i} U(\left|r_i - r_j\right|)\boldsymbol{\delta} z \tag{2.50}$$

Where $\left|r_i - r_j\right| = \sqrt{\left(x_i - x_j\right)^2 + \left(y_i - y_j\right)^2 + \left(z_i - z_j\right)^2}$ and $\boldsymbol{\delta}$ is unit vector.Based on the chain rule in differential equation:

$$-\frac{\partial}{\partial x_i} U(\left|r_i - r_j\right|) = -\frac{\partial}{\partial \left|r_i - r_j\right|} U(\left|r_i - r_j\right|) \frac{x_i - x_j}{\left|r_i - r_j\right|} \tag{2.51}$$

the repulsive force can be rewritten as follows:

$$\mathbf{F}_{ji} = -\frac{\partial}{\partial \left|r_i - r_j\right|} U(\left|r_i - r_j\right|) \frac{\mathbf{r}_i - \mathbf{r}_j}{\left|r_i - r_j\right|} \tag{2.52}$$

Some other potential, such as Lennard-Jones, soft potential are also commonly used in the Brownian simulation. However, it is not obvious how the parameters in those models adjust with the molecule discretization $N_{k,s.}$ That's the reason why they developed such kind of potential (Jendrejack, 2003).

In the theta solvents, polymer molecule can't distinguish the polymer and solvent at larger length scale, which means polymers can't feel 'itself'. The theta effects can be simply realized by removing the potential. In a bad solvent, polymer tends to contract, which means polymer prefer to get together, which can be achieved by adding an attractive bead-bead potential.

### 2.3.6. Physical confinement

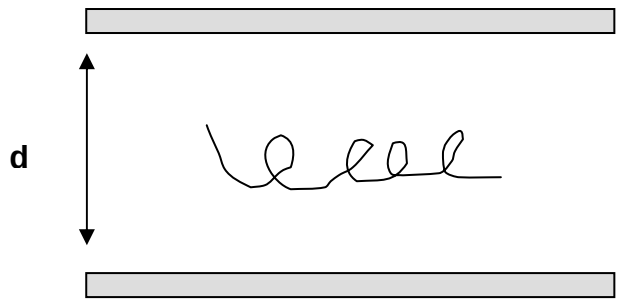


Figure 2.9 illustration of polymer chain confined in a slit with a gap width of d

To realize the physical boundary condition due to confined geometry as shown in Figure 2.9, a bead-wall repulsive potential has been considered as follows (Jendrejack *et al*, 2004):

$$\begin{aligned} U_i^{wall} &= \frac{A_{wall}}{3b_k\delta_{wall}^2}(h-\delta_{wall})^3 \quad , for \quad h<\delta_{wall} \\ &= 0 \quad . for \quad h \geq \delta_{wall} \end{aligned} \tag{2.53}$$

So the repulsive force for bead *i* from the wall can be given as follows:

$$\begin{aligned} F_i^{wall} &= -\frac{\partial}{\partial h}U_i^{wall} = -\frac{A_{wall}}{b_k\delta_{wall}^2}(h-\delta_{wall})^2 \quad , for \quad h<\delta_{wall} \\ &= 0 \quad . for \quad h \geq \delta_{wall} \end{aligned} \tag{2.54}$$

Where *h* is the perpendicular distance between bead *i* and the wall. $\delta_{wall}$ is the cut-off distance for the molecule to feel the repulsive force from the wall and $A_{\text{wall}}$ is the repulsive energy constant. Here we use $A_{\text{wall}}$ =25 $k_BT$ and $\delta_{wall}$ =0.236 *um*. Since we want to guarantee that no beads can penetrate the geometry, we assume the parallel

walls are perfect elastic. During the process, if bead is the outside the wall, the wall can reflect the bead back into the same depth without affecting the bead displacement in the direction parallel to the wall. From above statement, it can be seen that the repulsive force from the wall is a short-range influence (the effective region is 0.236 *um*) compared with the long-range hydrodynamic interaction.

## Reference

Doyle, P.S. and Underhill, P.T., *Brownian dynamics simulations of polymers and soft matter*, In S. Yip, editor, *Handbook of Materials Modeling, volume I.* Kluwer Academic Publishers, 2004.

J S.Hur,E S G.Shaqfeh,R G.Larson *Brownian dynamics simulations of DNA molecules in shear flow*, J.Rheol.44,713-742,2000.

R.G.Larson, *The rheology of dilute solutions of flexible polymers: Progress and problem*s, J.Rheol.49 (1), 1-70, 2005

Ottinger,H.C., *Stochastic Process in Polymeric Liquids*, Springer,Berlin,1995

C.C.Hsieh, L.Li,R. G.Larson, *Modeling hydrodynamic interaction in Brownian dynamics: simulations of extensional flows of dilute solutions of DNA and polystyrene*', J.Non-Newtonian Fluid Mech.113,147-191,2003

R.M.Jendrejack, D.C.Schwartz, J.J.de Pablo, M.D.Graham, *Shear-induced migration in flowing polymer solutions: simulation of long-chain DNA in microchannels*, J.Chem Phys,120,2513-2529,2004

R.M.Jendrejack, *Multiscale Simulations of Dilute-Solution Macromolecular Dynamics in Macroscopic and Microscopic Geometries*, Doctoral dissertation, 2003

COMSOL AB Sweden, FEMLAB 3.0,http://www.femlab.com

E.R. Dufresne, T.M. Squires, M.P.Brenner, *Hydrodynamic Coupling of Two Brownian Spheres to a Planar Surface*, Phys. Rev. Lett. 85, 3317,2000

R.L. Schiek, E.S.G.Shaqfeh, *Cross-stream line migration of slender Brownian fibres in plane Poiseuille flow*, J.Fluid Mech., 332, 1997

# Chapter 3 Numerical Scheme

*Since the starting point — the stochastic differential equation has been developed in the last chapter, we must integrate the equation forward in time in order to get the trajectories of the molecule. Two most common integration schemes for FENE dumbbell and Bead-spring model are introduced in this chapter.*

## 3.1 Simulation scheme[4]

### 3.1.1. Explicit Euler Scheme

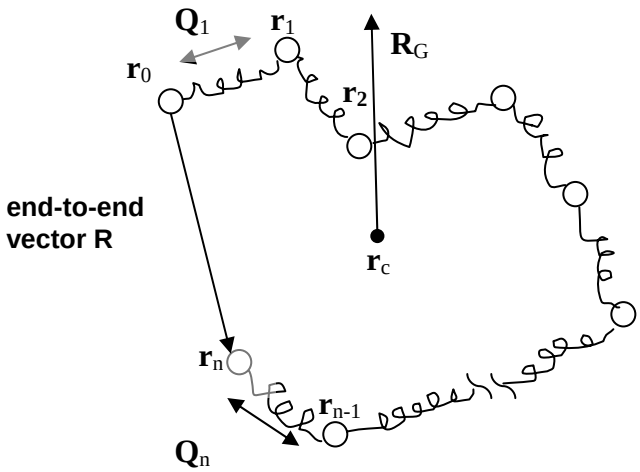


Figure 3.1 illustration of the position vector $\mathbf{r}_i$, end-to-end vector $\mathbf{R}$,center of mass $\mathbf{r}_c$, radius of gyration $\mathbf{R}_G$ in bead-spring model

The governing equation is given as Eq(2.25) as follows:

$$\mathbf{r}_i(t+\Delta t)=\mathbf{r}_i(t)+\left(\boldsymbol{\kappa}\cdot\mathbf{r}_i(t)+\frac{1}{\zeta}\mathbf{F}_i^s\right)dt+\left(\frac{6k_BTdt}{\zeta}\right)^{1/2}\mathbf{n}_i$$

To integrate this equation, the simplest scheme is the explicit Euler scheme. By marching the time, we can update the position of beads. In addition, the trajectories of the connector vector $\mathbf{Q}_i$ (t), center of mass $\mathbf{r}_c$(t) and the radius of gyration $\boldsymbol{R}_G$(t) shown in Figure 3.1 can be given as follows:

$$\mathbf{Q}_i=\mathbf{r}_{i+1}-\mathbf{r}_{i+1} \tag{3.1}$$

$$\mathbf{r}_c=\frac{1}{N}\sum_{i=1}^{N}\mathbf{r}_i \tag{3.2}$$

$$\mathbf{R}_G=\frac{1}{N}\sum_{i=1}^{N}(\mathbf{r}_i-\mathbf{r}_c)^2 \tag{3.3}$$

Substituting Equation (2.4) into Equation (2.25) leads to:

[4] To illustrate the scheme, Free draining model is taken as the example for simplicity

$$\mathbf{r}_i(t+\Delta t)=\begin{cases}\mathbf{r}_1(t)+\left(\boldsymbol{\kappa}\cdot\mathbf{r}_i(t)+\frac{1}{\zeta}\mathbf{F}_1^s\right)dt+\left(\frac{6k_BTdt}{\zeta}\right)^{1/2}\mathbf{n}_i, i=1\\ \mathbf{r}_i(t)+\left(\boldsymbol{\kappa}\cdot\mathbf{r}_i(t)+\frac{1}{\zeta}(\mathbf{F}_i^{sb}-\mathbf{F}_{i-1}^{sb})\right)dt+\left(\frac{6k_BTdt}{\zeta}\right)^{1/2}\mathbf{n}_i, 1<i<N\\ \mathbf{r}_N(t)+\left(\boldsymbol{\kappa}\cdot\mathbf{r}_N(t)-\frac{1}{\zeta}\mathbf{F}_{N-1}^{sb}\right)dt+\left(\frac{6k_BTdt}{\zeta}\right)^{1/2}\mathbf{n}_i, i=N\end{cases} \tag{3.4}$$

If we take FENE dumbbell model for example, equation (3.4) for two beads becomes

$$\mathbf{r}_1(t+\Delta t)=\mathbf{r}_1(t)+\left(\boldsymbol{\kappa}\cdot\mathbf{r}_1(t)+\frac{1}{\zeta}\frac{H\mathbf{Q}_1}{1-\left(\frac{Q_1}{L_s}\right)^2}\right)dt+\left(\frac{6k_BTdt}{\zeta}\right)^{1/2}\mathbf{n}_1, i=1 \tag{3.5}$$

$$\mathbf{r}_2(t+\Delta t)=\mathbf{r}_2(t)+\left(\boldsymbol{\kappa}\cdot\mathbf{r}_2(t)-\frac{1}{\zeta}\frac{H\mathbf{Q}_1}{1-\left(\frac{Q_1}{L_s}\right)^2}\right)dt+\left(\frac{6k_BTdt}{\zeta}\right)^{1/2}\mathbf{n}_2, i=1 \tag{3.6}$$

Those equations can be decoupled into three components ***x,y,z***, take Equation (3.5) in simple shear flow for example:

$$\begin{cases}r_{1,x}(t+\Delta t)=r_{1,x}(t)+\left(\dot{\gamma}r_{1,x}(t)+\frac{1}{\zeta}\frac{HQ_{1,x}}{1-\left(\frac{Q_1}{L_s}\right)^2}\right)dt+\left(\frac{6k_BTdt}{\zeta}\right)^{1/2}n_{1,x}\\ r_{1,y}(t+\Delta t)=r_{1,y}(t)+\frac{1}{\zeta}\frac{HQ_{1,y}}{1-\left(\frac{Q_1}{L_s}\right)^2}dt+\left(\frac{6k_BTdt}{\zeta}\right)^{1/2}n_{1,y}\\ r_{1,z}(t+\Delta t)=r_{1,z}(t)+\frac{1}{\zeta}\frac{HQ_{1,z}}{1-\left(\frac{Q_1}{L_s}\right)^2}dt+\left(\frac{6k_BTdt}{\zeta}\right)^{1/2}n_{1,z}\end{cases} \tag{3.7}$$

By updating the time, we can update the bead position in three directions, and then collect the molecular configurations by Equation (3.1)-(3.3).

However, we have to choose the small time step t $=10^{-4}$-$10^{-5}$s for explicit Euler method (we will discuss the choice of parameters later). If the time step is larger than that, the maximum extension length would be larger than the contour length of the

chain, which is unphysical. Since the use of random variables in the simulation and a finite number of trajectories in the ensemble, there will be intrinsic statistical noise to the method. According to the theory of statistics, the magnitude of this error is proportional to $N^{-1/2}_T$ where $N_T$ is the number if they are independent trajectories. (Doyle *et al* 2004)

### 3.1.2. Predictor-Corrector Method

Due to the weak convergence of the *Euler* scheme and its relatively high error, Öttinger (1995) developed a more efficient second-order algorithm developed by updating the dumbbell trajectories of connector vector first. If we take differences between Equation (2.25) with successive indices *i* for FENE dumbbell model, we can get the equations as follows:

***predictor:***

$$\bar{\mathbf{Q}}_1(t+\Delta t) = \mathbf{Q}_1(t) + \left( \boldsymbol{\kappa}\cdot\mathbf{Q}_1(t) - \frac{2}{\zeta}\frac{H\mathbf{Q}_1}{1-\left(\frac{\mathrm{Q}_1}{L_s}\right)^2} \right) dt + \left(\frac{6k_B T dt}{\zeta}\right)^{1/2} (\mathbf{n}_1 - \mathbf{n}_2) \quad (3.8)$$

Where $\bar{\mathbf{Q}}_1(t+\Delta t)$ is the predictor , here we use the value from *explicit Euler method* as the predictor.

***corrector:***

$$\mathbf{Q}_1(t+\Delta t) = \mathbf{Q}_1(t) + 0.5\left( \boldsymbol{\kappa}\cdot[\mathbf{Q}_1(t)+\bar{\mathbf{Q}}_1(t+\Delta t)] - \frac{2H}{\zeta}\left[\frac{\mathbf{Q}_1}{1-\left(\frac{\mathrm{Q}_1}{L_s}\right)^2} + \frac{\bar{\mathbf{Q}}_1(t+\Delta t)}{1-\left(\frac{\bar{\mathbf{Q}}_1(t+\Delta t)}{L_s}\right)^2}\right] \right) dt$$
$$+\left(\frac{6k_B T dt}{\zeta}\right)^{1/2} (\mathbf{n}_1 - \mathbf{n}_2)$$

(3.9)

Equation (3.9) also can be decoupled into three directions in Cartesian coordinates. If we take the combination of Equation (2.25) and successive index *i*, then time evolution of the center of mass can be get:

$$\mathbf{r}_c(t+\Delta t) = \mathbf{r}_c(t) + \boldsymbol{\kappa}\cdot\mathbf{r}_c(t)dt + \left(\frac{6k_B T dt}{\xi}\right)^{1/2} \frac{1}{2}\sum_{i=1}^{2}\mathbf{n}_i, \quad (3.10)$$

Based on Equation(3.9) and Equation(3.10), we can get the trajectories of the internal connectors $\mathbf{Q}_i$(t) and the center of mass position vector $\mathbf{r}_c$, because we know the relationships between $\mathbf{Q}_i$(t), $\mathbf{r}_c$, and $\mathbf{r}_i$(t) as follows:

$$\mathbf{r}_1(t) = \mathbf{r}_c(t) - \sum_{j=1}^{N} \frac{N-j}{N} \mathbf{Q}_j(t) = \mathbf{r}_c(t) - \frac{1}{2}\mathbf{Q}_j(t) \tag{3.11}$$

$$\mathbf{r}_i(t) = \mathbf{r}_1(t) + \sum_{j=1}^{i-1} \mathbf{Q}_j(t) = \mathbf{r}_1(t) + \mathbf{Q}_j(t) \tag{3.12}$$

Compared to *explicit Euler method*, predictor-corrector method don't have good performance on increasing speed on each step, but it saves computing time by increasing the step size, since this method can prevent the molecular extension beyond the maximal length efficiently.

## 3.2 Dimensionless parameter

For *FENE dumbbell* model, we scale the length with $\sqrt{k_B T / H}$ and the time with $\tau_F$, where $\tau_F$ is the characteristic time of FENE dumbbell and we assume it is the relaxation time of molecular stretch (defined in chapter 4). In order to characterize the flow strength, the *Weissenberg number* is defined as follows, which indicates the chain relaxation time scale relative to the characteristic flow time scale:

$$Wi = \dot{\gamma}\tau_F \tag{3.13}$$

where $\dot{\gamma}$ is shear rate.In Bead-spring model, the characteristic time and length is the relaxation time τ of molecular stretch (defined in chapter 4) and Kuhn length $\boldsymbol{b_k}$ respectively. Therefore, Weissenberg number for Bead-spring model can be defined as follows:

$$Wi = \dot{\gamma}\tau \tag{3.14}$$

## 3.3 Pseudo random number generator

In our simulation, it is needed to generate a large number of random numbers, which is the stochastic origin of the equation. At first, we used the build-in function *random_number* ( ) in FORTRAN. When we tried to optimize the code to reduce computational time, we found the build-in function almost uses most of the time,

which is very time-expensive. Therefore, it would be a good idea to code the random number generator by ourselves.

System-supplied random number generators are always *linear congruential generators*, which generate a sequence of integers $I_1, I_2, I_3, \ldots$, each between 0 and m-1(a large number) by the recurrence relation as follows:

$$I_{j+1} = aI_j + c \tag{3.15}$$

then get the *modulus* based on *m* as follows:

$$v = \mathrm{mod}(I_{j+1}, m) \tag{3.16}$$

then divided by *m*

$$U = v / m \tag{3.17}$$

Where *a* and *c* are positive integers called the *multiplier* and *increment* respectively. If *m*, *a*, *c* are properly chosen and repeating this recurrence relation over a period, all possible numbers *U* between 0 and 1 will occur at some point.

Here we will take random number generator proposed by Lewis, Goodman and Miller in 1969, which has passed almost all the theoretical tests in the past years (Press *et al* ,1992). Here are their parameters for the random number generator:

$$a = 7^5 = 16807 \quad c = 0 \qquad m = 2^{21} - 1 = 2147483647 \tag{3.18}$$

Implementing the algorithm (3.16)-(3.18), a sequence of random number uniformly distributed in [0, 1] can be generated. To get a sequence of random number uniformly distributed in [-1,1], the algorithm need to be modified as follows:

$$U = -1 + 2 \times v / m \tag{3.19}$$

After tested, this random number generator reduces half of the total time compared with that by build-in function in FORTRAN.

## Reference

Doyle, P.S. and Underhill, P.T. *Brownian dynamics simulations of polymers and soft matter*, In S. Yip, editor, *Handbook of Materials Modeling, volume I.* Kluwer Academic Publishers, 2004.

Ottinger,H.C., *Stochastic Process in Polymeric Liquids,* Springer,Berlin,1995

I.Ghosh,G H.Mckinley, R A.Brown,R C.Armstrong, *Deficiencies of FENE dumbell models in describing the rapid strenching of dilute polymer solutions*,.J.Rheol.45,721-758, 2001.

W.H.Press, S.A. Teukolsky, William T. Vetterling, B. P. Flannery, *NUMERICAL RECIPES IN FORTRAN 77: THE ART OF SCIENTIFIC COMPUTING*, Cambridge University Press, 1992

# Chapter 4 Choices of parameter

*Since the local physicochemical properties along polymer chains are not that important, bead-rod model and bead spring model is enough to capture some critical non-linear properties of polymer chains. Although the properties will be unphysical as the chains approach full extension and local details become important, many cases especially for DNA can be found that bead-rod and bead-spring model can give agreement with the experimental data if reasonable parameters are chosen, such bead numbers( Hur et al ,2000). In this chapter, parameters and observable will be introduced*

## 4.1 Parameters

From aspects of implementation and parameter optimisation, FENE dumbbell model and Bead- spring model are definitely the best candidates because the Bead-rod model is very expensive on computing time, although it can lead more accurate results.

The earliest accurate predictions of polymer configuration under flow were carried out successfully for long, fluorescently stained DNA molecules in dilute solutions. Chu and his co-workers imaged the configuration of DNA molecules in the well-defined flow in the mid 1990's (Perkins *et al*, 1995), their experimental data should be the most important reference data for us to compare with. According to their works, the most commonly used DNA molecule was the biologically derived λ-phage DNA and hence perfectly monodisperse double stranded DNA molecule, with a contour length of 21-22 *μm* and 0.066 *μm* for the persistence length. Good results have been achieved by the bead-rod model and bead-spring model (Hur *et al*, 2000). Since we know the contour length and persistence length of DNA, the total number of persistence length should be 21/0.066=318, which means the Kuhn steps should be 150-160, because Kuhn length is twice the persistence length. Although λ-phage DNA is a long chain, it has a relatively low extensibility and a larger radius of gyration, around $\boldsymbol{R}_G$=0.73 *μm*, indicating the root-mean-square end-o-end distance of the chain $\langle \boldsymbol{R}^2 \rangle_0^{1/2} = \sqrt{6} R_G$ =1.8 *μm*, which is also closed to $\langle \boldsymbol{R}^2 \rangle_0^{1/2} = \boldsymbol{N}^{1/2} \boldsymbol{b_k}$=1.62**,** when the Kuhn steps $\boldsymbol{N}$ were 150 and the Kuhn length $\boldsymbol{b_k}$ =21/150=0.066 *μm*(Larson, 2005). In conclusion, our

parameters used in *FENE dumbbell* and *Bead-spring* model can be summarized as the following table 4.1-4.4.

***Table 4.1 Environmental parameters***

| | |
|---|---|
| $k_B$ $(J/K)$ | 1.38e-23 |
| $T$ $(K)$ | 296 |
| Gap width $(\mu m)$ | 3 or 6.36 |
| viscosity of the solvent $\eta_s$ $(Pa{\cdot}s)$ | 1e-3 |

***Table 4.2 Parameters in FENE dumbbell model***

| | |
|---|---|
| Bead number in Bead-rod model $N_k$ | 150 |
| Kuhn length $\boldsymbol{b_k}$ $(\mu m)$ | 0.132 |
| Hydrodynamic radius a $(\mu m)$ | 0.0693 |
| Contour length $L$ $(\mu m)$ | 21 |

***Table 4.3 Parameters in Bead-spring model***

| | |
|---|---|
| Bead number in Bead-spring model $N_s$ | 10 |
| Kuhn length $\boldsymbol{b_k}$ $(\mu m)$ | 0.132 |
| Effective persistence length $\lambda_p$ $(\mu m)$ | 0.066 |
| Maximum length for each spring $L_S$ $(\mu m)$ | 2.33 |
| Hydrodynamic radius a $(\mu m)$ | 0.0693 |

***Table 4.4 Implementation parameters***

| | |
|---|---|
| Time step size $(s)$ | 1e-4~1e-5 |
| Time step | 1e+6~1e+7 |

## 4.2 Observable

In order to characterise the behaviours of the polymer in different cases, the following parameters will be considered in this work

### 4.2.1. Molecular stretch X of the chain

the real-time molecular stretch $\underline{\boldsymbol{X}}$ of the chain can be defined as the maximum length between bead and bead along the main flow direction. In other words, it is the projected length of the molecule in the flow direction (Jendrejack *et al.* 2004):

$$\underline{X} = \max(r_{i,x}) - \min(r_{i,x}) \tag{4.1}$$

where $r_{i,x}$ is the position vector of bead $i$ in the flow direction. The steady state of stretch at given condition can be defined as the ensemble average over N trials:

$$X = \frac{1}{N}\sum_{n=1}^{N} \underline{X}_n \tag{4.2}$$

where *n* is the *n*th trial.

### 4.2.2. The longest relaxation time of molecular stretch

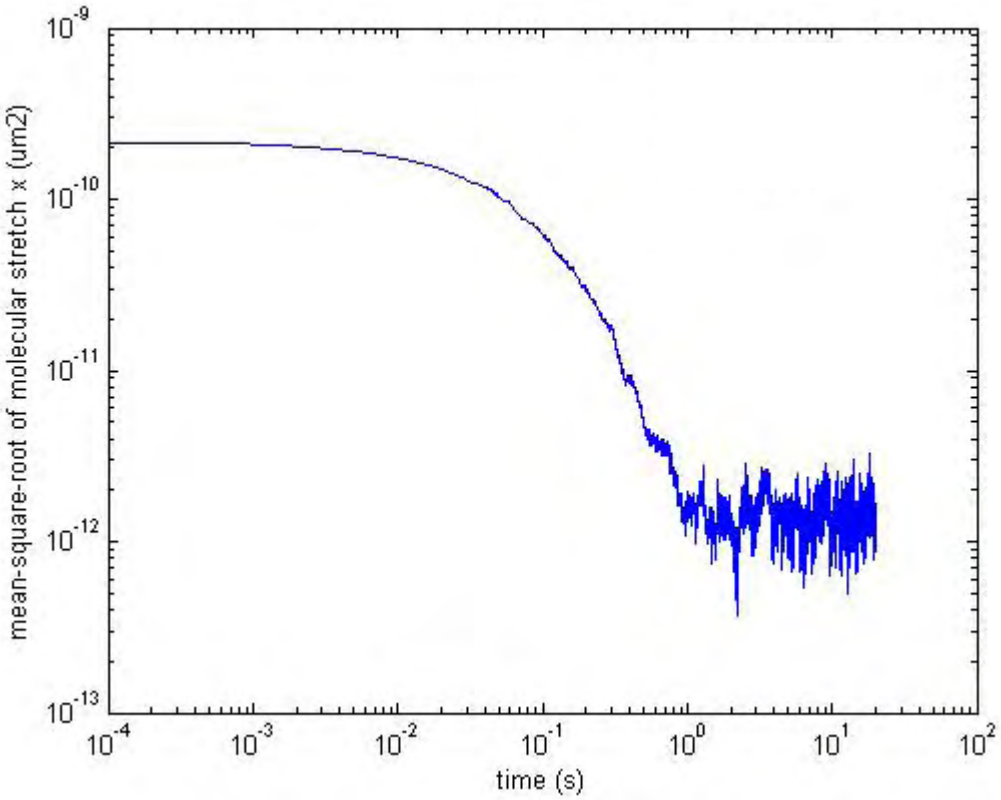


Figure 4.1 Relaxation curve of square of molecular stretch $x^2$ of 21 $um^2$ DNA by bead-spring model

The relaxation time of the molecular stretch is introduced to characterize the flow strength. To obtain the longest relaxation time $\tau_1$, we start the simulation from an initial value of the stretch ***x/L*** =0.7 along the flow direction and run the simulation in absence of flow and confined walls until the chains are completely relaxed. Averaging the results over 40 repeat simulations, we can get a relaxation curve of square of molecular stretch $x^2$ as shown in Figure 4.1.The final 9 % of the curve can be fit into an exponential curve as follows:

$$\left\langle x^2 \right\rangle = A\exp(-\frac{t}{\tau_1}) + B \tag{4.3}$$

where $\tau_1$ is the longest effective relaxation time, which is 0.11-0.13s for Bead-spring (10 beads) model and 0.063 for FENE dumbbell model. This relaxation time is close to the simulation result 0.095s by Jendrejack *et al* (2004). In addition, this relaxation time indicates that the time step should not be larger than this value, therefore our time step from $10^{-4}$-$10^{-5}$ second sounds reasonable.

### 4.2.3. The radius of gyration Rg of the chain

The radius of gyration can be defined as follows:

$$R_g = \left\langle \frac{1}{N_b} \sum_{i=1}^{N_b} \left| r_i - r_c \right|^2 \right\rangle \tag{4.4}$$

where $\mathbf{r}_c$ is the center of mass of the chain as follows:

$$\mathbf{r}_c = \frac{1}{N} \sum_{i=1}^{N} \mathbf{r}_i \tag{4.5}$$

where N is the number of beads and *i* is the index of the bead

### 4.2.4. Orientation and configuration thickness of the molecule in the shear flow

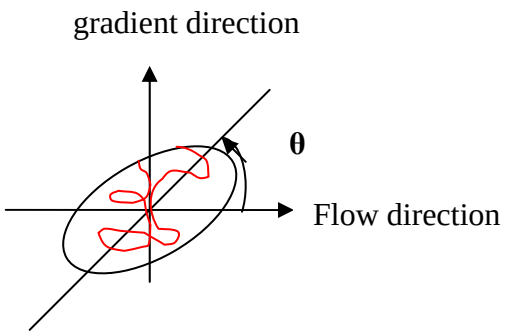


Figure 4.2 illustration of orientation of polymer in the shear flow

In order to charaterize the orientation of single molecule in the shear flow, the angle between the chain and flow direction should be computed. First, it is necessary to define the radius of gyration tensor related with section **4.2.3** as follows:

$$\mathbf{G} = \frac{1}{2N^2} [\sum_{i=1}^{N} \sum_{j=1}^{N} (\mathbf{r}_i - \mathbf{r}_j)(\mathbf{r}_i - \mathbf{r}_j)] \tag{4.6}$$

where $\mathbf{r_i}$ is the position vector of *i*th bead, *N* is the bead number of the chain. The mean orientation angle as illustrated in Figure 4.2 in the shear flow can be defined as follows:

$$\theta = \frac{1}{2} \tan^{-1} \left( \frac{2\langle G_{xy} \rangle}{\langle G_{xx} \rangle - \langle G_{yy} \rangle} \right) \tag{4.7}$$

Where $G_{xy}$, $G_{xx}$, $G_{yy}$ are the elements of the radius of gyration tensor. *x* is the flow direction; *y* is the velocity gradient direction. Here the angle is defined to be positive when measured from the flow direction to positive velocity gradient direction. The mean configuration thickness $\delta_y$ of the molecule in the velocity gradient direction can be defined as follows:

$$\delta_y = \sqrt{G_{yy}} \tag{4.8}$$

### 4.2.5. Diffusivity coefficient of the chain

In this case, polymer diffuses in the solution by Brownian kicks, the displacement of center of mass in three directions can be given as the follows:

$$x^2 = y^2 = z^2 = 2Dt \tag{4.9}$$

then

$$R^2 = 6Dt \tag{4.10}$$

Where D is the diffusion coefficient. Here is the plot of the <$\boldsymbol{R}^2$> *vs t* of 21 *um* DNA by bead-spring model (10 beads) in the free solution without flow to check whether the parameters are suitable.

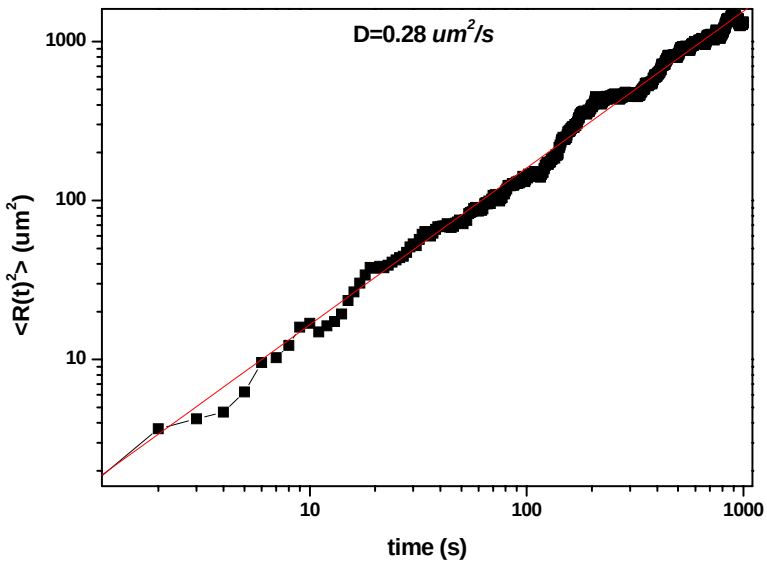


Figure 4.2 Mean-square displacement of center of mass vs, t for Bead-spring model (10)

As shown in Figure 4.2, the diffusion coefficient D of the chain is 0.286 $\mu m^2/s$. Compared with the input value 0.281 $\mu m^2/s$ we set in the simulation, Error= (0.286-0.281)/0.281=0.18%, which indicates the validity of our method of obtaining the coefficient from the simulations

### 4.2.6. steady state of center of mass distribution and width of center of mass distribution

The steady state center of mass distribuation in the cross section of the channel can be defined as follows:

$$P_c(y,z) = \left\langle \delta(y - y_{c,n})\delta(z - z_{c,n}) \right\rangle_N \tag{4.11}$$

where $y_{c,n}$ and $z_{c,n}$ is the coordinates of center-of-mass in $y$ and $z$ direction at observation n and N is the total number of trials for the simulation (Jendrejack et al,2004).

In order to characterize to the depletion layer in the channel, the second moment of the center-of-mass distribution in the cross section of the channel is introduced as follows.

$$w^2 = \int (y^2 + z^2) P_c(y,z) dydz \tag{4.12}$$

The quantity $w/w_{eq}$ gives a measure of the width of the center of mass distribution relative to the equilibrium value (Jendrejack et al, 2004). If $w/w_{eq}$ is increasing, it indicates that the chain is migrating towards to the wall and vice verse.

## Reference

J.S.Hur, E.S.G.Shaqfeh, R.G.Larson, *Brownian dynamics in simulations of single DNA molecules in shear flow*, J.Rheol.44, 713-742,2000

T.Perkins, D.E.Smith, R.G.Larson, S.Chu, *Stretching of a single Tethered Polymer in a Uniform flow* , Science, 268, 83-87,1995

R.G.Larson, *The rheology of dilute solutions of flexible polymers: Progress and problem*s, J.Rheol.49, 1-70 , 2005

M.Chopra, R.G.Larson, *Brownian dynamics simulations of isolated polymer molecules in shear flow near adsorbin and nonadsorbing surface*, J.Rheol.46,831- 862,2002

R.M.Jendrejack, D.C.Schwartz, J.J.de Pablo, M.D.Graham, *Shear-induced migration in flowing polymer solutions: simulation of long-chain DNA in microchannels*, J.Chem Phys,120,2513-2529,2004

# Chapter 5 DNA in equilibrium[5]

*Before analyzing the sheared DNA in confined geometry, it is instructive to consider the motion of single DNA molecule in equilibrium. With the variation of the length scale of the geometry, the static properties of the chain are significant affected. This can give us a simple picture about the dynamics of single DNA molecule in equilibrium with confined boundaries.*

## 5.1 Free solution in equilibrium

### 5.1.1. Analytical result

In order to offer a comparison to the simulation, theoretical analysis is carried on first. For simplicity, we take FENE dumbbell model to carry the theoretical analysis. Since we have introduced the force law in the FENE dumbbell model as follows, we can get the energy for each configuration **Q,** which is the end-to-end distance vector:

$$\mathbf{F} = \frac{H\mathbf{Q}}{1-\frac{Q^2}{Q_{\max}^2}} \tag{5.1}$$

$$E_p(\mathbf{Q}) = \int_0^Q \mathbf{F}\cdot d\mathbf{Q} = \int_0^Q \frac{H\mathbf{Q}}{1-\frac{Q^2}{Q_{\max}^2}}\cdot d\mathbf{Q} = -\frac{1}{2}HQ_{\max}^2 \ln(1-\frac{Q^2}{Q_{\max}^2}) \tag{5.2}$$

Where $Q_{\max}$ is the maximum molecular extension which means the contour length in FENE dumbbell model and $E_p$ is the potential energy for this configuration. Thus, the configuration-space distribution function can be calculated based on the theory of statistical physics as follows:

$$\iint f(\mathbf{Q},\mathbf{P})d\mathbf{Q}d\mathbf{P} = 1 \tag{5.3}$$

$$\psi(\mathbf{Q}) = \int f(\mathbf{Q},\mathbf{P})d\mathbf{P} \tag{5.4}$$

Where $\psi(\mathbf{Q})$ is the configuration-space distribution function and ***f(Q,P)*** is the phase-space distribution function. To calculate this function, an important result from

[5] **Note:** In this chapter, we didn't consider hydrodynamic interaction if not specified

classical statistical mechanics will be used: for a system at equilibrium, $f(\mathbf{Q},\boldsymbol{P})$ is a canonical distribution:

$$f(\mathbf{Q},P)=\mathbf{Z}^{-1}\exp(-H/k_BT) \tag{5.5}$$

Where $H$ is the **Hamiltonian**, the sum of the kinetic energy $E_k$ and potential energy $E_p$ and **Z** is partition function, which can be given as follows:

$$Z=\int\int\exp(-\mathrm{H}/k_BT)d\boldsymbol{Q}d\boldsymbol{P}=\int_{-\infty}^{+\infty}\exp(-E_k/k_BT)d\boldsymbol{P}\int_0^{Q_{\max}}\exp(-E_p/k_BT)d\boldsymbol{Q} \tag{5.6}$$

By inserting Equation (5.2), it leads to:

$$Z=\int_{-\infty}^{+\infty}\exp(-E_k/k_BT)d\boldsymbol{P}\int_0^{Q_{\max}}\left[(1-\frac{Q^2}{Q_{\max}^2})^{\frac{HQ_{\max}^2}{2k_BT}}\right]d\boldsymbol{Q} \tag{5.7}$$

By inserting Equation (5.5),Equation (5.4) can be rewritten as follows :

$$\begin{aligned}\psi(\mathbf{Q})&=\int\mathbf{Z}^{-1}\exp(-H/k_BT)d\mathbf{P}\\&=\exp(-E_p/k_BT)\int_{-\infty}^{+\infty}\mathbf{Z}^{-1}\exp(-E_k/k_BT)d\mathbf{P}\end{aligned} \tag{5.8}$$

So the probability density of finding an end-to-end vector $\boldsymbol{Q}$ can be defined as follows:

$$\psi(\mathbf{Q})=[1-\frac{Q^2}{Q_{\max}^2}]^{\frac{HQ_{\max}^2}{2k_BT}}\Bigg/\int_0^{Q_{\max}}\left[(1-\frac{Q^2}{Q_{\max}^2})^{\frac{HQ_{\max}^2}{2k_BT}}\right]4\pi Q^2dQ \tag{5.9}$$

This leads to the probability density of finding an end-to-end distance $Q$ as follows:

$$P(Q)=4\pi Q^2\psi(Q)=4\pi Q^2[1-\frac{Q^2}{Q_{\max}^2}]^{\frac{HQ_{\max}^2}{2k_BT}}\Bigg/\int_0^{Q_{\max}}\left[(1-\frac{Q^2}{Q_{\max}^2})^{\frac{HQ_{\max}^2}{2k_BT}}\right]4\pi Q^2dQ \tag{5.10}$$

Since we know the spring constant $H=\frac{3k_BT}{(N_K-1)b^2}$, the constant in Eq (5.10) can be rewritten as follows:

$$\frac{HQ_{\max}^2}{2k_BT}=\frac{3}{2}(N_k-1) \tag{5.11}$$

Figure 5.1 represents the probability distribution of end-to-end distance Q for 21 *um* DNA molecule in equilibrium. It can be founded that when in equilibrium, the end-to-end distance Q in the solution is less than 0.2 and the distribution is a Gaussian distribution. The mean value is $\left\langle\mathbf{Q}^2\right\rangle_0^{1/2}$=1.57 *um*, which is close to the numerical result around 1.66 $\mu m$ (Chopra *et al*, 2002).

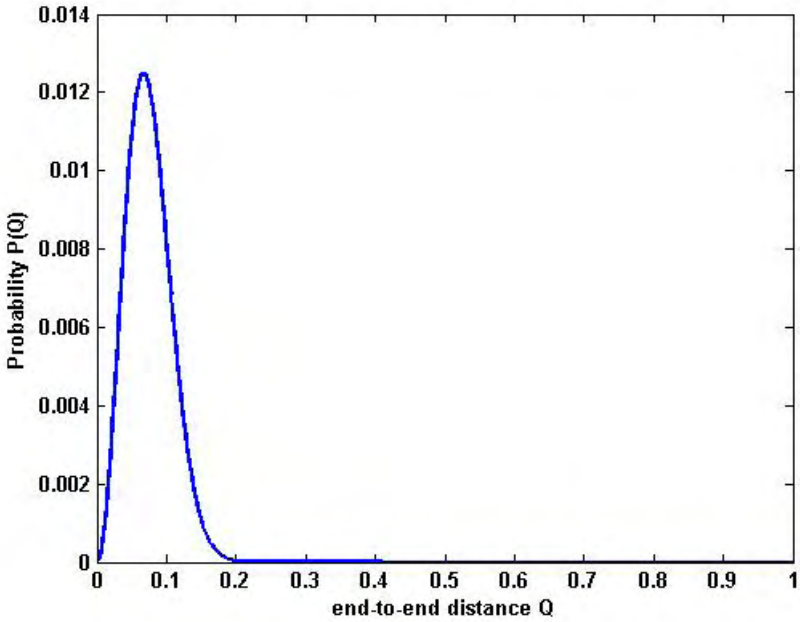


Figure 5.1 Probability distribution function of end-to-end distance for 21 *um* DNA molecule( Kuhn step =150 ) by FENE dumbbell model, where the bin size is 0.001 and end-to-end distance normalized by the maximum spring length $Q_{max}$

### 5.1.2 Simulation result

In order to compare with the analytical results, DNA in free solution in equilibrium is considered first. In this case, polymer molecule only experience the Brownian kicks from surrounding solvent molecules, drag force which resists the movements, and entropic spring forces which resist configurations changes of polymer molecules. For this case, the molecular motion has been studied for 100s, and the length of time step is chosen to $10^{-4}$-$10^{-5}$ s. During this period, all the configuration data will be stored in every 0.1 s around one relaxation time in order to collect the statistically significant data for analysing the behaviour of the molecules with flow. In this way, we sampled 40-100 chains to get the ensemble properties of polymer, so the total number of measure points is 40000-100000, which should be large enough to get good approximation to real behaviour of polymers

FENE Dumbbell and Bead-spring model (10 beads) are implemented with their corresponding force laws. By averaging those ensembles, statistical properties of single chain in equilibrium can be shown in the following table.

***Table 5.1 Comparison of statistical properties by bead-spring and FENE model***

| | Chorpra *et al*(2002) | Bead-spring(10) | FENE |
|---|---|---|---|
| Equilibrium strech $\langle x^2 \rangle^{1/2} / L$ ( μm) | 1.26(experimental) | 1.13 | 0.74 |
| End-to-end distance $\langle \mathbf{R}_0^2 \rangle^{1/2}$ ( μm) | 1.66 | 1.43 | 1.48 |
| Radius of gyration $\langle \mathbf{R}_G^2 \rangle^{1/2}$ ( μm) | 0.68 | 0.64 | 0.74 |
| $\langle \mathbf{R}_0^2 \rangle^{1/2} / \langle \mathbf{R}_G^2 \rangle^{1/2}$ | 2.44 | 2.23 | 2.00 |

As shown in Table 5.1, it can be seen that Bead-spring model have better agreements with experimental value and simulation results in equilibrium in free solution from Chorpra *et al* (2002) compared with FENE dumbbell model. However, it seems the equilibrium stretch in the model doesn't agree very well with the experimental value, which indicates better parameters for bead-spring model can be found.

## 5.2 Confined solution in equilibrium

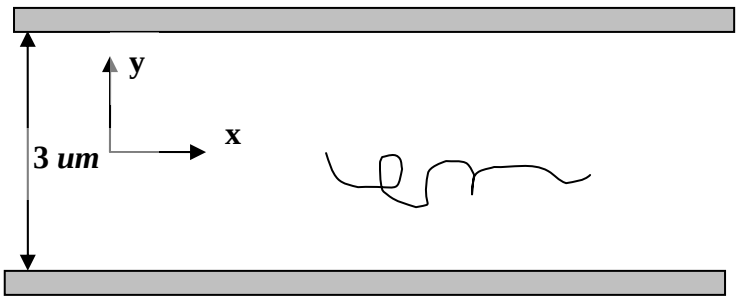


Figure 5.2 illustration of polymer in equilibrium in the infinite parallel walls

Here we consider molecules are confined in the slit between the two infinite long parallel hard plates with a fixed distance (3 *μm*) between each other as shown in Figure 5.2[6].This width is roughly 2 times of mean-square-root of end-to-end distance $\langle \boldsymbol{R}^2 \rangle_0^{1/2}$ (1.66 *μm*) and 5 times of the radius of gyration $\boldsymbol{R}_G$ (0.68 *μm*). This value is not only large enough for DNA molecule to display the their near-bulk solution behaviour, but also small enough to keep the frequent interaction of molecule with the walls. The flow direction is only in *x* direction, which is parallel to the walls and the *y* direction is normal to the wall (Chropa *et al*, 2002). Running this simulation, the statistical properties are shown in Table 5.2 as follows:

[6] Here we treat the wall as pure elastic wall, please refer section 3.1 for details.

***Table 5.2 comparison of statistical properties withwall and without wall by bead-spring(Free-draining and Bulk HI) model***

| | without wall | with wall (FD) | with wall (Bulk HI) |
|---|---|---|---|
| Equilibrium strech $\langle x^2 \rangle^{1/2} / L$ ( μm) | 1.121 | 1.12 | 1.129 |
| End-to-end distance $\langle R_0^2 \rangle^{1/2}$ ( μm) | 1.43 | 1.37 | 1.35 |
| Radius of gyration $\langle R_G^2 \rangle^{1/2}$ ( μm) | 0.64 | 0.626 | 0.619 |
| $\langle R_0^2 \rangle^{1/2} / \langle R_G^2 \rangle^{1/2}$ | 2.23 | 2.19 | 2.18 |

As shown in Table 5.2, it can be seen that mean square root of end-to-end distance and radius of gyration is reduced to some extent but not very much, which means the chain is squeezed slightly due to confined effect from the walls, but the confined effect is not very strong in the length scale of this confined geometry. This can be supported by that the equilibrium stretch in Bulk HI model slightly increases. In addition, it can be seen the equilibrium stretch predicted by FD model is not affected by the presence of the wall. The reason will be discussed in the end of this chapter.

In addition, Figure 5.3 illustrates a trend that probability density of center of mass varies from zero (or close to 0) close to the wall, to the bulk value in the center of the channel. In this case, polymers will only experience confinement in *y* direction, theoretical solution is reported by Casassa (I.Teraoka, 2002) as follows:

$$P(y, y') = \frac{2}{d} \sum_{k=1}^{\infty} \sin \frac{k\pi y}{d} \sin \frac{k\pi y'}{d} \exp[-(k\pi R_g / d)^2] \qquad (5.12)$$

Where $P(y,y')$ is the probability density function of finding a chain at particular *y* away from a given *y'* and *d* is the gap width .In this case, *y'* =*d*/2 ,which is the center of the gap.

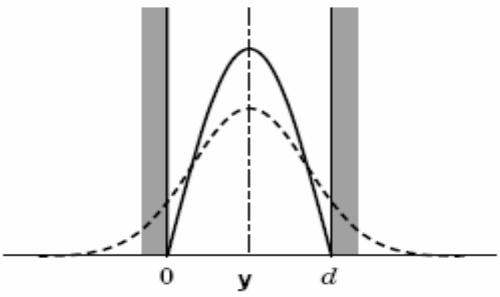


Figure 5.3 Probability density distribution of center of mass for a Gaussian chain confined inside two parallel plates with gap width=d. The dash line represents unconfined chain and solid line means confined chain (Teraoka, 2002)

Figure 5.4 represents the comparison of probability density distribution of center-of-mass by FENE dumbbell model, Bead-spring model and analytical results. It can be seen that for FENE dumbbell model, the probability density of center-of-mass decreases more slowly from wall to the centre compared with Bead-spring model. Bead spring model has better agreement with theoretical result near the wall compared with FENE dumbbell model, but it overpredicts at the center of the channel. In addition, the probability density is not zero at the wall for FENE dumbbell model. The reason for this discrepancy could be the use of a finite number of beads in the simulation. To improve the degree of discretization of model, the difference close to wall can be reduced, which can be concluded from the results of the bead-spring model with 10 beads. From the same point of view, increasing the number of internal mode in the bead-spring model will make the results closer to the real behaviour of the polymer.

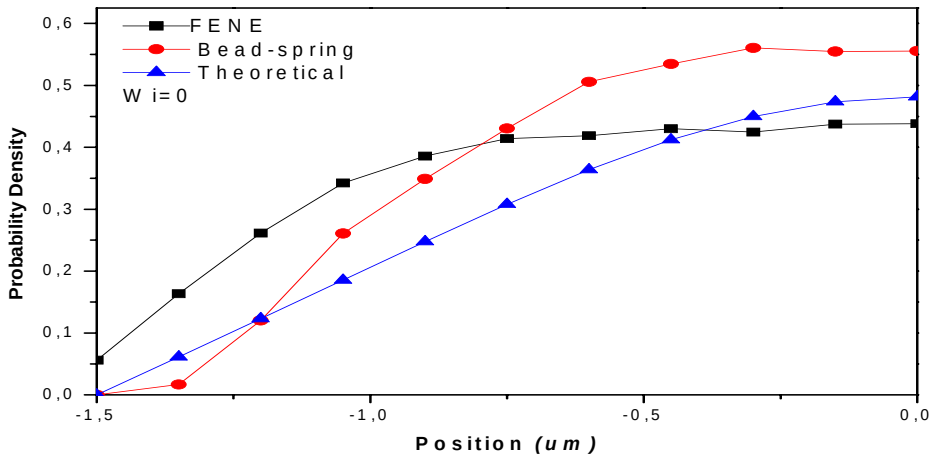


Figure 5.4 Comparision of probability density distribution of center of mass for Bead-spring model (10) , FENE dumbbell model and theoretical result in equilibrium. The distribution shown is half of the symmetric profile in the cross section of the channel

Having analysed probability density distribution of chain segments in the channels, we will present the distribution of fractional extension in the flow direction at **Wi=0** for Bead-spring model (10) and FENE dumbbell model as shown in Figure 5.5. It can be seen that both distributions display a shape of Gaussian-like distribution as we have shown in Figure 5.1. Although the statistical properties of both models are almost the same, Bead-spring model has better agreements with experimental data (Hur *et al* 2000) and theoretical analysis.

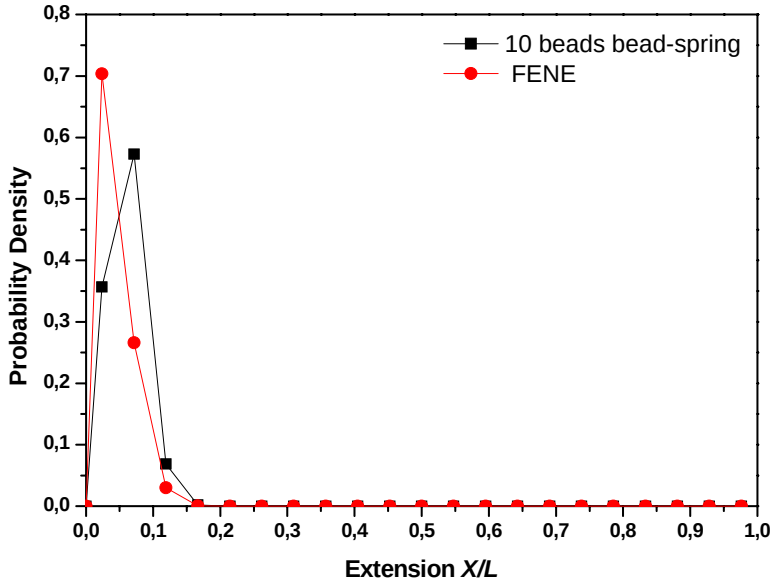


Figure 5.5 Probability distribution of fractional extension for Bead-spring model (10) and FENE dumbbell model in equilibrium

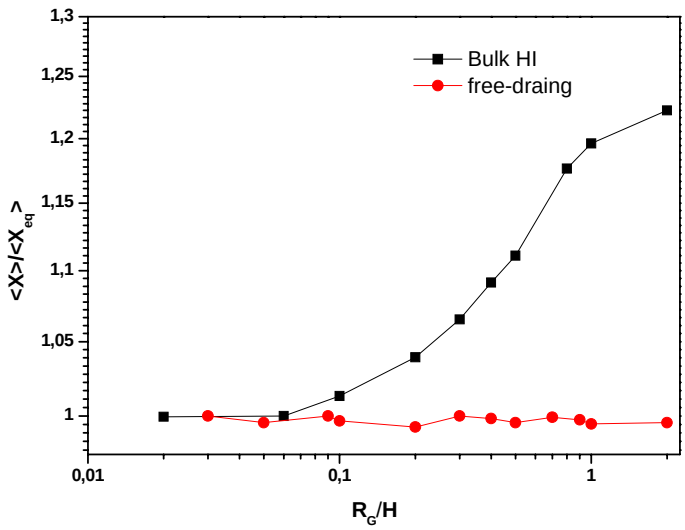


Figure 5.6 Dimensionless molecular stretch as a function of channel width for 21 *um* DNA in equilibrium by Bulk HI and FD model (please refer to this model on section 2.3.4), $\langle X \rangle$ and $\langle X \rangle_{eq}$ is the equilibrium stretch in confined geometries and free solution respectively. H is the channel width of the slit.

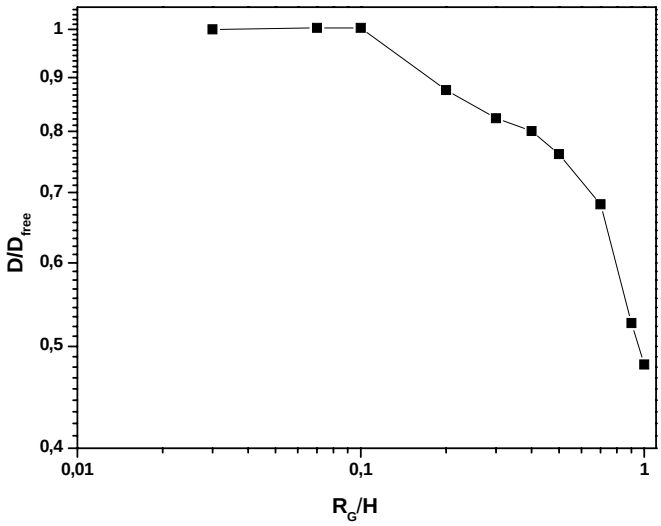


Figure 5.7 Normalized diffusivity of the chain as a function of channel width for 21 *um* DNA in equilibrium by Bulk HI model (please refer to this model on chapter 7), $\boldsymbol{D}_{\text{free}}$ and $\boldsymbol{D}$ is the diffusivity of the chain in free solution and confined geometry respectively. H is the channel width of the slit.

Figure 5.6 represents the equilibrium stretch of 21 *um* DNA molecule as a function of the channel width in microchannels by free-draining model (without hydrodynamic interaction and excluded volume interaction) and Bulk HI model[7] (hydrodynamic interaction). It can be seen that there is a transition region: the static confinement effect appears at $R_G/H \approx 0.1$, which means when H lowers down to around $10R_G$, the chain will be strongly confined; Larger than this value, the confinement is not pronounced. However, in the highly confined regime, for example when $R_G/H > 2$ is not accurate, because the original bead-wall potential is not suitable for this model anymore, since the bead-wall repulsive potential of the two walls in our model begins to interfere with each other at this length scale. Compared to the chain in the channel with a square cross section (Jendrejack et al, 2003), the stretch in the slit has a weaker dependence on the channel width; there should be no plateau at the regime of smaller channel width; the stretch should continue to increase as the decrease of the channel width.

[7] Please refer the concepts of Free-draining model and Bulk HI model in section 2.3.4 and section 7.2

In addition, it can be seen that free-draining model can not predict the transition regime of dimensionless molecular stretch from larger channel width to smaller channel width and the stretch remains almost constant shown in Figure 5.6, it is quite reasonable: Free-draining polymer chain in this parallel plates is equivalent to an ideal chain in 3D random walk with confinement in y direction (wall-normal direction).The stretch in other two unconfined directions *x* and *z* don't change, since the random walk in each direction is independent of each other.

In fact, Free-draining model with exclude volume interaction (but without hydrodynamic interaction) also are examined. However, it gives the same prediction with Free-draining model. At the first sight, this result is a little confusing. Because according to theoretical prediction (de Gennes, 1979), the strong confinement will also be expected at highly confined regime in a model with exclude volume interaction. However, if you recall how we include this excluded volume interaction in Equation (2.27) in chapter 2, it will be clear that we only consider the bonded excluded volume interaction (the EV between a bead and its successive bead) and the repulsive interactions between this bead and other surrounding beads are not explored, since we switch off the bead-bead hydrodynamic interaction. This will lead to a weaker EV effect even in extremely confined geometries.

It is related with *Langevin equation* Equation (2.27): it can be seen that all the non-bonded interactions between bead and bead have to be incorporated through hydrodynamic interaction. This also explains why we only see the confinement on center of mass distribution, but almost no confined effect is predicted in molecular stretch in the confined geometry for Free-draining model shown in table 5.2.

Besides the confinement on molecular stretch due to the confined geometry, the diffusivity of the chain is also significantly affected by the confined boundary shown in Figure 5.7. The simulations show that from around $R_G/H \approx 0.1$, the diffusivity starts to decrease significantly, which means highly confined effect will lead to a smaller diffusion coefficient. This critical value for highly confined effect agrees with the critical channel width in the molecular stretch. In addition, if we correlated with simulation results in Figure 5.6 and 5.7, it can be noted that less stretched chains move faster than highly stretched chains does. This is because the diffusivity of the

chain will decrease when hydrodynamic interaction between the segments is being screened with the decrease of channel width.

In conclusion, the equilibrium properties and configurations in free solution and confined geometries have been studied in this chapter. First, the confined boundaries will change the distribution of center of mass. Second, we observed the equilibrium properties, such as molecule stretch and diffusivity of the chain began to be significant affected by the geometry at around $H=10R_G$, which indicates that at $H<10R_G$, polymers can be considered to be highly confined.

## Reference

I.Teraoka, *Polymer Solutions: An introduction to Physical Properties*, Wiley- Interscience, 2002

J S.Hur,E S G.Shaqfeh,R G.Larson *Brownian dynamics simulations of DNA molecules in shear flow*, J.Rheol.44,713-742,2000.

R.G.Larson, *The rheology of dilute solutions of flexible polymers: Progress and problem*s, J.Rheol.49 (1), 1-70 , 2005

R.M.Jendrejack, D.C.Schwarts, M.D.Graham, J.J.de Pablo, *Effect of confinement on DNA dynamics in microfluidic devices*, J .Chem Phys,119,1165-1173, 2003

De Gennes,'*Scaling Concepts in Polymer physics*',Cornell University Press,1979

M.Chopra, R.G.Larson, *Brownian dynamics simulations of isolated polymer molecules in shear flow near adsorbin and nonadsorbing surface*, J.Rheol.46,831- 862,2002

# Chapter 6 DNA in homogenous flow[8]

*In this chapter, we turn to the investigation of nonequilibrium properties of single DNA molecule inside the confined geometry under simple shear flow. Both orientation and elongation of the chain are investigated numerically as a function of flow strength (Wi).*

## 6.1 Geometry and flow field

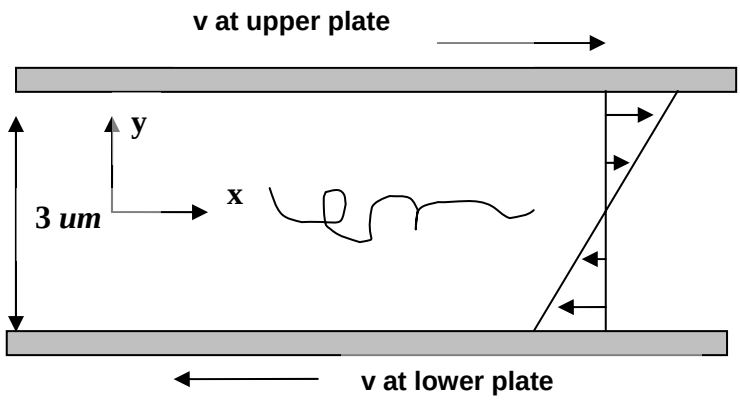


Figure 6.1 illustration of polymer in the infinite parallel walls moving in opposite direction.

In this chapter, we consider the dynamics of single DNA molecule inside two infinite long parallel plates (gap width H=3 *um*) .The centerline of the channel is along the *x* axis, which is the direction of the imposed flow field. The cross section is in the *y*-*z* plane .The imposed simple shear flow field can be given as follows:

$$\mathbf{v}_x(y) = \dot{\gamma} y \quad , \mathbf{v}_y = \mathbf{v}_z = 0 \tag{6.1}$$

Where $\dot{\gamma}$ is shear rate. To our knowledge, shear rate is a constant independent of the position in the channel under simple shear flow. Therefore, the velocity gradient in the direction perpendicular to the wall is zero.

## 6.2 Simulation result

Figure 6.2 shows the center of mass distribution of DNA in the cross section of the channel under shear by FENE dumbbell model. It can be seen that in this case, the region of the depletion layer near the wall didn't change with the increase of the flow strength, which agrees well with the results in a plane coquette flow reported by Larson *et al* (2002). Their results also indicate that the migration of DNA isn't affected by the flow strength the under simple shear flow by FENE dumbbell model.

[8] If not specified, the model used in this chapter don't include the hydrodynamic interaction.

The reason may be that the FENE dumbbell can not reproduce the complexity of the configurational restrictions on the chain close to a confined boundary.

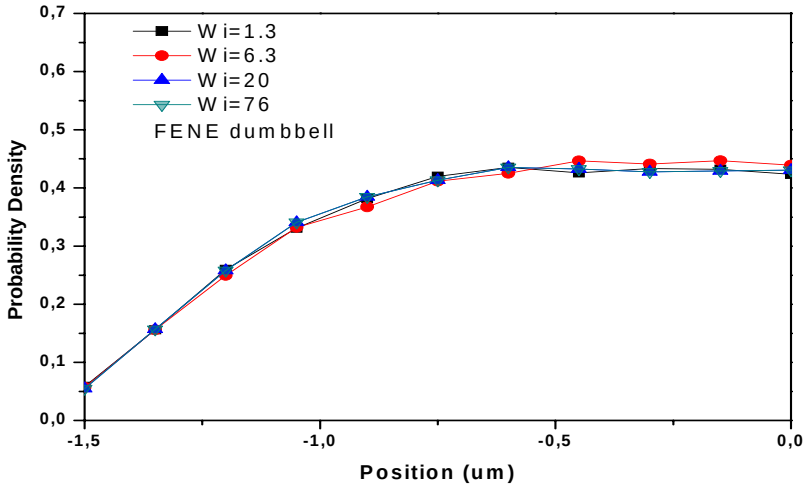


Figure 6.2 Probability density distribution of center of mass for FENE dumbbell model with flow at different Wi in the silt H=3 *um*

For Bead-spring model, it is similar with FENE dumbbell model. As shown in Figure 6.3, it can be seen the probability density distribution of the center-of -mass near the wall didn't change so much with the flow strength. However, Larson *et al.* (2002) reported depletion layer near the wall should be decreased by the increase of the flow strength. They hypothesized that the size of the chain will shrink in the shear gradient direction at strong flow strength, which will allow the polymer to approach closer to the wall. However, according to the results from the same group (Fang *et al*, 2005), the opposite trends have been found. In addition, Pablo *et al* (1992) hold that the thickness of depletion layer near the wall for Bead-rod model would decrease with the increase of the flow strength from lower to intermediate flow strength, but increase from intermediate flow strength to strong flow strength. They argued that at lower shear rate, molecules would tend to align itself to the flow direction, thereby allowing itself approach closer to the wall; at higher shear rate, molecule would rotate mole rapidly, therefore it has more chances to interact with wall, which leads to the increase of the thickness of the depletion layer of the wall. However, the region with configuration restriction effect or steric effect from the wall is only around 1/3 to 1/2 of $R_G$, so the presence of the wall only affects on the chain very close to the wall. Therefore, with the increase of flow strength, the depletion region should not change

so much. Although weak migration behavior to the wall reported by Larson *et al* (2002),it is still not consistent with the experimental results (Seo *et al*,1996).

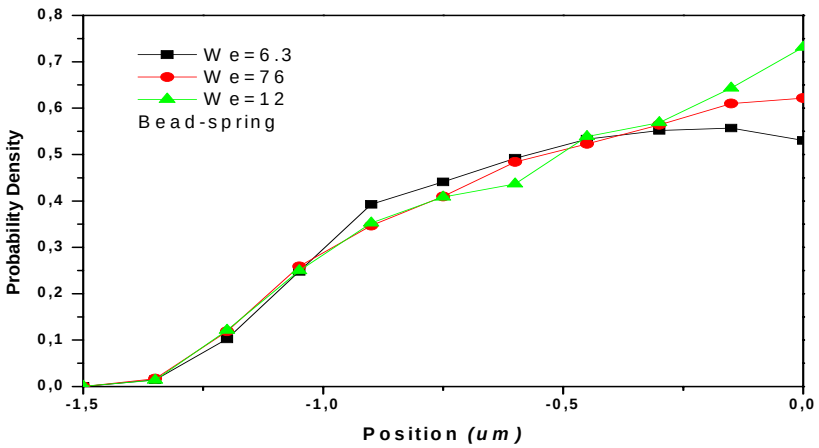


Figure 6.3 Probability density distribution of center of mass for 21*um* DNA by Bead-spring model with flow at different Wi in the silt H=3 *um*

In order to test Larson's idea, the mean orientation <θ> and the mean thickness $\delta_y$ of DNA molecule in free solution and confined geometry at various flow strength are examined in Figure 6.5. It can be seen that with the increase of the flow strength, the mean orientation and the mean thickness $\delta_y$ will decrease, which indicates the chain becomes slightly thinner in the velocity gradient direction and tends to align itself closer to the flow direction. Those trends can be supported by the experimental results at Wi <100 in free solution from Teixiara *et al* (2005) in Figure 6.4,

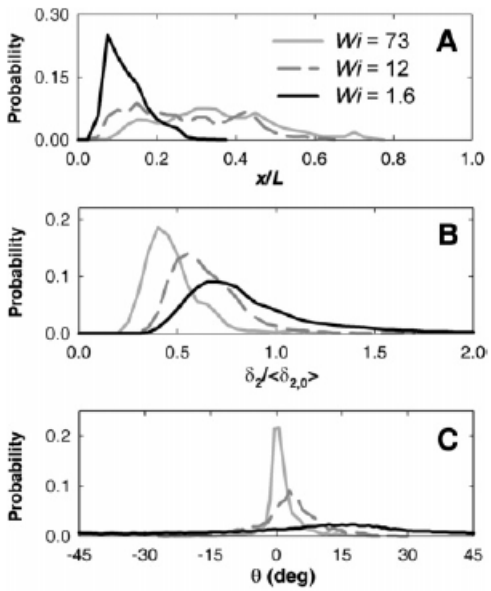


Figure 6.4 Probability distributions of (A) extension, (B) thickness, and (C) orientation. Both 22 *um* DNA (*Wi* =1.6 and 12) and 80 *um* DNA (*Wi*= 73) are shown. The bin sizes are 0.025, 0.05, and 1°, respectively (Teixiara *et al* ,2005)

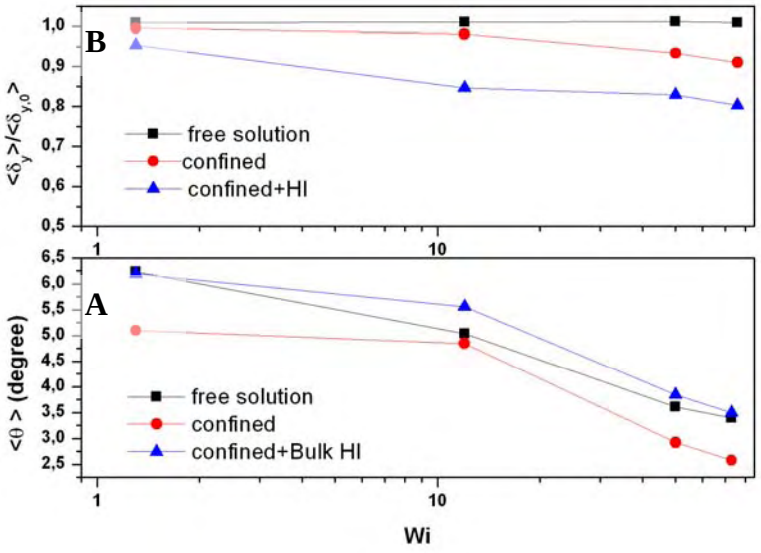


Figure 6.5 Mean orientation <θ> and mean thckness $\delta_y$ in the velocity gradient direction for 21*um* DNA in free solution (Free-draining) and confined geometry (Free-draining and Bulk HI) by Bead-spring model under simple shear flow at different Wi in the silt H=3 *um*

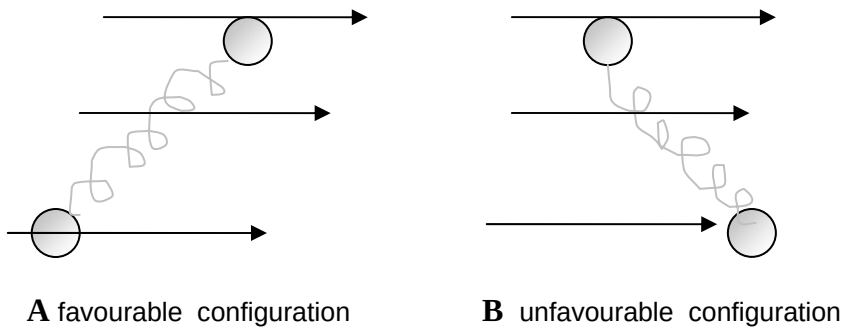


Figure 6.6 illustration of the favourable configuration in the shear flow

though their angle decays faster than that in our case. The reason is unknown.

In Figure 6.5A, it can be seen that the mean orientation <θ> is positive, which means the configuration in Figure 6.6**A** in the flow is favourable in the shear flow. This hypothesis of favourable configuration can be supported by the probability distribution of orientation in free solution and in the confined geometry under simple shear flow shown in Figure 6.7, in which positive angles are more probable to appear. This agrees qualitatively well with experimental results by Teixiara *et al* (2005) in Figure 6.4C. In addition, the width of probability distribution of orientation becomes narrower and shift to the mean orientation <θ> close to 0, with the increase of the

flow strength shown in Figure 6.7, which indicates that the chain will be confined in the narrower spectrum of orientation space with the increase of the flow strength.

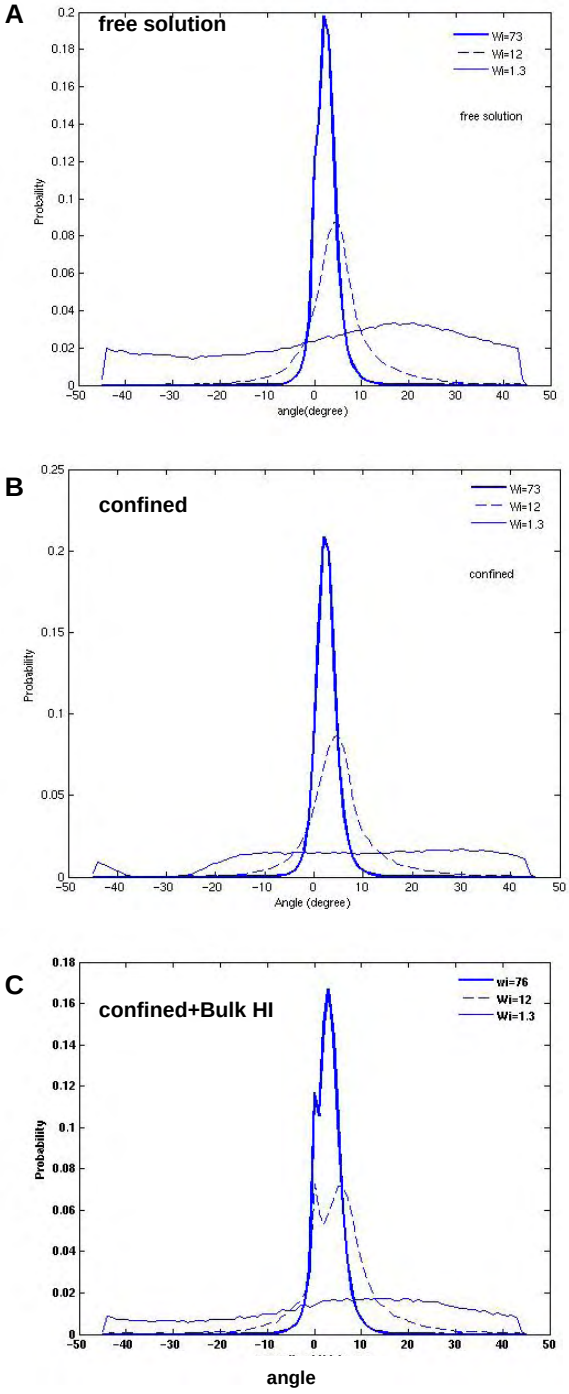


Figure 6.7 Probability distribution of orientation of single DNA molecule in free solution and confined geometry (with and without HI) under simple shear flow by Bead-spring model. The bin size is 1$^{o}$, and probability is normalized by the total number of the sample data-200000.

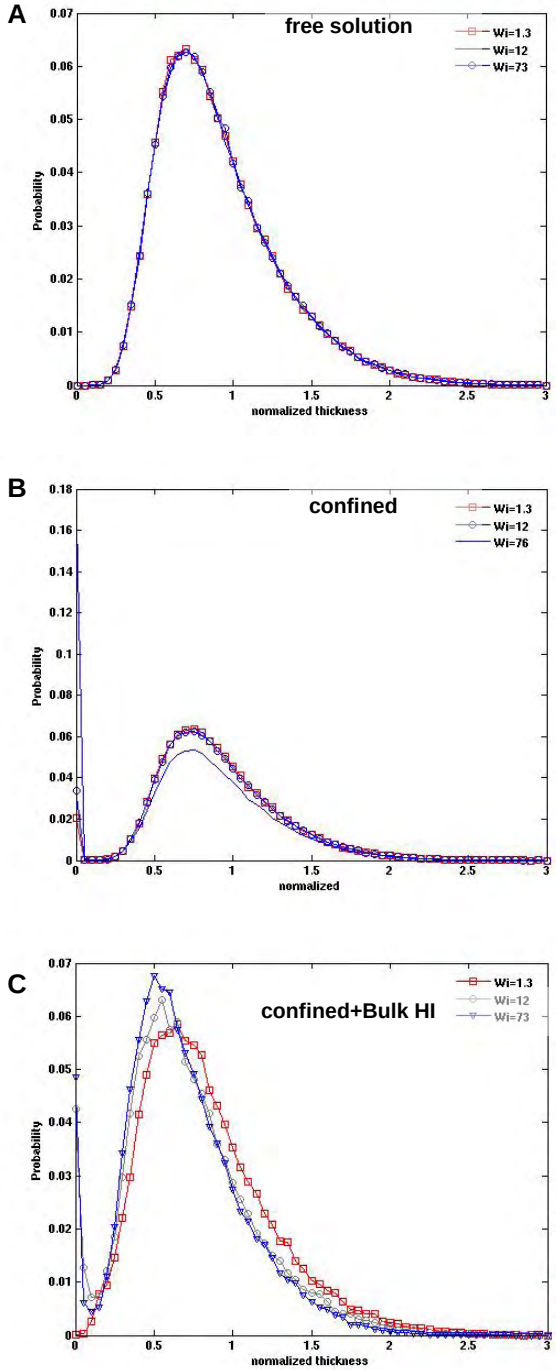


Figure 6.8 Probability distribution of thickness in velocity gradient direction of single DNA molecule in free solution and confined geometry (with and without HI) under simple shear flow by Bead-spring model. The bin size is 0,05, and Probability is normalized by the total number of the sample data-200000.

However, we didn't find that the mean thickness $\delta_y$ of single molecule in gradient direction change so much but almost remain constant as shown in Figure 6.5B for the case *free solution* and *confined geometry* by *Free-draining model*, even the probability distribution of the thickness almost remain unaffected by the flow strength shown in Figure 6.8A,B. However, when *hydrodynamic interaction* (Bulk HI) comes into the play, things become different. The mean thickness $\delta_y$ decay a lot with the increase of flow strength compared with other two models shown in Figure 6.5B, which can be supported by that the thickness distribution shifts to small thickness direction with increase of the flow strength shown in Figure 6.8C. The result about $\delta_y$ predicted by considering the hydrodynamic interaction is similar with the experimental result in Figure 6.4B, which indicates hydrodynamic interaction can strongly induce the decrease of the mean thickness $\delta_y$

Furthermore, as shown in Figure 6.7-6.8, only the model with hydrodynamic interaction (*Bulk HI*) gives correct predictions on all the dynamic properties compared with the experimental results in Figure 6.4, though other two models (Free solution and confined solution by *Free draining* model) gives partial correct predictions, which hydrodynamic interaction plays an important role on the variation of the shape of molecule in the solution under shear flow but less important on other properties, such as the distribution of orientation.

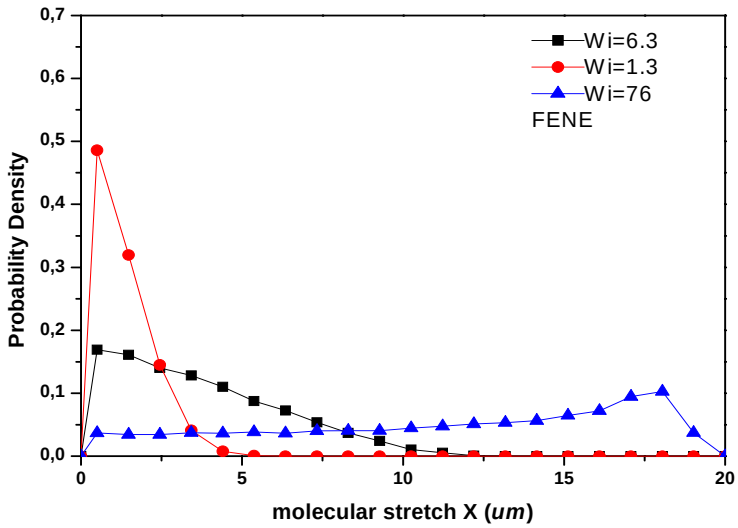


Figure 6.9 Probability distribution of fractional extension for 21*um* DNA by FENE dumbbell model with flow at different Wi

In figure 6.9-6.10, comparisons of probability distribution of molecular stretch at different Weissenberg numbers for FENE dumbbell and Bead-spring model are presented. Here, molecular stretch means the average 'extension' along the flow direction or channel direction. It can be seen that at Wi=1.3, the chain does not differ much from the equilibrium state in free solution and the distribution is close to a Gaussian shape, which indicates the chain remains coiled state most of the time. At the intermediate value Wi=6.3, the chain is stretched to some small extension. As the flow strength goes to high, such as Wi=76, the chain is unfolded to a large degree.

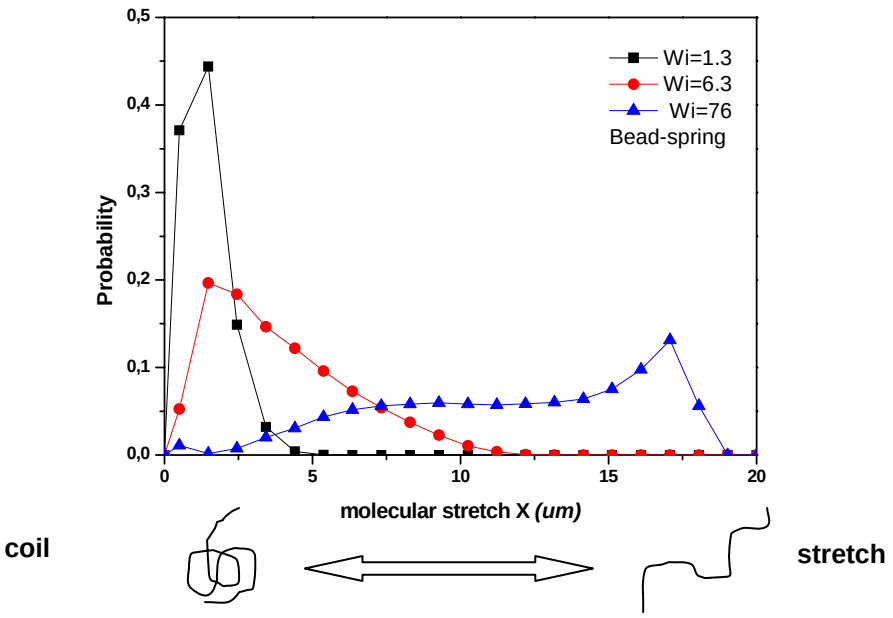


Figure 6.10 Probability distribution of fractional extension and corresponding configuration for 21*um* DNA by Bead-spring model with flow

The width of distribution is broadened and it seems that molecular configuration with high extension seems to be more probable to appear. This result agrees qualitatively well with the prediction by Celani *et al* (2005). Compared with the results for DNA molecule from Simth *et al* (1999), Hur *et al* (2000) and experimental results in Figure 6.4 our results have excellent agreement with them at the lower Weissenberg numbers, but their measurements didn't show a peak at near the maximum stretch in the higher flow strength. Their results indicate every configuration of the molecular stretch is almost equally probable to appear. This difference may come from the bead number we use (10) is smaller than their value (20). Of course, we can use more beads to get more accurate result, but it can be seen the difference is not very large, which is enough to capture the essence of the phenomena in the length and time scale of our

confined geometry shown in Figure 6.1. In addition, as the increase of flow strength, the fractional molecular stretch asymptotes to around 0.5 shown in Figure 6.11 , which is similar with the value of 0.5 from Hur *et al* (2000). This is interesting: it means the average molecular stretch will remain 0.5 even at very high shear rate. Larson (2005) explained these phenomena according to the observation by Simth *et al* (1999): The chain tends to align itself to the flow direction under flow strength. However, Brownian force will kick the beads out of the shear plane with a positive or negative angle shown in Figure 6.13. According to our knowledge on fluid dynamics, a simple shear flow can be regarded as the superimposition of pure elongation flow and pure rotation flow shown in Figure 6.12. Due to the coupling of those two flow effects, the dynamics of polymer molecules in the shear flow will become complicated. After being kicked out of the shear plane, there will be two possibilities for a stretched chain: for the positive angle, drag force will stretch molecular further and the vorticity will derive the molecular back to the shear plane; for negative angle, drag force will help the chain relax and vorticity will carry it to the shear plane shown in Figure 6.13. After coming back, the molecule will be kicked out of the shear plane and then repeat the above process. During this process, DNA molecule will experience stretching, tumbling, coiling state irregularly. Based on this mechanism, although molecule has more chances to stretch, it also has a substantial probability to tumble, so the average stretch approaches to 0.5 even at the higher shear rate (Larson, 2005)

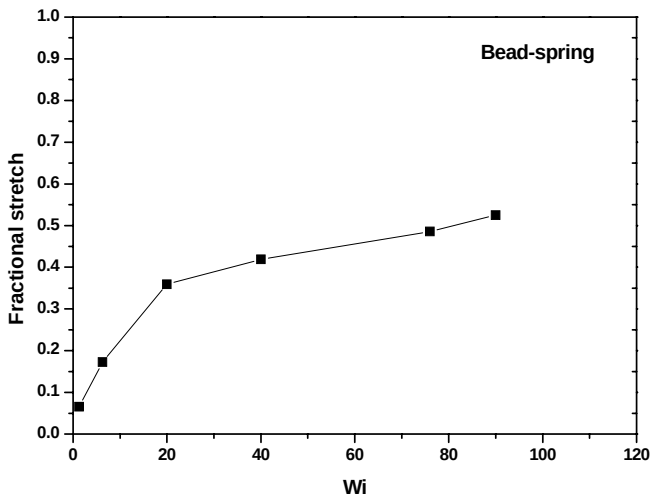


Figure 6.11 average fractional extension of 21*um* DNA by Bead-spring model at different Wi

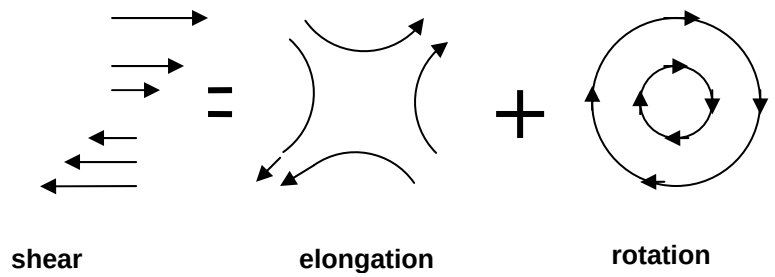


Figure 6.12 illustration of simple shear flow can be regarded as the superposition of the pure elongation flow and pure rotation flow

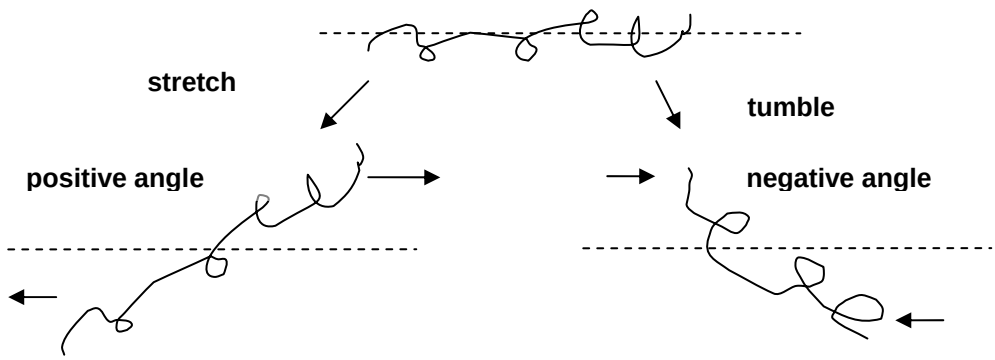


Figure 6.13 illustration of the tumbling dynamics of polymer in the simple shear flow

In this chapter, dynamics of DNA molecule under simple shear flow in the confined geometry is investigated. It can be seen that statistical properties of single DNA molecule, such as probability density distribution of center of mass in physical space, have been significantly affected. As the increase of flow strength, the chain will be confined in a narrower orientation space and hydrodynamic interaction becomes important when we consider the variation of the size of molecule in the velocity gradient direction. This indicates that hydrodynamic interaction will play an import role on some nonequilibrium properties, and we will discuss this effect in detail in chapter 7.

So far, migration behavior of DNA molecule due to the variation of the flow strength is not discovered in those models without including hydrodynamic interaction, which doesn't agree with experimental results (Ausserre et al, 1991, Seo et al, 1996) and simulation results from others (Hur et al 2000, Pablo et al 1992). There are several reasons for these discrepancy mentioned by Pablo et al (1992): first, we neglect the hydrodynamic interaction between bead and bead. Second, hydrodynamic interaction created by the confined geometry has been neglected for simplicity. Third, since molecules have less probability to appear to the region near the wall, it should create

inhomogeneous flow, but we assume the flow field won't be disturbed. Those simplifications should be questioned; we will incorporate those effects into the next chapter.

## Reference

M.Chopra, R.G.Larson, *Brownian dynamics simulations of isolated polymer molecules in shear flow near adsorbin and nonadsorbing surface*, J.Rheol.46,831- 862,2002

J.J.de Pablo, H.C.Ottiinger , *Hydrodynamic Changes of the Depletion Layer of Dilute Polymer Solutions Near a wall* ,AlchE Journal,308,1992

Ausserre, D., J.Edwards, J.Lecourtier, H.Hervet, F.Rondelez, *Hydrodynamic thickening of the depletion layer in colloidal solutions*, Europhys,Lett,14,33-38,1991

Y.H.Seo, O.O.Park, M.S.Chun, *The behavior of the velocity enhancement in microcapillary flows of flexible water-soluable polymers*,J.Chem.Eng.Jpn,29,611,1996

R.E. Teixeira, H P. Babcock,E.S. G. Shaqfeh, S.Chu, *Shear Thinning and Tumbling Dynamics of Single Polymers in the Flow-Gradient Plane* , Macromolecules 38, 581-592,2005

Simth,D.E, H.P.Babcock, S.Chu, *Single polymer dynamics in steady shear flow*, Science 283,1724-1727,1999

J S.Hur,E S G.Shaqfeh,R G.Larson *Brownian dynamics simulations of DNA molecules in shear flow*, J.Rheol.44,713-742,2000.

R.G.Larson, *The rheology of dilute solutions of flexible polymers: Progress and problems*, J.Rheol.49 (1), 1-70, 2005

L.F, H.Hu, R.G.Larson, *DNA configurations and concentration in shearing flow near a glass surface in a microchannel*, J. Rheol.49,127-138,2005

A. Celani, A.Puliafito, K.Turitsyn, *Polymers in linear shear flow: a numerical study*, Europhys. Lett., 70 , 464-470, 2005

# Chapter 7 DNA in inhomogeneous flow

*In the last chapter, Dynamics of single DNA molecule in the confined geometry under the homogenous flow (simple shear flow) has been investigated. It can be seen that DNA molecules display different behaviors in confined geometry compared to the case in the free solution. But we didn't find the migration effect near the wall as people reported migration toward the wall (Pablo et al 1992, Larson et al. 2002) or migration to the center of the channel (Seo et al 1996, Jendrejack et al, 2004). As mentioned before, that's because we did some assumptions for simplicity. In this chapter, those neglected effects in our model will be taken into the play, especially the influence of the wall to the hydrodynamic flow.*

## 7.1 Geometry and flow field

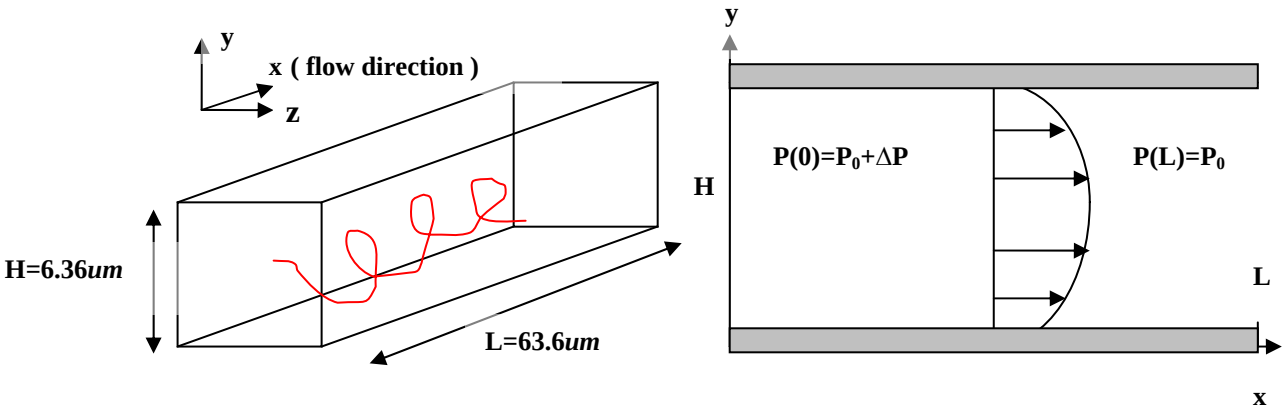


Figure 7.1 illustration of single DNA molecule in a microchannel with a square cross section and velocity profile under pressure-driven flow. *x* is the flow direction

In this chapter, we considered the dynamics of single DNA molecule in an infinite long microchannel with a square cross section (gap width H=6.36 *um*) .The center line of the channel is along the *x* axis, which is the direction of the imposed flow field. Thus, the cross section is in the *y-z* plane .The imposed pressure-driven flow field can be given by Jendrejack *et al* (2004) as follows:

$$\mathbf{v}_x(y,z) = \frac{4H^2}{\eta\pi^3}\left(-\frac{dp}{dx}\right)\sum_{k=1,3,5\ldots}^{\infty}(-1)^{(k-1)/2}\times\left[1-\frac{\cosh(k\pi z/H)}{\cosh(k\pi/2)}\right]\frac{\cos(k\pi y/H)}{k^3} \quad (7.1)$$

Where -*dp/dx* is the pressure difference along the flow direction, $\eta$ is the viscosity of the solution, *H* is the width of the channel. The strength of the flow is defined by an effective shear rate, $\dot{\gamma}_{eff} = 2v_{\max} / H$, where $\mathbf{v}_{\max} = |\mathbf{v}((y=0, z=0))|$ is the velocity at the center line of the channel.

## 7.2 Hydrodynamic Interaction model

In this chapter, three models with different levels to treat hydrodynamic interaction are compared[9]. The hydrodynamic interaction can be incorporated into Brownian dynamics through hydrodynamic interaction tensor $\mathbf{\Omega}_{ij}$ in the diffusion tensor $\mathbf{D}_{ij}$ shown in Equation (2.27) and (2.30) as follows:

$$\frac{d\mathbf{r}_i}{dt} = \boldsymbol{\kappa} \cdot \mathbf{r}_i + \sum_{j=1}^{N} \frac{\partial}{\partial \mathbf{r}_j} \cdot \mathbf{D}_{ij} + \sum_{j=1}^{N} \frac{\mathbf{D}_{ij}}{k_B T} \mathbf{F}_i^s + \left(\frac{6}{dt}\right)^{1/2} \sum_{j=1}^{N} \mathbf{B}_{ij} \cdot \mathbf{n}_i$$

$$\mathbf{D}_{ij} = k_B T \left(\frac{1}{6\pi\eta_s a} \mathbf{I}\delta_{ij} + \mathbf{\Omega}_{ij}\right)$$

The simplest model to treat the hydrodynamic interaction is ***Free-Draining*** model, which means the hydrodynamic interaction $\mathbf{\Omega}_{ij}$ is neglected and a bead will not be affected by the flow field due to the motion of its surrounding beads. Therefore, the diffusion tensor can be expressed as follows:

$$\mathbf{D}_{ij}^{FD} = \frac{k_B T}{6\pi\eta a} \delta_{ij} \mathbf{I} \tag{7.2}$$

Here it can be seen that $\mathbf{D}_{ij}^{FD}$ is a symmetric, isotropic and position-independent tensor.

A more accurate approximation to describe the hydrodynamic interaction is ***Bulk Hydrodynamic*** *Interaction* model. Hydrodynamic interaction between bead and bead in free solution is included into the diffusion tensor as follows:

$$\mathbf{D}_{ij}^{Bulk} = k_B T \left[ \frac{1}{6\pi\eta a} \delta_{ij} \mathbf{I} + (1-\delta_{ij}) \mathbf{\Omega}^{RPY}{}_{ij} \right] \tag{7.3}$$

Where $\mathbf{\Omega}^{RPY}{}_{ij}$ is the *Rotne-Prager-Yamakawa (RPY) Tensor* mentioned in chapter 2. It is a symmetric, but anisotropic and inter-configuration dependent tensor, which leads to configuration-dependent and anisotropic diffusion tensor.

[9] These three models we have metioned in Chapter 2

However, the most accurate model-***Full Hydrodynamic Interaction*** model is to take the influence from the confined geometry into the play. Usually, this term can be neglected because the length scale of the microchannel is much larger than the radius of gyration of DNA molecule. However, in our case, the length scale can be comparable to the radius of gyration, therefore the correct term from the wall becomes important to the dynamics of DNA molecule in the microchannel. Thus, the diffusion tensor in *Full HI* model can be given as follows:

$$\mathbf{D}_{ij}^{Full} = k_B T \left[ \frac{1}{6\pi\eta a} \delta_{ij} \mathbf{I} + (1-\delta_{ij}) \mathbf{\Omega}^{RPY}{}_{ij} + \mathbf{\Omega}^{wall}{}_{ij} \right] \tag{7.4}$$

Where $\mathbf{D}_{ij}^{Full}$ is supposed to be an asymmetric, but anisotropic, inter-configuration and position dependent tensor due to the configuration dependent bead-bead hydrodynamic interaction and position-dependent wall hydrodynamic interaction.

## 7.3 Simulation result

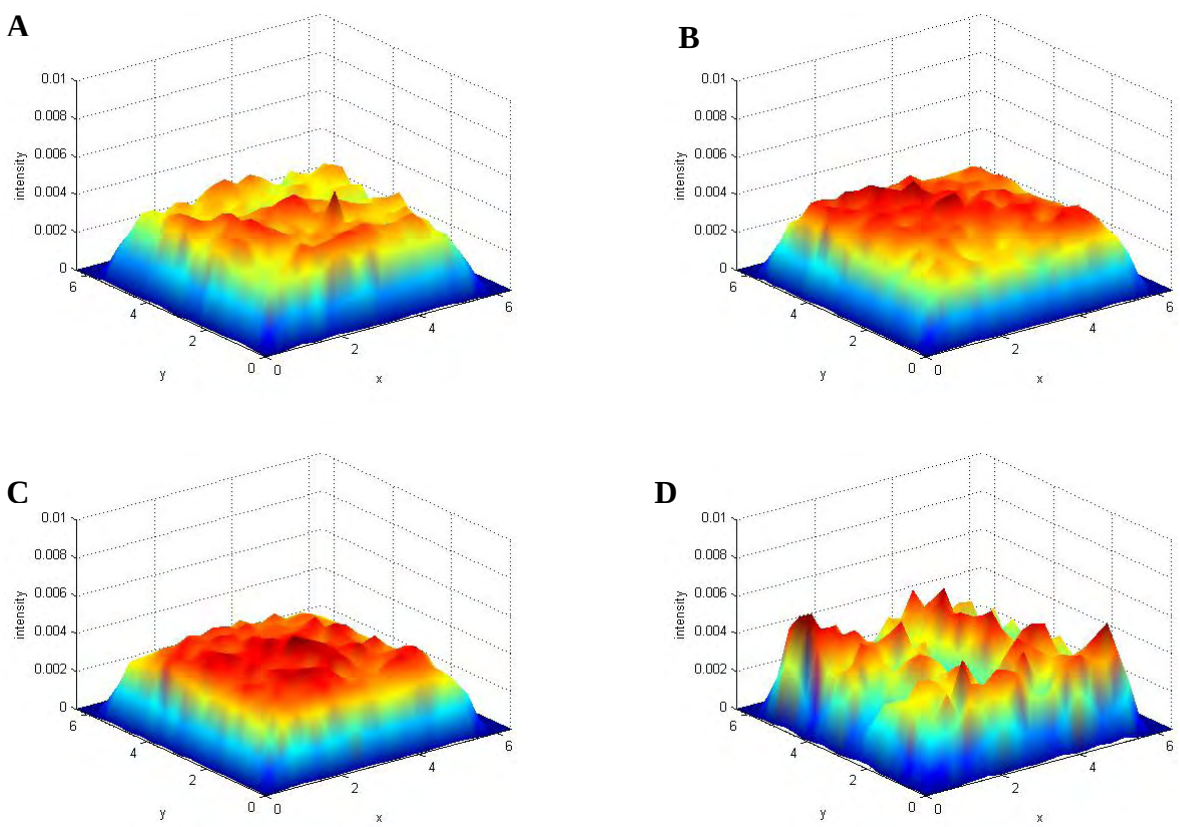


Figure 7.2 Steady state of center-of-mass distribution in the cross section (*y-z* plane) of the channel for a 21*um* DNA chain in a 6.3 *um* wide channel by Free-draining model: A. $\dot{\gamma}_{\text{eff}} = 0\,\text{s}^{-1}$( Wi=0 ) , B. $\dot{\gamma}_{\text{eff}} = 3.98\,\text{s}^{-1}$( Wi=0.44 ) , C. $\dot{\gamma}_{\text{eff}} = 30.8\,\text{s}^{-1}$ ( Wi=3.39 ), D. $\dot{\gamma}_{\text{eff}} = 308\,\text{s}^{-1}$( Wi=33.9 )

The effect of the flow strength on the probability distribution of center-of-mass is represented in Figure 7.2 for a 21 *um* DNA molecule by ***Free-draining*** *model*. At equilibrium (Wi=0), the center-of-mass has a uniform distribution across the channel, except a depletion layer near the wall (Blue area) due to steric hindrance from the wall. As the increase of the flow strength, the depletion layer near the wall is unaffected, which can be quantified by the width of the center-of-mass in the Figure 7.8.This is similar with the phenomena we observed in the simple shear flow in chapter 6 (the reason will be discussed later). However, this is not consistent with the experimental results by Fang *et al* (2004), they reported that the depletion layer will be enlarged with the increase of the flow strength.

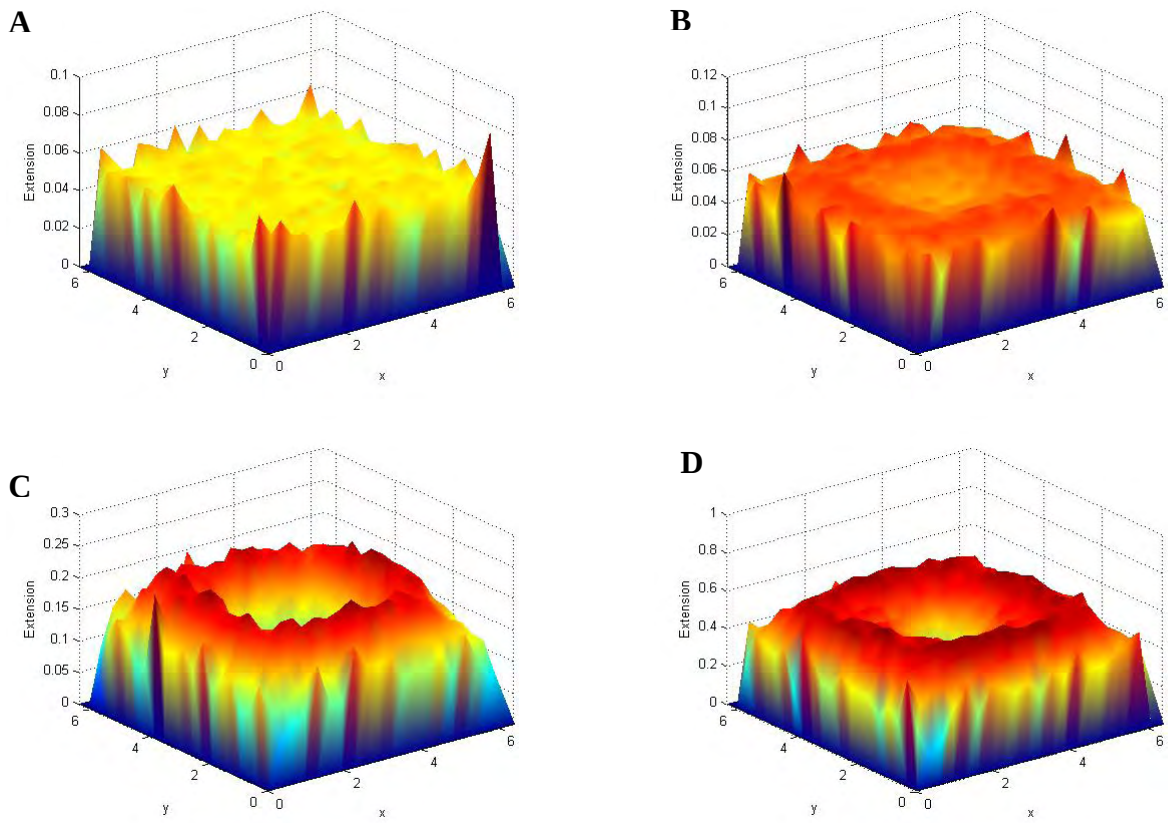


Figure 7.3 Steady state of stretch as a function of position of center-of-mass in the cross section (*y-z* plane) of the channel for a 21*um* DNA chain in a 6.3 *um* wide channel by Free-draining model : A. $\dot{\gamma}_{\text{eff}} = 0\,\text{s}^{-1}$( Wi=0 ) , B. $\dot{\gamma}_{\text{eff}} = 3.98\,\text{s}^{-1}$( Wi=0.44 ) , C. $\dot{\gamma}_{\text{eff}} = 30.8\,\text{s}^{-1}$ ( Wi=3.39 ), D. $\dot{\gamma}_{\text{eff}} = 308\,\text{s}^{-1}$( Wi=3.39 ).The data around the edges are nosiy due to the small observations near the wall(the error is proportional to $\boldsymbol{N}^{-1/2}$ where $\boldsymbol{N}$ is the number of independent observations.)

Figure 7.3 represents the influence of flow strength on the probability distribution of chain stretch in the cross section of the channel for a 21 *um* DNA molecule by *Free-draining model*. These plots are plotted as the average stretch at given position in the cross section in order to decouple it from the probability of finding a chain at this position. It can be seen that the distribution is uniform at equilibrium (the blue area means the small probability of finding a chain there), the chain in the depletion layer is slightly more elongated than that in the center of the channel due to the steric hinderance. It's because only higher stretched chain parallel to wall can survive in the region near the wall as illustrated in Figure 7.4. Because less restricted configuration has a larger thickness in the direction perpendicular to the wall, so at the same distance above the wall, the chain with this configuration can be pushed away from the wall first. Therefore, it leads to a lower density of center-of-mass near the wall but higher average strength there.

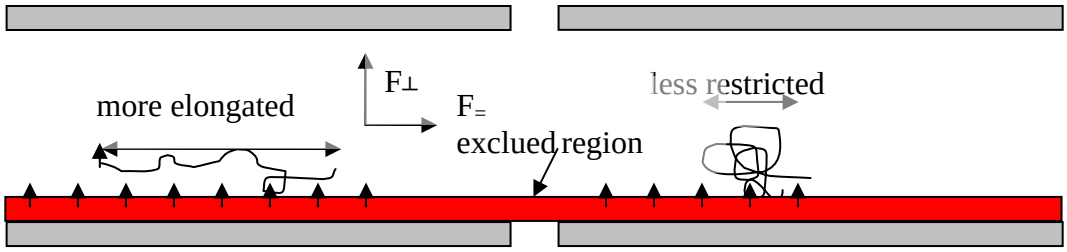


Figure 7.4 illustration of configurations of the chain near the lower wall. The red area is the region where the chain can feel the repulsive force from the lower wall.

As the increase of the flow strength, the chain is highly elongated if we compared the 4 plots in the Figure 7.3. The probability distribution of the chain extension becomes highly nonuniform compared with the equilibrium case. At higher Weissenberg number, the chain near the wall are strongly aligned and elongated to the flow direction against the randomizing influence of Brownian motion, but the chain near the center is less elongated at the center line of the channel, and a minimum of the averaged stretch is shown in Figure 7.3 B, C, D. This is due to the inhomogeneous properties of the parabolic flow, the local velocity gradient near the wall is higher than that near the center of the channel, which means the shear rate near the wall is higher than that near the center.

In Figure 7.5 A, B, C, the effect of the flow strength on the probability distribution of center-of-mass is represented for a 21 *um* DNA molecule by ***Bulk HI*** *model*.

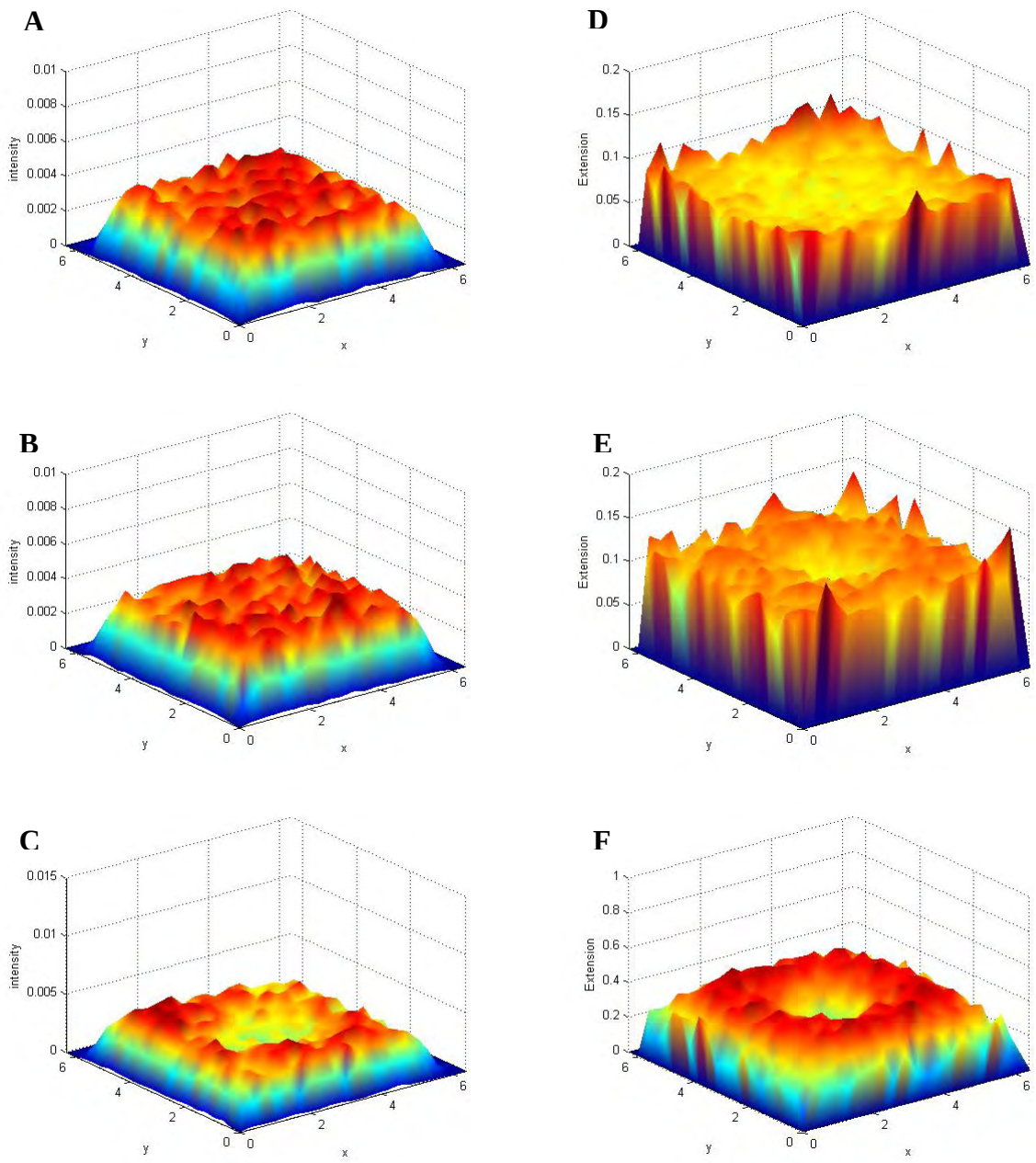


Figure 7.5 Steady state center-of-mass distribution and Steady state stretch as a function of position of center-of-mass in the cross section (*y-z* plane) of the channel for a 21*um* DNA chain in a 6.3 *um* wide channel by ***Bulk HI*** model. A,D $\dot{\gamma}_{\text{eff}} = 3.98\ \text{s}^{-1}$( Wi=0.44 ) , B,E $\dot{\gamma}_{\text{eff}} = 30.8\ \text{s}^{-1}$ ( Wi=3.39 ), C,F $\dot{\gamma}_{\text{eff}} = 308\ \text{s}^{-1}$( Wi=33.9 )

At lower Weissenberg regime, the probability distribution of the center-of-mass is fairly uniform except the depletion layer near the wall as shown in Figure 7.5 A, B; at the higher Weissenberg regime, the distribution becomes nonuniform.

Figure 7.5 C indicates a nonmonotonic probability distribution of the center-of-mass *at stronger flow strength* : moving from the wall to center of the channel, the probability of finding a chain, first increases from 0 near the wall to a maximum off

the centerline (near the wall), then decrease to a local minimum at the centerline. The maximum is the consequence of the competition between the steric hinderance from the wall and the spatial variation of the bead-bead hydrodynamic interation produced by the inhomogeneous flow. The steric effect will give the repulsive force to drive the molecule (very close to the wall) away from the wall, but the spatial variation of the diffusivity along the chain in the velocity gradient direction will make the chain migrate out of regions of lower shear rate to regions of higher shear rate. Therefore, a maximum appears near the wall, which can be illustrated as a simple picture in Figure 7.6. As known from Chapter 6, the chain has fewer configurations in gradient direction and orientates almost parallel to the flow direction at strong shear rate; at smaller shear rate, the chain has more configurations in gradient direction. Therefore, the ***simple mechanism*** is: the chain near the center (lower shear rate) migrates towards wall due to an implicitly position-dependent diffusivity (induced by the configuration-dependent hydrodynamic interaction). When it enters into the excluded region near the wall, the contribution to the drift toward wall from the diffusion becomes less important; at the same time, the drift term toward the center contributed by the repulsive wall becomes important. At a particular point near the wall, the upward drift term will be equal or larger than the downward drift term. This is where the maximum is.

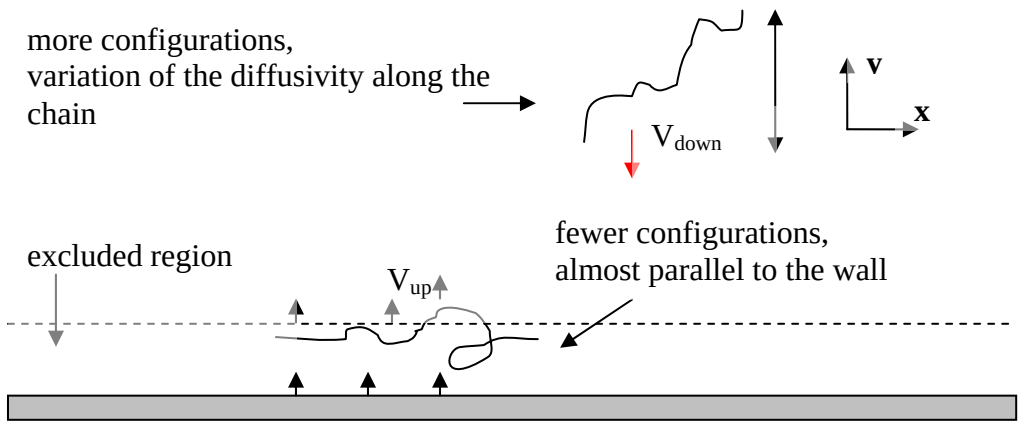


Figure 7.6 illustration of the mechanism of migration behavior of the chain in the microchannel predicted by Bulk HI model. The area below the dash line is the region where the chain can feel the repulsive force from the lower wall. Here we only plot the lower wall for simplicity. ***x*** and **y** is flow direction and its velocity gradient direction.

In addition, it can be seen in Figure 7.8 that as the increase of the flow strength, the width of center-of-mass is slightly increased, which indicates the chain migrates toward the wall and leads to a thinner depletion layer. It is because the flow strength

increases, the velocity gradient perpendicular to the wall is increased compared to the smaller flow strength, which indicates the variation of diffusivity along the chain(near the center) is larger at stronger flow strength. This stronger driving force under the stronger flow strength makes the chain migrate towards the wall further compared with the case in smaller flow strength.

Figure 7.5 D, E, F show the average stretch in the cross section is increased with the increase of the flow strength and the distribution is still nonuniform as we observed in the *Free-draining* model. At lower Weissenberg number, the average stretch decreases monotonically from the maximum near the wall to the minimum in the center. The reason is the same: higher local velocity gradient induced the higher extension near the wall. The only difference is that the average stretch in the local minimum is not as low as that predicted by Free-draining model if we compared with Figure 7.3C and Figure 7.5 E. The reason is unknown. It may be because part of the less stretched chains migrate toward wall and highly elongated chains will migrate toward the center, so the probability of finding a less stretched chain becomes smaller near the center, therefore the chain in the center of the channel is predicted with higher average stretch in Bulk HI model compared with that predicted by Free-draining model. In other words, because of the migration of less stretched chain, you can find a less extended chain in the region near the wall with a relatively higher probability, and more higher stretch molecules near the center, which means the average stretch in the region near the center is higher and a relatively smaller stretch is predicted near the wall compared with that in Figure 7.3

So far, it seems that we got a reasonable result for the migration behavior, but this is not the case, which has an opposite trend on migration behavior. It is because we didn’t treat the contribution to the flow field from the wall in an accurate way. Although the steric effect has been considered, it is only restricted itself in a boundary layer near the wall, which is a short-range interaction and will not influence the whole velocity field. Therefore, it is necessary to include the *wall hydrodynamic interaction*, which is *Full HI* model, to see any difference there.

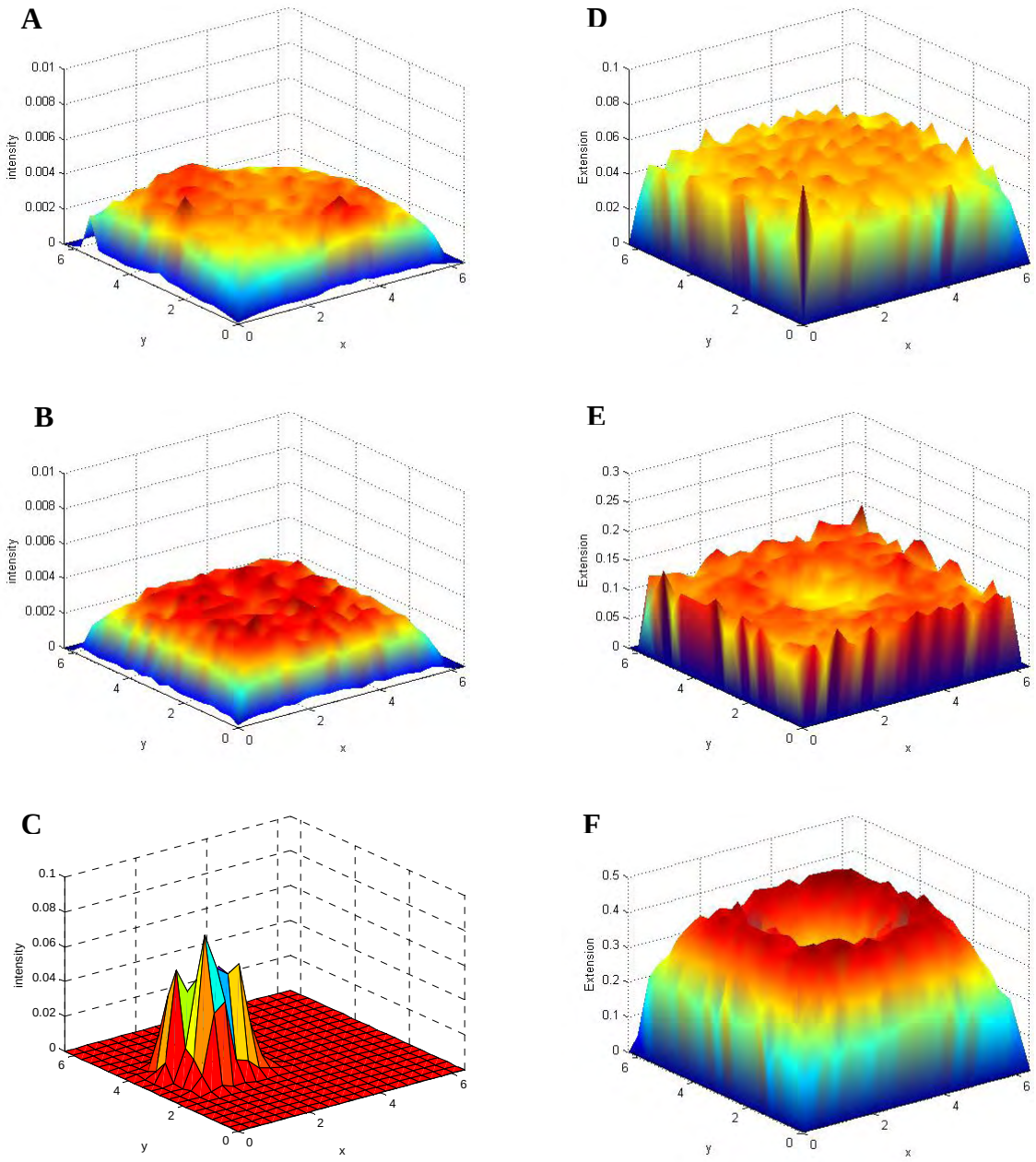


Figure 7.7 Steady state center-of-mass distribution and Steady state of stretch as a function of position of center-of-mass in the cross section (*y-z* plane) of the channel for a 21*um* DNA chain in a 6.3 *um* wide channel by ***Full HI*** model. A,D $\dot{\gamma}_{\text{eff}} = 3.98\ \text{s}^{-1}$( Wi=0.44 ) , B,E $\dot{\gamma}_{\text{eff}} = 30.8\ \text{s}^{-1}$ ( Wi=3.39 ), C,F $\dot{\gamma}_{\text{eff}} = 308\ \text{s}^{-1}$( Wi=33.9 )

Figures 7.7 A, B, C illustrate the effect of flow strength on the probability distribution of the center-of-mass distribution. It can be seen that as the increase of the flow strength, a hydrodynamic-induced depletion layer (red area) is forming and depletion effect is quite strong at stronger flow strength. This can be supported by Figure7.8: the width of center-of-mass distribution in the cross section of the channel is decreasing with the increase of the flow strength, which indicates the depletion layer

is enlarging. Figure 7.7 C also indicates the distribution increases nonmonotonically from the pronounced depletion area near the wall and peaks at the halfway between the wall and the center, and then decreases to the local minimum in the center. This is due to the Brownian drift away from the centerline and deterministic drift away from the wall (due to the asymmetry of the bead mobility and wall hydrodynamic interaction due to the presence of the wall). The details of the mechanism will be discussed in the next section.

Figure 7.7 D,E,F show the average stretch in the cross section is increased with the increase of the flow strength. At the lower Weissenberg number, the distribution is fairly uniform, except the depletion layer near wall; higher strength appears there which is similar with those we have observed in the previous two models. At stronger flow strength, the maximum of average stretch seems to peak at halfway between the center and wall. This maybe because the less stretched chain will migrate toward the wall, while highly elongated chain near the wall drift away from the wall due to the presence of the wall. Therefore, the competition of those two effects leads to nonmontonical distribution of molecular stretch in the cross-section of the channel.

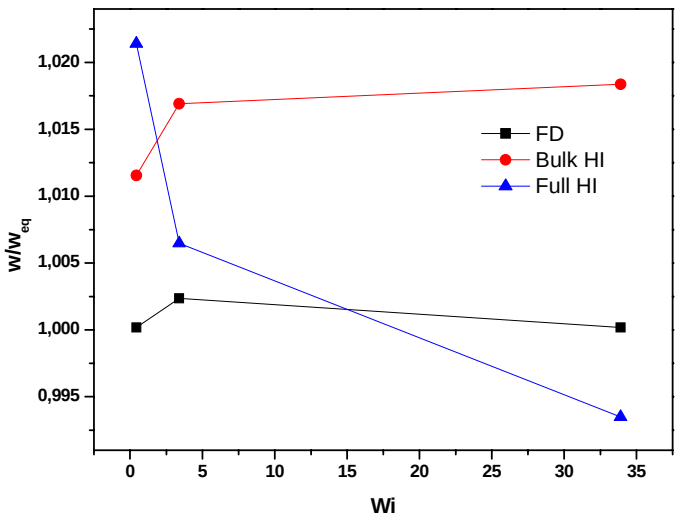


Figure 7.8 Width of the steady-state center-of-mass distribution $w$ (relative to equilibrium $w_{eq}$) in the microchannel as a function of flow strength for 21 *um* DNA by Free-draining model (black),Bulk HI model (red),and Full HI model (blue).

Figure 7.8 represents the width of the steady-state center-of-mass distribution normalized by the equilibrium width as a function of flow strength. Results are shown for *Free-draining* model, *Bulk HI* model, and *Full HI* model. It can be seen that the width is unaffected with the variation of the flow strength in *Free-draining* model, which means migration effect is not expected by this model. For *Bulk HI* model, the width slightly increases with the flow strength, which indicates weak migration toward the wall. In addition to *Full* HI model, the width decrease a lot compared with other two models, therefore migration away from the wall is predicted and the depletion layer increases with the flow strength. Those results indicate that molecular migration away from the wall is induced by the coupling of bead-bead hydrodynamic interaction and hydrodynamic effect from the confined geometry.The mechanism in details will be discussed in the next section.

## *7.4 Mechanism on migration behavior*

### 7.4.1. General analytical approach

In the last section, the different migration behaviors under pressure-driven flow in the confined geometry have been predicted by different hydrodynamic interaction model. So far, only Full HI model gives a correct prediction to migration behavior. The depletion layer is significant affected by the variation of the flow strength, which indicates the chain migrates toward the center of the microchannel. Various mechanisms have been explored in order to explain the migration behavior in confined geometries. From Jendrejack *et al*'s work (2004), it is now well accepted that configuration dependent hydrodynamic interaction coupled with inhomogenous shear flow and confined boundaries are most likely responsible for the migration across streamlines. In this section, Jendrejack's idea is followed and simple modified mechanism will be proposed.

To explain those phenomena, the theoretical analysis of elastic dumbbell model (two beads connected by a spring) is carried through the generalized diffusion equation. The probability distribution function $\Psi$ for a single dumbbell is a function of positions of two beads ($\mathbf{r}_1$, $\mathbf{r}_2$) and time (t) in physical space. So the continuity equation for $\Psi$ ($\mathbf{r}_1$, $\mathbf{r}_2$,t) can be given as follows (Bird *et al*, 1987):

$$\frac{\partial \Psi}{\partial t} = -(\frac{\partial}{\partial \mathbf{r}_1} \cdot \dot{\mathbf{r}}_1 \Psi) - (\frac{\partial}{\partial \mathbf{r}_2} \cdot \dot{\mathbf{r}}_2 \Psi) \tag{7.5}$$

where $\dot{\mathbf{r}}_1, \dot{\mathbf{r}}_2$ is the velocity of beads at the $\mathbf{r}_1$, $\mathbf{r}_2$. Since the relationship between $\mathbf{r}_1$, $\mathbf{r}_2$ and center of mass $\mathbf{r}_c$ and the connector vector $\mathbf{q}$ as follows:

$$2\mathbf{r}_c = (\mathbf{r}_1 + \mathbf{r}_2) \tag{7.6}$$

$$\mathbf{q} = \mathbf{r}_2 - \mathbf{r}_1 \tag{7.7}$$

$$\mathbf{r}_1 = \mathbf{r}_c - \frac{1}{2}\mathbf{q} \tag{7.8}$$

$$\mathbf{r}_2 = \mathbf{r}_c + \frac{1}{2}\mathbf{q} \tag{7.9}$$

So the following derivatives can be got:

$$\frac{\partial}{\partial \mathbf{r}_c} = \frac{\partial}{\partial \mathbf{r}_1}\frac{\partial \mathbf{r}_1}{\partial \mathbf{r}_c}\bigg|_{\mathbf{q}} + \frac{\partial}{\partial \mathbf{r}_2}\frac{\partial \mathbf{r}_2}{\partial \mathbf{r}_c}\bigg|_{\mathbf{q}} = \frac{\partial}{\partial \mathbf{r}_1} + \frac{\partial}{\partial \mathbf{r}_2} \tag{7.10}$$

$$\frac{\partial}{\partial \mathbf{q}} = \frac{\partial}{\partial \mathbf{r}_1}\frac{\partial \mathbf{r}_1}{\partial \mathbf{q}}\bigg|_{\mathbf{r}_c} + \frac{\partial}{\partial \mathbf{r}_2}\frac{\partial \mathbf{r}_2}{\partial \mathbf{q}}\bigg|_{\mathbf{r}_c} = \frac{1}{2}\left(\frac{\partial}{\partial \mathbf{r}_2} - \frac{\partial}{\partial \mathbf{r}_1}\right) \tag{7.11}$$

Subsituting (7.6)-(7.11) into (7.5), Equation (7.5) can be rewritten as follows:

$$\begin{aligned}\frac{\partial \Psi}{\partial t} &= -\left(\frac{\partial}{\partial \mathbf{r}_1}\cdot \dot{\mathbf{r}}_1 \Psi\right) - \left(\frac{\partial}{\partial \mathbf{r}_2}\cdot \dot{\mathbf{r}}_2 \Psi\right) \\ &= -\left(\frac{1}{2}\frac{\partial}{\partial \mathbf{r}_c} - \frac{\partial}{\partial \mathbf{q}}\right)\cdot \dot{\mathbf{r}}_1 \Psi - \left(\frac{1}{2}\frac{\partial}{\partial \mathbf{r}_c} + \frac{\partial}{\partial \mathbf{q}}\right)\cdot \dot{\mathbf{r}}_2 \Psi \\ &= -\left(\frac{\partial}{\partial \mathbf{r}_c}\cdot \dot{\mathbf{r}}_c \Psi\right) - \left(\frac{\partial}{\partial \mathbf{q}}\cdot \dot{\mathbf{q}} \Psi\right)\end{aligned} \tag{7.12}$$

Where the average velocity of center of mass $\mathbf{r}_c$ is given as follows (Bird *et al* 1977)

$$2\dot{\mathbf{r}}_c = \boldsymbol{\kappa}\cdot(\mathbf{r}_1 + \mathbf{r}_2) + \sum_{i,j=1}^{2} \mathbf{D}_{ij}\cdot\frac{\mathbf{F}_j^s}{k_B T} - \sum_{i,j=1}^{2} \mathbf{D}_{ij}\cdot\frac{\partial}{\partial \mathbf{r}_j}\ln\Psi \tag{7.13}$$

and average time evolution rate of connector vector $\dot{\mathbf{q}}$ is :

$$\dot{\mathbf{q}} = \boldsymbol{\kappa}\cdot(\mathbf{r}_2 - \mathbf{r}_1) + \sum_{j=1}^{2}(\mathbf{D}_{2j} - \mathbf{D}_{1j})\cdot\frac{\mathbf{F}_j^s}{k_B T} - \sum_{j=1}^{2}(\mathbf{D}_{2j} - \mathbf{D}_{1j})\cdot\frac{\partial}{\partial \mathbf{r}_j}\ln\Psi \tag{7.14}$$

Now it can be seen that the probability distribution function $\Psi$ can be rewritten as a function $\Psi(\mathbf{r}_c, \mathbf{q}, t)$ of center of mass $\mathbf{r}_c$ and the connector vector $\mathbf{q}$. But what we are really interested in the relationship between $\Psi$ and position center of mass $\mathbf{r}_c$. Therefore, we integrate Equation (7.12) in order to decouple the influence of $\mathbf{q}$ and $\mathbf{r}_c$ :

$$C(\mathbf{r}_c, t) = \int \Psi(\mathbf{r}_c, \mathbf{q}, t) d\mathbf{q} \tag{7.15}$$

So the continuity equation for center of mass $\mathbf{r}_c$ can be given as follows:

$$\frac{\partial C(\mathbf{r}_c, t)}{\partial t} = -\nabla_{\mathbf{r}_c}\cdot \mathbf{j}_c \tag{7.16}$$

where $C(\mathbf{r}_c,t)$ is the probability distribution of center of mass $\mathbf{r}_c$ and $\mathbf{j}_c = \langle \dot{\mathbf{r}}_c \rangle C$ is the momentum-space-averaged center-of-mass, integrated over the internal degrees of freedom of the chain, and the average is defined as follow:

$$\langle A \rangle = \int A\Psi d\mathbf{q} \tag{7.17}$$

Therefore $\langle \dot{\mathbf{r}}_c \rangle C$ can be got by multiplying Equation (7.13) by $\Psi$ and integrate by connector vector $\mathbf{q}$ :

First, we rewrite the r as follows $\mathbf{r}_c$:

$$\dot{\mathbf{r}}_c = \mathbf{v}_c + \frac{1}{2}\bar{\mathbf{\Omega}} \cdot \mathbf{F}^s - (\frac{1}{4}\hat{\mathbf{D}}\frac{\partial}{\partial \mathbf{r}_c}\ln\Psi - \frac{1}{2}\bar{\mathbf{D}}\frac{\partial}{\partial \mathbf{q}}\ln\Psi) \tag{7.18}$$

Where

$$\mathbf{F}^s = \mathbf{F}_1^s = -\mathbf{F}_2^s \tag{7.19}$$

$$v_c = \frac{1}{2}\boldsymbol{\kappa} \cdot (\mathbf{r}_1 + \mathbf{r}_2) \tag{7.20}$$

$$\hat{\mathbf{D}} = (\mathbf{D}_{11} + \mathbf{D}_{22}) + (\mathbf{D}_{21} + \mathbf{D}_{12}) \tag{7.21}$$

$$\bar{\mathbf{\Omega}} = (\mathbf{\Omega}_{11} - \mathbf{\Omega}_{22}) + (\mathbf{\Omega}_{21} - \mathbf{\Omega}_{12}) \tag{7.22}$$

$$\bar{\mathbf{D}} = \bar{\mathbf{\Omega}} k_B T \tag{7.23}$$

Thus $\mathbf{j}_c = \langle \dot{\mathbf{r}}_c \rangle C$ can be expressed as follows (Jendrejack *et al*,2004):

$$\mathbf{j}_c = \left[ \langle \mathbf{v}_c \rangle + \left\langle \frac{1}{2}\frac{\bar{\mathbf{D}}}{k_B T} \cdot \mathbf{F}^s \right\rangle \right] C - \left\langle \frac{\partial}{\partial \mathbf{q}} \cdot (\frac{1}{2}\bar{\mathbf{D}}C) \right\rangle - \left\langle \frac{1}{4}\frac{\partial}{\partial \mathbf{r}_c} \cdot (\hat{\mathbf{D}}C) \right\rangle$$

$$= \left[ \langle \mathbf{v}_c \rangle + \left\langle \frac{1}{2}\bar{\mathbf{\Omega}} \cdot \mathbf{F}^s \right\rangle \right] C - \frac{1}{4}[2\left\langle \frac{\partial}{\partial \mathbf{q}} \cdot \bar{\mathbf{D}} \right\rangle - \left\langle \frac{\partial}{\partial \mathbf{r}_c} \cdot (\mathbf{D}_{11} + \mathbf{D}_{22}) \right\rangle + \left\langle \frac{\partial}{\partial \mathbf{r}_c} \cdot \hat{\mathbf{D}} \right\rangle ]C - \frac{1}{4}\hat{\mathbf{D}} \cdot \left\langle \frac{\partial}{\partial \mathbf{r}_c} C \right\rangle \tag{7.24}$$

The steady state solution condition for Equation (7.16) is $-\nabla_{\mathbf{r}_c} \cdot \mathbf{j}_c = 0$, but in our case, the confined boundary condition is :

$$\mathbf{j}_{c,y} = 0 \text{ at the wall} \tag{7.25}$$

$$\mathbf{j}_{c,z} = 0 \text{ at the wall} \tag{7.26}$$

It leads to $\mathbf{j}_{c,x}$ =0, therefore the steady state solution condition can be simplified as follows:

$$\mathbf{j}_c = 0 \tag{7.27}$$

With the corresponding boundary conditions, the corresponding distribution of center of mass $C(\mathbf{r}_c)$ in the physical space is supposed to be solved by an analytical way. However, this is just for dumbbell model; kinetic theory for advanced model such as bead-spring model can be much more mathematically complicated.

In equation (7.22), $C(\mathbf{r}_c)$ can be regarded as probability distribution function in physical space of the confined geometry and the terms proportional to $C(\mathbf{r}_c)$ can be regarded as a 'drift' term to the probability distribution. The 'drift' or 'migration' also can be understood in this way: the probability distribution in the confined geometry will change with the variation of the flow strength.

First, we try to give a physical explanation to those terms. For pressure-driven flow in the channel, the first term $\langle \mathbf{v}_c \rangle C(\mathbf{r}_c)$ is the contribution from the flow field, but this term is zero in the wall-normal directions, because the components of the flow field in wall-normal directions are zero, which indicates the imposed flow field can not induce the migration effect directly.

The second term $\left\langle \frac{1}{2}\bar{\mathbf{\Omega}} \cdot \mathbf{F}^s \right\rangle C(\mathbf{r}_c)$ indicates that a dumbbell in tension or (compression) near a solid boundary may experience a deterministic drift which is not necessary along the streamline (Jendrejack *et al* 2004) due to the difference on bead mobility $(\mathbf{\Omega}_{11} - \mathbf{\Omega}_{22})$ and bead-bead interaction $(\mathbf{\Omega}_{21} - \mathbf{\Omega}_{12})$ in the inhomogeneous flow.

The term behind the first two terms is the Brownian contribution to the drift. In fact, this term is something between deterministic and stochastic in nature, since this term is the coupling of the diffusivity of the dumbbell and Brownian portion. If the diffusivity is position-dependent, at least implicitly position-dependent, this contribution becomes non-completely Brownian. Further insight into this term, there are four parts: the first term in average $\left\langle \frac{\partial}{\partial \mathbf{q}} \cdot \bar{\mathbf{D}} \right\rangle$ is the contribution due to the variation on the difference of bead mobility $(\mathbf{\Omega}_{11} - \mathbf{\Omega}_{22})$ and bead-bead hydrodynamic interaction $(\mathbf{\Omega}_{21} - \mathbf{\Omega}_{12})$; the second $\left\langle \frac{\partial}{\partial \mathbf{r}_c} \cdot (\mathbf{\Omega}_{11} + \mathbf{\Omega}_{22}) \right\rangle$ and third term $\left\langle \frac{\partial}{\partial \mathbf{r}_c} \cdot \hat{\mathbf{D}} \right\rangle$ indicates the

contribution due to the spatial variation on the bead mobility and bead-bead hydrodynamic interaction. The last term represents the typical Ficknian diffusion: $\left\langle \frac{1}{4}\hat{\mathbf{D}} \right\rangle \cdot \frac{\partial C}{\partial \mathbf{r}_c}$ ,where $\left\langle \frac{1}{4}\hat{\mathbf{D}} \right\rangle$ is the Kirkwood diffusivity ,averaged over all the internal coordinates (Jendrejack *et al* 2004).With this starting point, we will give a physical explanation to the phenomena in chapter 6,7.

### 7.4.2. Migration in Free-draining model

For the case of chain in homogenous flow in Chapter 6, Free-draining model is used by neglecting bead-bead interaction and wall hydrodynamic interaction, which indicates the diffusivity of the chain is constant and independent of the position in the channel. Therefore, the following condition can be deduced:

$$\mathbf{D}_{11} = \mathbf{D}_{22} = \frac{k_B T}{\zeta}\mathbf{I},\ \mathbf{D}_{12} = \mathbf{D}_{21} = 0 \tag{7.28}$$

Thus, Equation (7.24) can be simplified as follows:

$$\mathbf{j}_c = \langle \mathbf{v}_c \rangle C - \left\langle \frac{1}{4}\hat{\mathbf{D}} \right\rangle \cdot \frac{\partial}{\partial \mathbf{r}_c} C \tag{7.29}$$

Since probability distribution is only function of $y_c$[10] at steady state, the components of $\mathbf{j}_c$ in wall-normal direction for simple shear flow is given as follows:

$$\begin{aligned} \mathbf{j}_{cy} &= -\left\langle \frac{1}{4}(\mathbf{D}_{11} + \mathbf{D}_{22}) \right\rangle_{yy} \cdot \frac{\partial}{\partial y_c} C(y_c) \\ &= -\frac{k_B T}{2\zeta} \frac{\partial}{\partial y_c} C(y_c) \end{aligned} \tag{7.30}$$

where $y_c$ is the distance away from the centerline of the channel. It can be seen that there is no deterministic drift, only Brownian contribution (Fickian diffusion with confined boundaries), which predicts a uniform distribution and can not be influenced by variations of the flow strength. Therefore, Free-draining model in the simple flow can not predict migration behavior.

For the case of the chain in the inhomogeneous flow in chapter 7, Equation (7.30) is still suitable for this case, because the diffusivity of the chain is still not configuration

[10] In fact, probability distribution is also dependent on $z_c$ , but direction y and z is symmetric, so we can assume C is only dependent of $y_c$ for simplicity.

or position-dependent. Therefore, deterministic migration still can not be predicted in this case with the change of the flow strength. This analysis of both cases by Free draining model is consistent with the numerical results in Figure 6.3 (chapter 6) and Figure 7.2 respectively.

In general, the Free-draining model is basically a partially confined random walk. The segments of the chain undergo random interactions with its bonded neighbors and solvents. No deterministic migration will occur, even in inhomogeneous flow.

### 7.4.3. Migration with Bulk Hydrodynamic interaction:

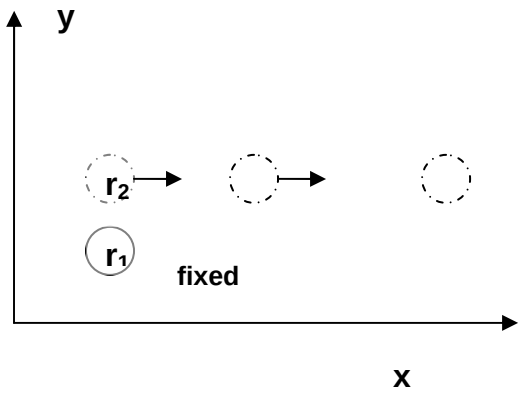


Figure 7.9 illustration of example system in Figure 7.10. In this case, the position $r_1$ of bead 1 is fixed and bead 2 is moving away from bead 1 in x-direction without changing the distance between bead 1 and bead 2 in y direction

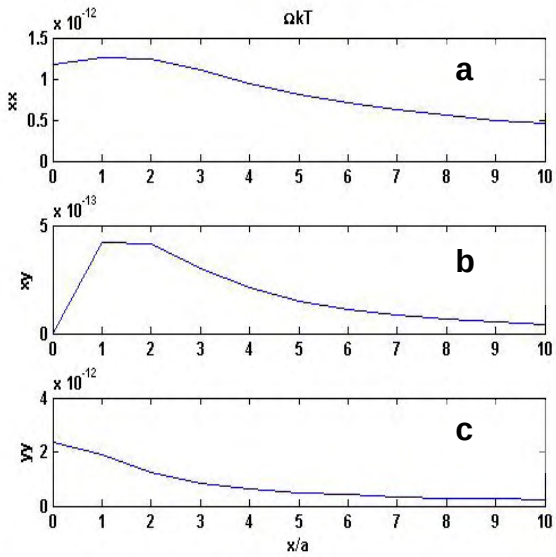


Figure 7.10 illustration of configuration dependence of Oseen tensor in the case of Figure 7.9. a. *xx* component of $\mathbf{\Omega}^{OB}$ b. *xy* component c. *yy* componet,where a is the bead radius

Now, if we build up our model more accurately, *Bulk hydrodynamic interaction* is needed to taken into the play. In this model, bead-bead hydrodynamic interaction is configuration dependent illustrated in Figure 7.9, which leads to the anisotropic diffusivity. Figure 7.9 represents the one point force is fixed at $\mathbf{r}_1$ and another point force is moving away from $\mathbf{r}_1$ in *x* direction (the flow field direction) without changing the distance in *y* direction (wall-normal direction). In Figure 7.10, the

corresponding evolution of *Oseen* tensor is presented[11]. It can be seen that when bead 2 is moving away from bead 1, all components of *Oseen* tensor will decrease with the increase of $\boldsymbol{q}=\left|\mathbf{r}_2-\mathbf{r}_1\right|$. The most interesting part is Figure 7.10 C: *yy* component will fall off with the increase of the distance in $\boldsymbol{x}$ direction and decay slowly (until 5 times of bead radius)! It indicates that wall-parallel orientated point forces will induce a weaker bead-bead hydrodynamic interaction in the wall-normal direction. In other words, highly stretched molecule in the direction of flow field will have smaller diffusivity in velocity gradient direction (the wall-normal direction in our case) compared to less stretched chains. In simple shear flow, this never happens. However, in the pressure-driven flow, the shear rate is higher near the wall than that close to the center, which will induce an implicitly position-dependent diffusivity. With this idea in mind, theoretical analysis can be introduced.

In this case (pressure-driven flow, Bulk HI model), we use Oseen tensor for simplicity:

$$\mathbf{D}_{11}=\ \mathbf{D}_{22}=\frac{k_BT}{\zeta}\mathbf{I},\ \mathbf{D}_{12}=\mathbf{D}_{21}=\frac{k_BT}{\zeta}(\mathbf{I}+\zeta\boldsymbol{\Omega}_{12}^{OB}) \tag{7.31}$$

Thus, Equation (7.24) can be simplified as follows:

$$\mathbf{j}_c=\left\langle\mathbf{v}_c\right\rangle C-\frac{k_BT}{2}\left\langle\frac{\partial}{\partial\mathbf{r}_c}\cdot\boldsymbol{\Omega}_{12}^{OB}\right\rangle C-\frac{k_BT}{2\zeta}\left\langle(\mathbf{I}+\zeta\boldsymbol{\Omega}_{12}^{OB})\right\rangle\cdot\frac{\partial}{\partial\mathbf{r}_c}C \tag{7.32}$$

If we take the component of $\mathbf{j}_c$ in wall-normal direction,

$$\mathbf{j}_{cy}=-\frac{k_BT}{2}\left\langle\frac{\partial}{\partial y_c}\cdot\boldsymbol{\Omega}_{12}^{OB}\right\rangle_{yy}C\left(y_c\right)-\frac{k_BT}{2\zeta}\left\langle(\mathbf{I}+\zeta\boldsymbol{\Omega}_{12}^{OB})\right\rangle_{yy}\cdot\frac{\partial}{\partial y_c}C\left(y_c\right) \tag{7.33}$$

Because in the steady state, probability distribution function $C(\mathbf{r}_c)$ is only dependent on $y_c$ [12], so the component of $\mathbf{j}_c$ in wall-normal direction is given as follows

$$\mathbf{j}_{cy}=-\frac{k_BT}{2}\left\langle\frac{\partial}{\partial y_c}\cdot\boldsymbol{\Omega}_{12,yy}^{OB}\right\rangle C\left(y_c\right)-\frac{k_BT}{2\zeta}\left\langle(\mathbf{I}+\zeta\boldsymbol{\Omega}_{12,yy}^{OB})\right\rangle\cdot\frac{\partial}{\partial y_c}C\left(y_c\right)=0 \tag{7.34}$$

which leads to :

$$\frac{\partial\ln C(y_c)}{\partial y_c}=-\zeta\left\langle(1+\zeta\boldsymbol{\Omega}_{12,yy}^{OB})\right\rangle^{-1}\left\langle\frac{\partial}{\partial y_c}\boldsymbol{\Omega}_{12,yy}^{OB}\right\rangle \tag{7.35}$$

[11] RPY tensor also can be used,using Oseen tensor is only for simplicity.

[12] In fact, probability distribution is also dependent on $z_c$ , but direction *y* and *z* is symmetric, so we can assume C is only dependent on $y_c$ for simplicity.

As we have mentioned before, the diffusivity or *Oseen* tensor (bead-bead hydrodynamic interaction) is implicitly position dependent, the *yy* component $\mathbf{\Omega}_{12,yy}^{OB} \propto q^{-1}(1+q_y/q^2)$ (where $q=|\mathbf{q}|$ and $\mathbf{q}$ is the connector vector) will decrease monotonically to an asymptotic value from center to the wall under the pressure-driven flow and remains positive shown in Figure 7.10. In fact, the decay is very similar to Figure 7.10, but not the same. This is because the assumption of Figure 7.10 is the fixed separation distance in y direction, the real case is that the chain will be squeezed in the velocity gradient direction when the chain approaches the wall[13]. Fortunately, the thickness in this direction didn't change so much compared to the increase of the stretch in *x*-direction as we know from Chapter 6. Therefore, the case happened in Figure 7.10 C is dominant in the parabolic flow and the separation between two beads in y direction can be assumed to be fixed for simplicity. As shown in the Figure 7.10, the maximum of $\mathbf{\Omega}_{12,yy}^{OB}$ appears in the center (smallest stretch at there), thus $\frac{\partial}{\partial y_c}\mathbf{\Omega}_{12,yy}^{OB}=0$ at the center, therefore the minimum of $C(y_c)$ is predicted at the center and $C(y_c)$ will increase monotonically from the center to the wall, which agrees well with the numerical results we get in Figure 7.6 C. As the increase of the flow strength, $\mathbf{\Omega}_{12,yy}^{OB}$ decaies faster to the asymptotic value from center to the wall. Therefore, the probability distribution will become broader in the wall-normal direction with the increase of the flow strength, which means migration toward wall is predicted by the *Bulk HI* model due to the anisotropic diffusivity of the chain (induced by spatial variations on the configuration-dependent bead-bead hydrodynamic interaction)

### 7.4.4. Migration with wall hydrodynamic interaction:

In the above analysis, the contribution to migration from wall hydrodynamic effects has been neglected. For the pressure-driven flow in the microchannel, if the contribution to hydrodynamic interaction from the wall is considered, we have:

$$\mathbf{D}_{11}=\frac{k_BT}{\zeta}(\mathbf{I}+\zeta\mathbf{\Omega}_{11}^{w}) \tag{7.36}$$

[13] We have proved that the thickness in the velocity gradient direction will decrease with the increase of the flow strength in chapter 6;in the parabolic flow, shear rate is higher rate near the wall than that near the center. Therefore, the thickness will decrease when the chain approach the wall.

$$\mathbf{D}_{22} = \frac{k_B T}{\zeta}(\mathbf{I} + \zeta \mathbf{\Omega}_{22}^{w}) \tag{7.37}$$

$$\mathbf{D}_{12} = \frac{k_B T}{\zeta}(\mathbf{I} + \zeta \mathbf{\Omega}_{12}^{OB} + \zeta \mathbf{\Omega}_{12}^{w}) \tag{7.38}$$

$$\mathbf{D}_{21} = \frac{k_B T}{\zeta}(\mathbf{I} + \zeta \mathbf{\Omega}_{21}^{OB} + \zeta \mathbf{\Omega}_{21}^{w}) \tag{7.39}$$

If we neglect the Brownian drift term in Eq (7.22), Eq(7.22) can be simplified as follows:

$$\mathbf{j}_c = \frac{1}{2}\left[2\langle \mathbf{v}_c \rangle + \left\langle (\mathbf{\Omega}_{11}^{w} - \mathbf{\Omega}_{22}^{w}) + (\mathbf{\Omega}_{21}^{w} - \mathbf{\Omega}_{12}^{w}) \cdot \mathbf{F}^s \right\rangle\right] C - \left\langle \frac{1}{4}\hat{\mathbf{D}} \right\rangle \cdot \frac{\partial}{\partial \mathbf{r}_c} C \tag{7.40}$$

Since $C(\mathbf{r}_c)$ is only dependent on $y_c$, the component of $\mathbf{j}_c$ in the wall-perpendicular direction and it's deterministic portion(det) can be given by Eq(7.24):

$$\mathbf{j}_{cy} = \frac{1}{2}\left\langle (\mathbf{\Omega}_{11}^{w} - \mathbf{\Omega}_{22}^{w}) + (\mathbf{\Omega}_{21}^{w} - \mathbf{\Omega}_{12}^{w}) \cdot \mathbf{F}^s \right\rangle_{yy} C - \left\langle \frac{1}{4}\hat{\mathbf{D}} \right\rangle_{yy} \cdot \frac{\partial}{\partial y_c} C \tag{7.41}$$

$$\mathbf{j}_{cy}^{\text{det}} = \left\langle \bar{\mathbf{\Omega}}^{w}(y_c) \cdot \mathbf{F} \right\rangle_{y} C(y_c) \tag{7.42}$$

$$\bar{\mathbf{\Omega}}^{w} = (\mathbf{\Omega}_{11}^{w} - \mathbf{\Omega}_{22}^{w}) + (\mathbf{\Omega}_{21}^{w} - \mathbf{\Omega}_{12}^{w}) \tag{7.43}$$

It can be seen that $\bar{\mathbf{\Omega}}^{w}$ is proportional to the difference in bead motility $(\mathbf{\Omega}_{11}^{w} - \mathbf{\Omega}_{22}^{w})$ and asymmetric portion of bead-bead interaction $(\mathbf{\Omega}_{21}^{w} - \mathbf{\Omega}_{12}^{w})$ due to the presence of the wall compared with $\bar{\mathbf{\Omega}}$=0 for the case of Bulk HI model in the last section. If we can assume that deterministic term can balance with Fickian term at steady state, Eq (7.41) can be rewritten as follows:

$$\frac{\partial \ln C}{\partial y_c} = \frac{1}{2} \frac{\left\langle \bar{\mathbf{\Omega}}^{w} \cdot \mathbf{F}^s \right\rangle_{yy}}{\left\langle \frac{1}{4}\hat{\mathbf{D}} \right\rangle_{yy}} \tag{7.44}$$

Although there is no analytical expression for $\mathbf{\Omega}^{w}$ in this confined geometry, it can be seen that the distribution will depend on the coupling of the sign and magnitude of the spring force, the difference in bead motility and asymmetric portion of bead-bead interaction due to the presence of the wall, and the Kirkwood diffusivity. Since it is too complicated to get the analytical expression, we will try to give a simple picture what happens in the channel.

Figure 7.11 represents a characteristic configuration near the wall under parabolic flow: a highly stretched elastic dumbbell orientated parallel to the wall[14].In this case, hydrodynamic flow in the local region due to the point forces at the bead 1 and bead 2, can be described by *Oseen* tensor. Here we neglect the repulsive force from the wall, because the repulsive force is a short distance interaction, the chain can feel its presence only when the chain is very close the wall. Therefore, the chain only experiences the spring force in the wall-parallel direction. If the chain is in a free solution, the hydrodynamic flow generated by point forces at two beads is symmetric, so there is no preference for chain to move up or down; Things become different when the wall appears: Due to the impenetrable wall, the velocity at wall the must be zero. The wall must generate a reflection flow field in order to fulfill the no-slip condition. This reflection flow field will counteract the part of the downward hydrodynamic flow, which make the total hydrodynamic flow upward or away from the wall.

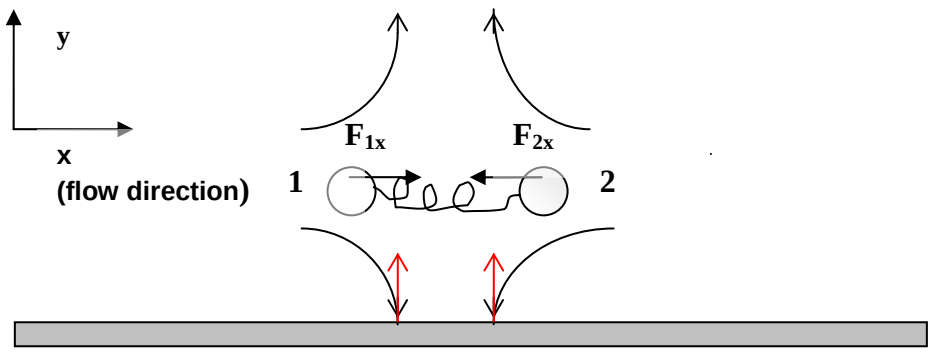


Figure 7.11 a elastic dumbbell in tension, parallel to the lower wall with $F_{1x}$= -$F_{2x,}$, induces the reflection flow field from the wall. Black line is the flow field induced by the point forces at bead 1 and bead 2, the red line is the refection flow field due to the presence of the wall. Here we assume that dumbbell is not very close to the wall in order to decouple the influence from the repulsive force from the wall and here we assume that the dumbbell can not feel the presence of the upper wall.

To illustrate this, recall that we have evaluated the hydrodynamic influence from wall- the correction term $\mathbf{\Omega}^{w}$ numerically in the chapter 2. Figure 7.12 represents the hydrodynamic influence due to the presence of the wall, please note Figure 7.12 only presents the reflection velocity contributed from the wall correction term, the contribution from *Oseen* tensor is not included. This can be interpreted as the chain (near the wall) in stretch orientated parallel to the wall will experience the drift

[14] The shear rate is higher near the wall under parabolic flow, so the chain tends to align with the flow direction, which we have known from chapter 6.

velocity away from the wall due to the horizontally orientated point forces, and higher stretched chain will experience a larger drift velocity. When the chain is far from the wall enough, the hydrodynamic flow by point forces at two beads will be symmetric again and the drift will disappear. In the above statement, we made an assumption: the diffusivity of the chain is not configuration dependent or position dependent. If the configuration-dependent diffusivity is considered, the drift direction will depend on the competition of the drift toward the center due to the presence of the wall and the drift toward the wall induced by the spatial variation on the difference of the bead-bead interaction under parabolic flow. From the numerical results in Figure 7.7C and results by Jendrejack *et al* (2004), the drift toward the center will dominate near the wall in the length scale of our confined geometry. When the chain is far from wall enough, the drift toward the wall will be dominant. Therefore, there must be a maximum for probability distribution $C(y_c)$ between the wall and center, which is consistent with the numerical result in the Figure 7.7 C.

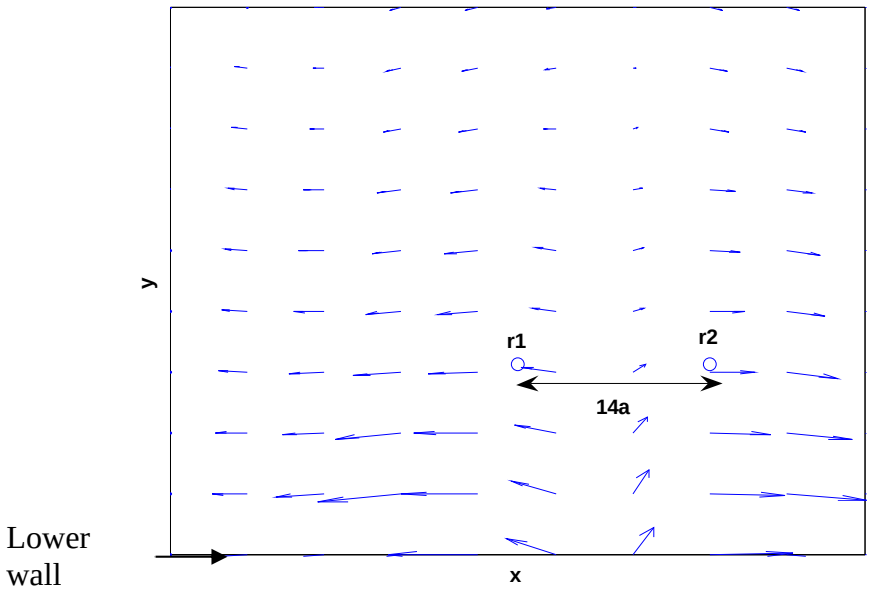


Figure 7.12 numerical solution of the reflection velocity field generated by the wall but induced by the points forces at $r_1$ and $r_2$ .In this case, the elastic dumbbell orients parallel to the lower wall with a stretch Q=14*a*,where a is the bead radius. The dumbbell only experiences the spring force in the x direction (the imposed flow direction).

In fact, we also examined the influence due to the orientation of the molecule near the wall. Figure 7.13 represents the similar case with Figure 7.12. In this plot, reflection velocity field in the case of dumbbell with different orientation is compared. It can be

seen that when molecule orientated smaller or larger than 45$^o$, it will migrate toward the wall, and hydrodynamic flow will drive the molecule to align with the flow direction during the process. However, it can be seen in Figure 6.6 in the chapter 6, molecule has more probability to orientate parallel to the wall. Therefore, the configuration with smaller angle close to zero should be dominant in the real case, which indicates the deterministic drift of molecule (near the wall) toward the center.

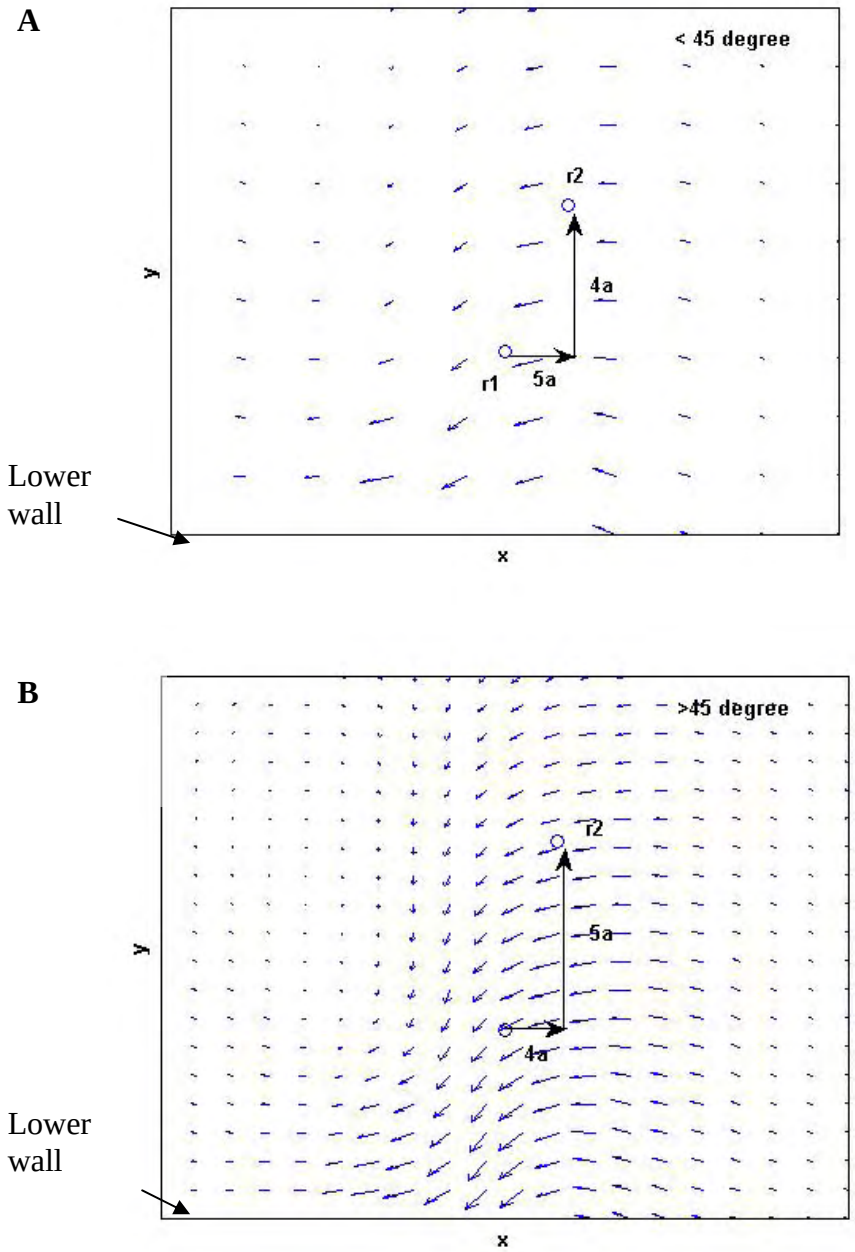


Figure 7.13 Comparsion of the reflection velocity field generated by the wall but induced by the points forces at $r_1$ and $r_2$ .In this case, the elastic dumbbell oriented smaller and larger than 45$^o$ with the imposed flow direction with a stretch Q= $\sqrt{41}\,a$,where $a$ is the radius of the bead.

In addition, as shown in Figure 7.7, as the increase of the flow strength, the reflection velocity field will become stronger compared with that at the same position with the smaller flow strength, since the higher stretched chain induces a stronger reflection velocity field. Therefore, the depletion layer will be significantly increased as the increase of the flow strength.

In fact, our explanation is a rather rough approach to migration behavior, especially the analytical part: the molecule is regarded as the dumbbell model, which indicates lots of contributions from internal configurations of molecule are not explored. However, the simple mechanism is still consistent with the simulation results by Jendrejack *et al* (2004): ***Full HI*** model will predict migration toward the center in the confined geometry, which displays flow induced evolution of configuration of polymer chain in an accurate fashion

## Reference

J.J.de Pablo, H.C.Ottiinger , *Hydrodynamic Changes of the Depletion Layer of Dilute Polymer Solutions Near a wall* ,AlchE Journal,308,1992

M.Chopra, R.G.Larson, *Brownian dynamics simulations of isolated polymer molecules in shear flow near adsorbin and nonadsorbing surface*, J.Rheol.46, 831- 862,2002

R.M.Jendrejack, D.C.Schwartz, J.J.de Pablo, M.D.Graham, *Shear-induced migration in flowing polymer solutions: simulation of long-chain DNA in microchannels*, J.Chem Phys,120,2513-2529,2004

Y.H.Seo, O.O.Park, M.S.Chun, *The behavior of the velocity enhancement in microcapillary flows of flexible water-soluable polymers*,J.Chem.Eng.Jpn,29,611,1996

L.F, H.Hu, R.G.Larson, *DNA configurations and concentration in shearing flow near a glass surface in a microchannel*, J. Rheol.49,127-138,2005

M.Chopra, R.G.Larson, *Brownian dynamics simulations of isolated polymer molecules in shear flow near adsorbing and non adsorbing surfaces* , J. Rheol.46,831-862,2002

R.B.Bird, C.F.Curtiss, R.C.Armstrong, O.Hassager, *Dynamics of Polymeric Liquids* Wiley ,Vol.2,1987

# Chapter 8 Conclusion and Future work

## 8.1 Conclusion

Simulations of dilute DNA solution in equilibrium in free solution and the confined geometries are performed in Chapter 5. We observed that there is a transition region for molecule stretch and diffusivity of the chain at H ≈10 $R_G$, where H is the width of the square channel and $R_G$ is the radius of gyration of polymer chain in free-solution. It indicates that the chain can be considered strong confined when the characteristic length scale of the confined geometry lowers down to certain value; otherwise, the chain will behave as it does in the free solution

In Chapter 6, simulations of dilute solution in simple shear flow in confined geometries are performed. Molecular orientation, molecule stretch and thickness in velocity gradient direction are examined and the results by Bulk HI model give qualitative agreements with the newest experimental data (Teixeira *et al*, 2005). Tumble dynamics of polymers in the shear flow proposed by Steven Chu is proved indirectly. In addition, migration behaviour is observed in this case, which is consistent with the mechanism we motioned in the chapter 7.

In Chapter 7, migration towards the center of microchannel is correctly predicted by Full HI model. Through the theoretical analysis of dumbbell model and simulation of bead-spring model, the following conclusions can be made on the migration beheavior:

a) There is deterministic hydrodynamic drift away from the walls. This is because highly stretched chain near the wall will generate a hydrodynamic flow field, which will induce a reflection flow field from the wall to break the symmetry of hydrodynamic flow and push the chain away from the wall.
b) There is non-completely Brownian drift, which couples with the spatial variation of configuration-dependent bead-bead hydrodynamic interaction, away from the centerline
c) The center-of-mass distribution of the steady state will depend on the competition of those two effects. In our geometry, the deterministic drift term will be dominant near the wall and the Brownian drift will be dominant near

the centreline of the channel. Therefore, a maximum is predicted at the halfway between the wall and center and nonmonotonical distribution of center-of-mass is predicted. In addition, the depletion layer is predicted to increase with the increase of flow strength.

## 8.2 Future Work

So far, we have presented simulation results in the microchannel with square cross section under simple shear flow and pressure-driven flow. Since the dynamics of polymers in confined geometry are extremely important for many natural and industrial processes, the following work may be interesting:

a) Different geometries will induce different hydrodynamic flow field from the boundaries, such as the channel with a triangle cross section has a fundamental interest for the SEC (Size Exclusion Chromatography) technology. In addition, the surface pattern in the channel would be interesting to explore for the purpose of bimolecular sorting.
b) In our project, the surface of the channel has a weaker repulsive potential to mimic the desorbing surface. In fact, adsorbing surface is subject to more extensive interests in science and technology.
c) More complex flow patterns are also interesting to consider. For example, a DNA molecule flowing into micro or nano-porous geometries is a contract flow, such kind of problem has a fundamental biological interest, eg. How virus gets though the membrane of cells.
d) Electromagnetic effect is also interesting to be examined. Deep understanding on how this effect influences the dynamics of biomolecules in the confined geometries will give lots of fresh ideas to the design of microfludic systems.
e) We are focusing on single molecule dynamics in this project for simplicity. In fact, the solution is concentrated in most of cases, therefore multi-chain system with different concentration effects will be interesting to be examined. With interchain entanglement, the project will become more complex.
f) To accomplish the above ideas, the algorithm needs to be optimized and more advanced computing resources and techniques are needed.

# Appendices

## A-1 Evaluation for Green's function

To evaluate the Green's function for the confined geometries, we need to set right boundary condition (2.44).

To get $\mathbf{v}'_{OB}$, using Equation (2.42), we can get

$$\mathbf{v}'_{OB} = \mathbf{\Omega}_{OB}(\mathbf{r}-\mathbf{r}_j)\cdot\mathbf{f}(\mathbf{r}_j) \tag{1.1}$$

For simplicity, we write the explicit expression for Equation (1.1)

$$\begin{pmatrix} v'_{OB,1} \\ v'_{OB,2} \\ v'_{OB,3} \end{pmatrix} = \begin{pmatrix} \Omega_{11}^{OB} & \Omega_{12}^{OB} & \Omega_{13}^{OB} \\ \Omega_{21}^{OB} & \Omega_{22}^{OB} & \Omega_{23}^{OB} \\ \Omega_{31}^{OB} & \Omega_{32}^{OB} & \Omega_{33}^{OB} \end{pmatrix} \cdot \begin{pmatrix} f_1 \\ f_2 \\ f_3 \end{pmatrix} \tag{1.2}$$

Here we always use $\mathbf{\Omega}^{RPY}$ instead of $\mathbf{\Omega}^{OB}$ .from Equation (2.33), we know:

$$\mathbf{\Omega}^{RPY}(\mathbf{r}-\mathbf{r}_j) = \frac{1}{8\pi\eta_S\left|\mathbf{r}-\mathbf{r}_j\right|}\left[C_1\mathbf{I} + C_2\frac{(\mathbf{r}-\mathbf{r}_j)(\mathbf{r}-\mathbf{r}_j)}{\left|\mathbf{r}-\mathbf{r}_j\right|^2}\right] \tag{1.3}$$

Here $\mathbf{r}_j$ is the point where the point force $\mathbf{f}(\mathbf{r}_j)$ generates a velocity perturbation $\mathbf{v}'_{OB}$ at $\mathbf{r}_i$ ,so $\mathbf{r}_j$ can be regarded as the source point and $\mathbf{r}_i$ should be your observation point or measurement point for velocity perturbation.

Here $\mathbf{I}$ is a unit tensor and $(\mathbf{r}-\mathbf{r}_j)(\mathbf{r}-\mathbf{r}_j)$ is a dyadic product as follows:

$$(\mathbf{r}-\mathbf{r}_j)(\mathbf{r}-\mathbf{r}_j) = \begin{pmatrix} (x-x_j)^2 & (x-x_j)(y-y_j) & (x-x_j)(z-z_j) \\ (y-y_j)(x-x_j) & (y-y_j)^2 & (y-y_j)(z-z_j) \\ (z-z_j)(y-y_j) & (z-z_j)(y-y_j) & (z-z_j)^2 \end{pmatrix} \tag{1.4}$$

Then we can write each component for the velocity perturbation $\mathbf{v}'_{OB}$

$$\begin{aligned} v'_{OB,1} &= \Omega_{11}^{OB}\cdot f_1 + \Omega_{12}^{OB}\cdot f_2 + \Omega_{13}^{OB}\cdot f_3 \\ &= \frac{1}{8\pi\eta_S\left|\mathbf{r}-\mathbf{r}_j\right|}\left[C_1 f_1 + C_2\frac{(x-x_j)^2 f_1 + (x-x_j)(y-y_j) f_2 + (x-x_j)(z-z_j) f_3}{\left|\mathbf{r}-\mathbf{r}_j\right|^2}\right] \end{aligned} \tag{1.5}$$

$$v'_{OB,2} = \Omega_{21}^{OB} \cdot f_1 + \Omega_{22}^{OB} \cdot f_2 + \Omega_{23}^{OB} \cdot f_3$$
$$= \frac{1}{8\pi\eta_S \left|\mathbf{r}-\mathbf{r}_j\right|}\left[ C_1 f_2 + C_2 \frac{(x-x_j)(y-y_j) f_1 + (y-y_j)^2 f_2 + (y-y_j)(z-z_j) f_3}{\left|\mathbf{r}-\mathbf{r}_j\right|^2} \right] \quad (1.6)$$

$$v'_{OB,3} = \Omega_{31}^{OB} \cdot f_1 + \Omega_{32}^{OB} \cdot f_2 + \Omega_{33}^{OB} \cdot f_3$$
$$= \frac{1}{8\pi\eta_S \left|\mathbf{r}-\mathbf{r}_j\right|}\left[ C_1 f_3 + C_2 \frac{(x-x_j)(z-z_j) f_1 + (z-z_j)(y-y_j) f_2 + (z-z_j)^2 f_3}{\left|\mathbf{r}-\mathbf{r}_j\right|^2} \right] \quad (1.7)$$

To use those equations, we take an assumption that the beads are well separated with each other.

After setting the boundary condition, we can get velocity perturbation field, then we can evaluate the Green's function for the wall numerically based on the grid.

$$\begin{pmatrix} \Omega_{11}^{W} \\ \Omega_{21}^{W} \\ \Omega_{31}^{W} \end{pmatrix} = \frac{1}{f_1} \mathbf{v}'_W \quad (1.8)$$

Where 1,2,3 is the three directions of the vector. The second and third column of the $\mathbf{\Omega}^W(\mathbf{x},\mathbf{x}_j)$ can be get in the similar way by applying the point force in the direction 2, 3, respectively. Here is a trick: when we evaluate each column of the Green's function, we need to set the point forces in other direction to zero and the point force in the corresponding direction to a unit point force. During the evaluation, the point force in the corresponding direction can be arbitrary value, because this Stokes equation is a linear equation, the magnitude of the force will be scaled up in the final stage. In addition, from another point of view, the Green's function here should only depend on the geometry, and is independent of the direction and magnitude of the point force. The magnitude of the point force will only influence the resulting velocity perturbation field, but when we evaluate the Green's function, this force will be removed anyway.

## A-2 Interpolation for Green's function

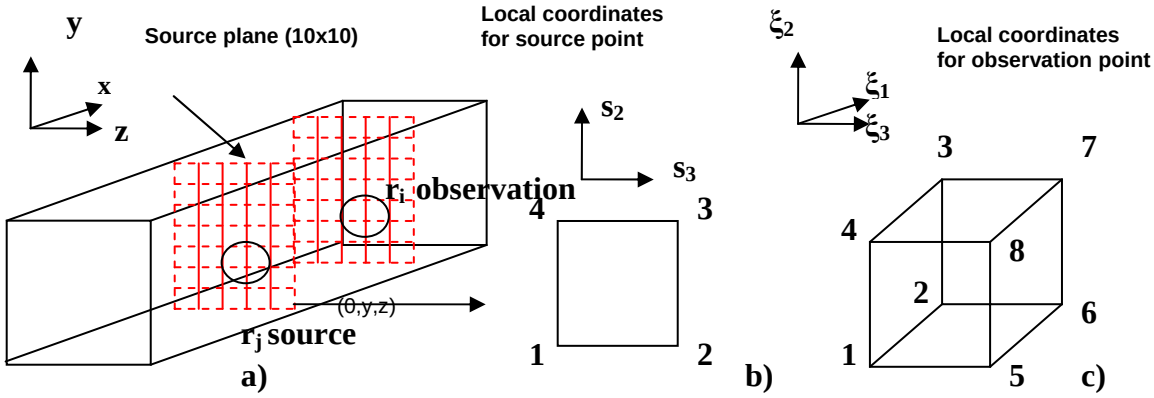


Figure a) sketch of the 3D FEM interpolation b) local coordinates for the source point $\mathbf{r}_j$ c) local coordinates for the observation point $\mathbf{r}_i$

Since we evaluated the Green's function from the wall on grid points (20x20x30, the observation points), we have to do 3D interpolation in order to evaluate the Green's function in the whole region of the channel. During the interpolation, we have two kinds of interpolation: one is the interpolation on the source point; the other is on the observation points.

Since we assume the channel is infinitely long, we don't have to evaluate all points in the channel as the source point. Choosing mid-plane in the channel (0,y,z) as the source plane due to the independence of source point in the *x* direction (flow direction) will reduce lots of computing time. In the evaluation, we will divide the source plane into 10x10 grid points. During the Brownian dynamic simulation, each time or iteration we can generate position of source point $\mathbf{r}_j$. and observation point $\mathbf{r}_i$ at each time or iteration. After converting their global coordinates into local coordinates, the following interpolation can be done:

At the given source grid point *j* (*j*=1,..,4) in the Figure b, the Green's function at any point of cubic box in Figure c can be interpolated by the observation grid point *i* (*i*=1,..,8) due to the source point can be written as follows:

$$\mathbf{\Omega}_{s,j} = \sum_{i=1}^{8} N_i \mathbf{\Omega}_i \quad , j = 1,2,3,4$$

where $N_i$ is the shape function for the observation point *i*, which can be defined as follows:

$$N_1 = \frac{1}{8}(1-\xi_1)(1-\xi_2)(1-\xi_3)$$
$$N_2 = \frac{1}{8}(1+\xi_1)(1-\xi_2)(1-\xi_3)$$
$$N_3 = \frac{1}{8}(1+\xi_1)(1+\xi_2)(1-\xi_3)$$
$$N_4 = \frac{1}{8}(1-\xi_1)(1+\xi_2)(1-\xi_3)$$
$$N_5 = \frac{1}{8}(1-\xi_1)(1-\xi_2)(1+\xi_3)$$
$$N_6 = \frac{1}{8}(1+\xi_1)(1-\xi_2)(1+\xi_3)$$
$$N_7 = \frac{1}{8}(1+\xi_1)(1+\xi_2)(1+\xi_3)$$
$$N_8 = \frac{1}{8}(1-\xi_1)(1+\xi_2)(1+\xi_3)$$

Where $\xi_1$, $\xi_2$, $\xi_3$ is the local coordinates for the observation points shown in the Figure c. It can be seen that the interpolation for observation point is a 3D interpolation, while the interpolation for the source point is actually 2D interpolation due to the infinite long effect of the channel in the flow direction we mentioned above.

Since we get the Green's function of any observation point $\mathbf{r}_i$ in the cubic box in Figure c due to the source point at grid point *j*, if the source point $\mathbf{r}_j$ in Figure b is in the square but not at the grid point, the Green's function can be interpolated as follows:

$$\mathbf{\Omega}(\mathbf{r}_i, \mathbf{r}_j) = \sum_{j=1}^{4} N_{s,j} \mathbf{\Omega}_{s,j}$$

where $N_{s,j}$ is the shape function for the source point $\mathbf{r}_j$ ,which can be defined as follows:

$$N_{s,1} = \frac{1}{4}(1-s_3)(1-s_2)$$
$$N_{s,2} = \frac{1}{4}(1+s_3)(1-s_2)$$

$$N_{s,3} = \frac{1}{4}(1+s_3)(1-s_2)$$
$$N_{s,4} = \frac{1}{4}(1-s_3)(1+s_2)$$

Where $s_2$,$s_3$ is the local coordinates for the source points.

Finally, $\mathbf{\Omega}(\mathbf{r}_i, \mathbf{r}_j)$ is the approximation of the Green's function for observation point $\mathbf{r}_i$ due to the point force at $\mathbf{r}_j$. To increase the accuracy of evaluation of the Green's function, decreasing the mesh size of each gird or increasing the discretization of the space is a choice, but the computing time will be significantly increased, since we have to locate the positions of source point and observation point first each time before starting the interpolation.

## *A-3 Chebyshev polynomial approximation*

$$\mathbf{D} = \mathbf{B} \cdot \mathbf{B}^T$$

**D** should be the symmetric semi-definite matrix, whose decomposition **B** in the above equation always can be efficiently solved by Cholesky decomposition. However, sometimes it fails during the simulation, so we can't make sure all eigenvalues of the diffusion tensor generated during the simulation is larger or equal to zero.

In addition, the decomposition of the diffusion tensor **D** is computational expensive and scales with $N^3$, while the Chebyshev decomposition scales with $N^{2.5}$(Kroger *et al*,2000; Jendrejack et al 2000) .Therefore, we introduce a method named Chebyshev polynomial approximation by Fixman (1986). B can be approximated by the following expression (Press *et al*, 1992):

$$\mathbf{B} = \sum_{k=1}^{L} c_k \mathbf{T}_{k-1}(D) - \frac{1}{2} c_1 \tag{2.1}$$

where

$$\begin{aligned} \mathbf{T_0} &= \mathbf{I} \\ \mathbf{T_1} &= d_a \mathbf{D} + d_b \mathbf{I} \\ \mathbf{T}_{l+1} &= 2\mathbf{C_1}\mathbf{C}_l - \mathbf{C}_{l-1} \end{aligned} \tag{2.2}$$

with

$$d_a = \frac{2}{\lambda_{\max} - \lambda_{\min}} \tag{2.3}$$

$$d_a = \frac{\lambda_{\max} + \lambda_{\min}}{\lambda_{\max} - \lambda_{\min}} \tag{2.4}$$

Where $\lambda_{\max}$ and $\lambda_{\min}$ is the maximum and minimum of **D**; $c_k$ is the Chebyschev coefficient , which can be obtained by the following way (Jendrejack *et al*,2000):

$$c_j = L^{-1} \sum_{k=1}^{L} \alpha_{kj}^{L} \sqrt{a_+ + a_- \cos[\pi(k-1/2)/L]} \tag{2.5}$$

Where

$$a_+ = (d_a + d_b)/2$$
$$a_- = (d_b - d_a)/2$$
$$\alpha_{kj}^{L} = 2\cos[\pi(j-1)(k-1/2)/L]$$

Here L is approximation degree. For a fixed L, Equation (2.1) is a polynomial which can approximate **B** in the interval [$\lambda_{\max}, \lambda_{\min}$].This approximation may be not better than other approximation from a point of view of accuracy, but it can be truncated to lower degree of M<L in a graceful way. It is difficult to find the minimal value of L, 50 are typical value used in our case (Press *et al*, 1992).

Because $\mathbf{B} \cdot d\mathbf{w}$ is our interest, whose polynomial **y** can be approximated by the same approach:

$$\mathbf{y} = \mathbf{B} \cdot d\mathbf{w} = \sum_{k=1}^{L} c_k \mathbf{x}_{K-1} \tag{2.6}$$

$$\mathbf{x}_0 = d\mathbf{w} \tag{2.7}$$

$$\mathbf{x}_1 = \mathbf{T}_1 \cdot d\mathbf{w} \tag{2.8}$$

$$\mathbf{x}_{l+1} = 2\mathbf{T}_1 \cdot \mathbf{x}_l - \mathbf{x}_{l-1} \tag{2.9}$$

The Chebyshev expansion is only valid within the chosen eigenvalue range; sometimes, a violation of the eigienvalue limits could happen. A method for error evaluation is proposed by R.M.Jendrejack *et al* (2004). Using Equation (2.6) and Equation (2.7) we can get

$$\lim_{L \to \infty} [\mathbf{y} \cdot \mathbf{y}] = d\mathbf{w} \cdot \mathbf{D} \cdot d\mathbf{w} \tag{2.10}$$

Assuming the eigenvalues we are using are valid. A relative error $E_f$ can be defined as follows(Jendrejack,2004):

$$E_f = \sqrt{\frac{\left|\mathbf{y}\cdot\mathbf{y} - d\mathbf{w}\cdot\mathbf{D}\cdot d\mathbf{w}\right|}{d\mathbf{w}\cdot\mathbf{D}\cdot d\mathbf{w}}} \tag{2.11}$$

Here, we give a initial guess of the eigenvalues of diffusion tensor D first ,then check if the error is acceptable. If it is not, we can compute another set of eigenvalues until the error requirement is satisfied.

In this way, we check the extent of violation of the fluctuation-disspation theorem is small enough to get a desired accuracy.

## *Reference:*

M.Kroger, A.Alba-Perez, M.Laso,H.C.Ottinger, *Variance reduced Brownian simulation of a bead-spring chain under steady flow considering hydrodynamic interaction effects*,J.Chem.Phys.113,4767,2000

R. M. Jendrejack, M. D. Graham, and J. J. de Pablo, *Hydrodynamic interactions in long chain polymers: Application of the Chebyshev polynomial approximation in stochastic simulations*, J. Chem. Phys.113,2894, 2000

Jendrejack, R. M., *Multiscale Simulations of Dilute-Solution Macromolecular Dynamics in Macroscopic and Microscopic Geometries*, Doctoral dissertation ,2003

W. Press, S. A. Teukolsky, W. T. Vetterling, and B. P. Flannery, *Numerical Recipes in Fortran*, 2nd ed. Cambridge University Press, Cambridge,1992

M. Fixman, *Construction of Langevin Forces in the Simulation of Hydrodynamic Interaction, Macromolecules* ,19, 1204,1986.

## *A-4 Construction of positive definite Hydrodynamic interaction tensor*

As we mentioned before, Oseen tensor in free solution will lead to unphysical properties of diffusion tensor, e.g. **negative translational diffusion coefficients** .The main origin is the treatment of segments as point sources of friction according to the

Oseen tensor (Yamakawa,1970). Hence RPY tensor is introduced to guarantee the diffusion tensor to be a positive-semidefinite for all the chain configurations.

Problem happens when we add the correction term $\mathbf{\Omega}^W(\mathbf{r},\mathbf{r}_j)$ from the geometry to the Green's function. During the simulation, the diffusion tensor **D** could become non-positive at some points, at which the program will break down. In order to keep the positive-semidefinite properties of diffusion tensor, we have to make some modifications to the diffusion tensor **D**. In the following, we will explain this issue.

First, we check the positive definiteness of $\mathbf{D}_{ij}$ (the hydrodynamic interaction tensor for a point force at $\mathbf{r}_j$) by determining the eigenvalues of 3×3 matrix. If $\mathbf{D}_{ij}$ is non-positive, it needs to be modified. For computational efficiency, one can set $\mathbf{D}_{ij} = c\mathbf{D}_{ii}$, where $c$<1 until $\mathbf{D}_{ij}$ becomes positive-definite. Here $c$ could be a constant, but if $c$ can be designed to be a function of relative distance between source point and observation point, the error due to modification of the diffusion tensor can be reduced to some extent (Jendrejack, *et al*, 2004).

## Reference

H. Yamakawa, *Transport properties of Polymer Chains in Dilute Solution: Hydrodynamic Interaction*, J. Chem. Phys.53, 436, 1970

R.M.Jendrejack, D.C.Schwartz, J.J.de Pablo, M.D.Graham, *Shear-induced migration in flowing polymer solutions: simulation of long-chain DNA in microchannels*, J.Chem Phys,120,2513-2529,2004